Universidade do Minho

Júlio André Machado Fernandes

Development of Power Converters for Electric Vehicle Charging with Photovoltaics Interface

Dissertação submetida na Universidade do Minho
para obtenção do grau de
Mestre em Engenharia Eletrónica e de Computadores

Trabalho realizado sob orientação do
Doutor Gabriel Pinto
e co-orientação do
Doutor Marcin Jarnut

Abril de 2017

DECLARAÇÃO

Júlio André Machado Fernandes

Endereço eletrónico: a62033@alunos.uminho.pt   Telefone: 919134295

Número do Cartão de Cidadão: 14163155

Título da Dissertação:

Development of Power Converters for Electric Vehicle Charging with Photovoltaics Interface

Orientador:

Doutor Gabriel Pinto (Departamento de Eletrónica Industrial - Universidade do Minho)

Co-orientador:

Doutor Marcin Jarnut (Departamento de Ciências da Computação, Engenharia Elétrica e Automação - Universidade de Zielona Góra)

Ano de conclusão: 2017

Dissertação submetida na Universidade do Minho para a obtenção do grau de Mestre em Engenharia Eletrónica e de Computadores

Universidade do Minho, ___/___/_____

Assinatura: _____

To the non-believers.

Acknowledgements

The making of this Project could not have been done if not for the support of some people to whom I give my most sincere thanks.

I would like to thank my supervisor at the University of Minho, Doctor Gabriel Pinto, for the patience and help given to me, not all of it practical but also the contribute he gave into the careful revise of this Dissertation and, most importantly, for giving me the opportunity to finish my work.

To my supervisor at the University of Zielona Góra, Doctor Marcin Jarnut, a big thank you for the ideas and the availability throughout the whole year I spent there. The opportunity to work and learn from him is certainly one of the most cherished memories that I brought back.

I would like to thank my girlfriend Ainara, for bringing me joy and happiness every day of my life. Thank you for all the patience throughout the last year and I hope I can make it up to you soon.

To all my co-workers, or better yet, friends and investigators in GEPE, I truly appreciate the good times spent working together and the Friday football matches. Thank you for the helping spirit that you always shown me. A special thank you goes to Doctor Vítor Monteiro, for letting me use the hardware he developed in order to finish all the experimental tests.

Last but not least, I would like to thank my mother Cristina, my sister Margarida and my grandparents Bernardino and Fátima for making me the man that I am today. I cannot thank you enough for the support you gave me, in every aspect, not only during this work but also during my whole life. To this day you all continue to teach me how to be the best that I can be. And I will gladly learn.

To all my friends outside of the university, especially my best friends Paulo and Vera, and all the people who left their mark and contribution, directly or indirectly, in the development of both the work and its author,

To all,

Thank you!

Development of Power Converters for Electric Vehicle Charging with Photovoltaics Interface
Júlio André Machado Fernandes - University of Minho

vii

Abstract

Currently, an increasing bet in electric mobility has been made, particularly in electric vehicles (EV) and plug-in hybrid vehicles (PHEV). However, in addition to the high initial costs, the EVs feature a very low autonomy when compared with a traditional car. By charging the batteries of the EV using a renewable energy source, it is possible to make the system virtually emissions-free, since the production of electric power, as well as inexhaustible, is made without the use of fossil fuels (e.g. natural gas and coal). In addition, the benefits to the economy of the country are also evident, since we are contributing to the decrease of importing costs of these fossil fuels.

As such, the main objective of this dissertation is the development and implementation of an integrated bi-directional converter (DC-DC and DC-AC) in order to connect an array of photovoltaic panels to the battery pack of an EV and to the power grid. In conventional systems, the electrical energy produced by the photovoltaic panels is injected into the grid and the batteries are charged from the grid. The aim is to develop a more efficient charging method which consists in charging the batteries directly from the PV panels. In this way it is possible to avoid the losses associated with the conversion of energy.

The converter will allow the charging of the EV's batteries directly from the PV panel, that is, without making DC-AC and AC-DC conversions, ensuring that the surplus energy is injected into the power grid. On the other hand, if the solar energy absorbed by the PV panel is insufficient to charge the batteries, the rest of the power needed to charge the batteries will be drawn from the grid. Naturally, if the batteries of the EV are already charged or no EV is connected to the system, all of the energy extracted from the PV panel will be injected into the power grid. Finally, the batteries will be able to deliver part of their stored energy to the power grid.

Keywords: Power Converters, Renewable Energies, Battery Charging, Electric Vehicles.

Resumo

Atualmente, tem vindo a ser feita uma aposta crescente na mobilidade elétrica, nomeadamente nos veículos elétricos (VE) e nos veículos híbridos *Plug-in* (PHEV). Contudo, para além do custo inicial elevado, os VEs apresentam uma autonomia muito baixa quando comparados com um automóvel tradicional. Ao carregar as baterias do VE através de uma fonte de energia renovável, é possível tornar o sistema virtualmente livre de emissões, uma vez que a produção de energia elétrica, para além de inesgotável, é feita sem o uso de combustíveis fósseis (e.g. gás natural e carvão). Para além disso, as vantagens para a economia do País também são evidentes, uma vez que estamos a contribuir para a diminuição dos gastos na importação dos referidos combustíveis fósseis.

O objetivo principal desta dissertação é o desenvolvimento e implementação de um conversor integrado bidirecional (CC-CC e CC-CA) de modo a ligar um *array* de painéis fotovoltaicos ao *pack* de baterias de um VE e à rede elétrica. Nos sistemas de carregamento convencionais, a energia elétrica produzida pelos painéis fotovoltaicos é injetada na rede elétrica e as baterias são carregadas a partir da rede. Pretende-se desenvolver um método de carregamento mais eficiente que consiste em carregar as baterias do VE diretamente dos painéis fotovoltaicos. Deste modo, evitam-se as perdas associadas à conversão de energia.

O conversor permitirá que as baterias do VE sejam carregadas diretamente do painel fotovoltaico, isto é, sem proceder a conversões de CC-CA e CA-CC, assegurando que a energia excedente é injetada na rede elétrica. Caso a energia solar absorvida pelo painel fotovoltaico seja insuficiente para fazer o carregamento das baterias, estas serão carregadas a partir da rede elétrica. Naturalmente, caso as baterias do VE já se encontrem carregadas ou nenhum VE se encontre ligado ao sistema, toda a energia extraída do painel fotovoltaico será injetada na rede elétrica. Finalmente, as baterias serão capazes de devolver parte da sua energia armazenada à rede elétrica.

Palavras-chave: Conversores de Potência, Energias Renováveis, Carregamento de Baterias, Veículos Elétricos.

Development of Power Converters for Electric Vehicle Charging with Photovoltaics Interface
Júlio André Machado Fernandes - University of Minho

xi

Development of Power Converters for Electric Vehicle Charging with Photovoltaics Interface
Júlio André Machado Fernandes - University of Minho

xiv

Index

Development of Power Converters for Electric Vehicle Charging with Photovoltaics Interface
Júlio André Machado Fernandes - University of Minho

xv

Development of Power Converters for Electric Vehicle Charging with Photovoltaics Interface
Júlio André Machado Fernandes - University of Minho

xvii

Figure Index

xx

Development of Power Converters for Electric Vehicle Charging with Photovoltaics Interface
Júlio André Machado Fernandes - University of Minho

Development of Power Converters for Electric Vehicle Charging with Photovoltaics Interface
Júlio André Machado Fernandes - University of Minho

xxi

xxii

Development of Power Converters for Electric Vehicle Charging with Photovoltaics Interface
Júlio André Machado Fernandes - University of Minho

Development of Power Converters for Electric Vehicle Charging with Photovoltaics Interface
Júlio André Machado Fernandes - University of Minho

xxiii

xxiv

Development of Power Converters for Electric Vehicle Charging with Photovoltaics Interface
Júlio André Machado Fernandes - University of Minho

Table Index

Appendix Index

List of Acronyms

AC	Alternating Current
ADC	Analog to Digital Converter
BCS	Battery Charging System
BEV	Battery Electric Vehicle
DAC	Digital to Analog Converter
DC	Direct Current
DSC	Digital Signal Controller
EODV	End of Discharge Voltage
ESR	Equivalent Series Resistance
ESS	Energy Storage System
EV	Electric Vehicle
HEV	Hybrid Electric Vehicle
G2V	Grid-To-Vehicle
IC	Incremental Conductance
ICE	Internal Combustion Engine
IDE	Integrated Development Environment
IEC	International Electrothecnical Comunity
IGBT	Insulated Gate Bipolar Transistor
MOSFET	Metal Oxide Semiconductor Field Effect Transistor
MPP	Maximum Power Point
MPPT	Maximum Power Point Tracker
MPV	Mid-point Voltage
NREAP	National Renewable Energy Action Plan
PCB	Printed Circuit Board
PFC	Power Factor Correction
PHEV	Plug-in Hybrid Electric Vehicle
PI	Proportional Integral
PLL	Phase Locked Loop
PV	Photovoltaic
PWM	Pulse Width Modulation
P&O	Perturb & Observe
RMS	Root Mean Square
SoC	State of Charge

Development of Power Converters for Electric Vehicle Charging with Photovoltaics Interface
Júlio André Machado Fernandes - University of Minho

xxix

SoD	State of Discharge
SoH	State of Health
SPI	Serial Peripheral Interface
SPWM	Sinusoidal Pulse Width Modulation
THD	Total Harmonic Distortion
UPS	Uninterruptable Power Supply
VSI	Voltage Source Inverter
V2G	Vehicle-To-Grid
V2H	Vehicle-To-Home

CHAPTER 1

Introduction

1.1. The Energy Paradigm in the Transport Sector

The consumption of energy, globally, has been increasing over the past decades, as corroborated by Figure 1.1. The information retrieved from the analysis of the figure allows us to conclude that, despite an increase in the consumption of energy provided by renewable sources, the vast majority of the consumed energy comes from non-renewable sources, like oil and coal.

Effectively, a new energy paradigm is growing recently, which will theoretically lead to the scarceness of primary energy sources and their imminent depletion. In Europe, there has been a noticeable decline in primary energy production as raw materials existing on European soil are being depleted or their exploration ceases to be economically viable.
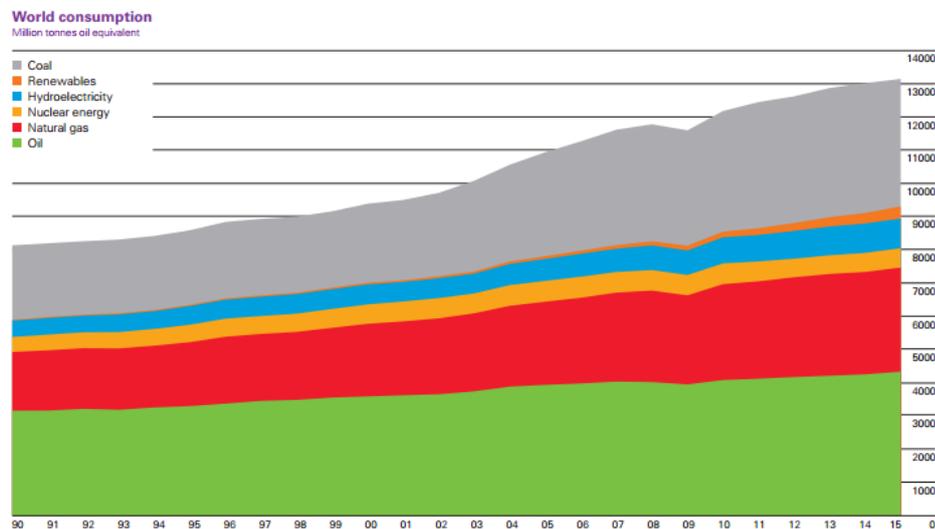
Figure 1.1 - Evolution of the yearly global energy consumption, in million tons of oil equivalent [1].

The effects of the increase of the energetic dependency, as energy importations are, by far, superior to the existing production, ultimately translate into the price escalation of the oil barrel. Account must be taken of the fact that the energy consumption in each country largely depends, among others, on the availability of natural resources for the production of primary energy. Considering that Portugal is not a rich country in terms of endogenous energy resources like oil but is still highly

Development of Power Converters for Electric Vehicle Charging with Photovoltaics Interface
Júlio André Machado Fernandes - University of Minho

1

dependent on them, it is safe to say that the significant increase in the energy price leads to disastrous consequences for the national economy.

Nevertheless, Portugal has shown a big expansion in the production of energy through renewable sources. Not only that, the total consumption of energy has been decreasing over the past few years, as shown in Figure 1.2. This is largely due to the recent economic crisis, which forced the population to adopt a new attitude towards the energy consumption.
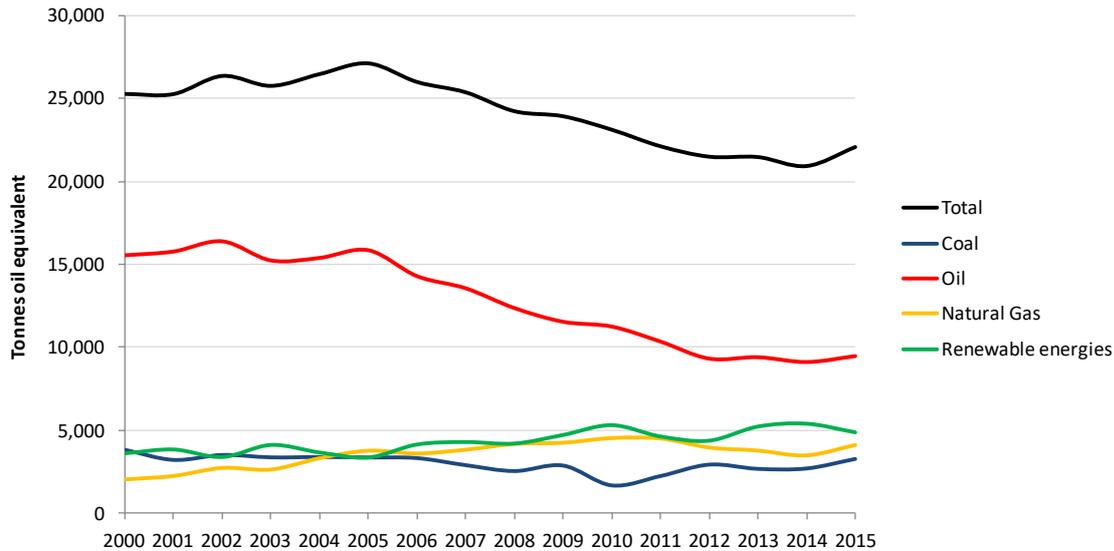
Figure 1.2 - Yearly primary energy consumption in Portugal by energy source [2].

Naturally, the transport sector is one that is still ruled by fossil fuels. Taking into account the consequences that the import of these resources can have economically, the fact is that the burning of fossil fuels is also one of the major causes for the increase in the concentration of greenhouse gases in the atmosphere. As such, it is of the upmost importance to find new solutions that can help us mitigate our external dependencies on oil based resources and, at the same time, reduce the emissions of pollutant gases into the atmosphere.

In the context of an efficient transport sector, the Electric Vehicle (EV) presents itself as a promising solution for the problems above mentioned. The development of these vehicles has been subject to new technological breakthroughs and, nowadays, numerous models of EVs can be found in the market, such as the Nissan Leaf and the Toyota Prius.

The proliferation of EVs can result in a promising change to the current paradigm in the transport sector mainly because the advantages that it presents from an environmental point of view.

1.2. Solar Photovoltaic Energy

The quest to harvest the solar energy that hits Earth for our own personal use is not properly recent. In fact, this quest began over 100 years ago when, in 1839, Edmond Becquerel discovered the photovoltaic effect. The technological challenge behind producing electricity from solar radiation is quite complex, so complex that to this day new technologies are still being discovered and "old" technologies are still being improved [3].

Curiously, the amount of solar radiation that Earth receives is more than enough to meet the World's consumption needs. Portugal has come a long way and now is one the countries with more electricity production though renewable energy sources. Currently, 53.2% of the electric energy produced comes from renewable sources [4]. Potentially, photovoltaic energy could have critical impact on the production of electricity in Portugal because it is one of the World's countries which receive the most sunlight, as shown in Figure 1.3. In average, Portugal has 2000-3000 hours of sunlight yearly for photovoltaic production [5].
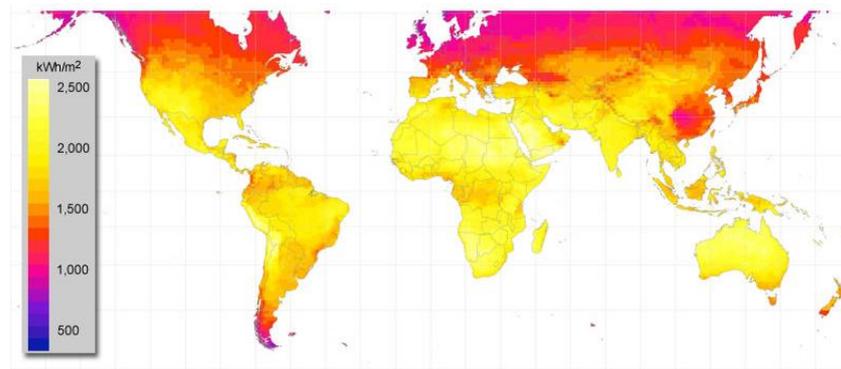
Figure 1.3 - Yearly indexes of solar irradiance in the World [6].

Photovoltaic energy, however, has little impact on the total production of electricity when compared with other renewable energy sources (e.g. wind, water). The reason behind this is the fact that it is a very costly technology. A bet must be made in order to develop technology instead of buying it. Only then will photovoltaic energy make its mark. Nevertheless, it is today the technology which sees more growth.

According to [7], in August of 2014, the production of photovoltaic energy grew 54.1% when compared with the previous year. This is largely due to the National Renewable Energy Action Plan (NREAP), in which certain goals were established, in terms of photovoltaic capacity, for each European country member. Table 1.1 presents for most European markets, the cumulative photovoltaic power installed by the end of 2014 as well as the required goals for 2020 [8] [9]:

Table 1.1 - Installed photovoltaic capacity in Europe under the NREAP.

Country	Installed Power [MW]	Proposed Power by NREAP [MW]	Target Reached
Portugal	414	720	No
Austria	767	322	Yes
Belgium	3104	1340	Yes
Bulgaria	1022	303	Yes
Croatia	33	52	No
Czech Republic	2134	1695	Yes
Denmark	608	6	Yes
France	5632	4860	Yes
Germany	38235	51753	No
Greece	2596	2200	Yes
Italy	18313	63	Yes
Malta	23	8000	No
Netherlands	1042	722	Yes
Poland	34	2	Yes
Romania	1223	260	Yes
Slovakia	524	300	Yes
Spain	5388	8367	No
United Kingdom	5230	2680	Yes

The analysis of allows to conclude that are many cases in which the installed power in 2014 was far higher than the original proposed. Other countries, such as Croatia, are on the brink of achieving the required installed capacity. However, we are still a long way from the goals stipulated for 2020 in which Portugal compromised to install 720 MW of solar capacity. As of now, to meet those requirements, 60 MW will need to be installed yearly until the deadline is reached.

1.3. Motivations

This work aims to contribute to the electric mobility landscape thereby trying to reduce the emissions of pollutant gases into the atmosphere and also provide an alternative to the over exploration of Earth's energy resources. Also, this work intends to contribute to the use of renewable energies to charge the batteries of the vehicles, as

4

Development of Power Converters for Electric Vehicle Charging with Photovoltaics Interface
Júlio André Machado Fernandes - University of Minho

currently few products on the market allow for a direct charging from renewable sources.

On a personal level, the main motivation was the possibility of developing a bidirectional power converter which allows for a controlled charge and discharge of the batteries. Aside from that, the fact that the development of the proposed system will involve all areas of Electronics, from Power Electronics to microcontroller programming, it will allow to consolidate all the knowledge that was acquired during the academic process.

1.4. Goals

This dissertation aims to continue a line of research initiated by the Group of Power Electronics and Energy (GEPE) from the University of Minho, in the areas of investigation regarding renewable energies and electric mobility.

As such, the main objective of this dissertation is the development and implementation of an integrated bi-directional converter (DC-DC and DC-AC) in order to connect an array of photovoltaic panels to the battery pack of an EV and to the power grid. In conventional systems, the electrical energy produced by the photovoltaic panels is injected into the grid and the batteries are charged from the grid. The aim is to develop a more efficient charging method which consists in charging the batteries directly from the PV panels. In this way we will avoid the losses associated with the conversion of energy. The converter will allow the following operation modes:

- Charging the batteries of the EV directly from the PV panel, that is, with minimum energy conversions, ensuring that the surplus energy is injected into the power grid;
- If the solar energy absorbed by the PV Panels is insufficient to charge the batteries, the rest of the power will be drawn from the grid;
- If the batteries of the EV are already charged or no EV is connected to the system, the energy extracted from the PV panel will be injected into the power grid;
- Deliver part of the energy stored in the batteries to the power grid.

1.5. Workplan

Conventionally, the batteries of the EV are charged from the power grid. This involves the conversion of AC signals to DC. To inject the energy from a PV to the power grid it is necessary to raise the output voltage to a value greater than the power grid's peak voltage (325 V) via a DC-DC converter, and then, use a DC-AC converter. The successive energy conversions have inherent losses due to the semiconductors (i.e. switching and conduction losses), thus decreasing the overall efficiency of the process. In order to mitigate these losses, it is intended, when possible, to make the battery charging directly from the PV, ensuring that the surplus is injected into the power grid and ensuring the possibility of loading from the grid in the absence of enough solar energy. The completion of this work entailed the following tasks:

- Research on the state of the art of bidirectional DC-DC converter topologies and their control algorithms;
- Research on the state of the art of bidirectional AC-DC converter topologies and their control algorithms;
- Research on the state of the art of MPPT algorithms;
- Study on the methods of battery charging;
- PSIM simulation of several power converters and choice of the converter topology to adopt for the system;
- PSIM simulation of all components of the system under various operating conditions;
- Development of a power converter prototype;
- Developed converter test and results validation.

1.6. Structure of the Dissertation

This dissertation is divided into 7 chapters. In the present chapter, the general outlook of the worldwide energy consumption is approached. Also the motivations and goals of this project are exposed.

In Chapter 2, an analysis of the state of the art of the electric mobility is presented. As such, the structures of the battery charging systems for EV's are presented in detail, as well as the contextualization with the Smart Grids. Also in Chapter 2, a review of the state of the art of photovoltaic energy is made. In this chapter, the different types of existing technologies can be found in addition with the most known algorithms for

6

Development of Power Converters for Electric Vehicle Charging with Photovoltaics Interface
Júlio André Machado Fernandes - University of Minho

Maximum Power Point Tracking, combined with the power converters utilized for those ends.

In Chapter 3, an in-depth look is taken into the most important topologies of bidirectional AC-DC and DC-DC converters within the scope of this project. Furthermore, a review of some current control techniques for AC-DC converters is also presented, as well some switching techniques for power semiconductors.

In Chapter 4, the design and development of the overall proposed converter system is approached. The chosen topologies for each converter and respective control strategies are presented and justified. Still in this chapter, the simulations that were made to the system in order to validate all of the different converters and control algorithms can be found.

In Chapter 5, the overall stages of implementation of the converter are exposed in detail. In here, the various components used for both the power stage and control system are presented.

In Chapter 6, relative to the Experimental Results of the Power Converter, are presented the obtained results when testing the system with different conditions of operation. Also in this chapter, the obtained results when delivering part of the stored energy of the batteries to the electrical power grid are presented.

Finally, in Chapter 7, the conclusions that were made of the finished project are presented, along with the proposals for future work that will improve the developed system.

Development of Power Converters for Electric Vehicle Charging with Photovoltaics Interface
Júlio André Machado Fernandes - University of Minho

7

Development of Power Converters for Electric Vehicle Charging with Photovoltaics Interface
Júlio André Machado Fernandes - University of Minho

6

CHAPTER 2

Electric Vehicle Charging Systems and Photovoltaics

2.1. Introduction

The first prototypes of electric vehicles date back to the beginning of the 20th century. XIX. Even though, at that time, vehicles with internal combustion engines already existed, the greater reliability, the absence of fumes, vibrations, noise and cold start were the main reasons for those EVs were the most sought after.

The invention of the electric starter motor in 1912, however, allowed eliminating one of the major disadvantages of cars with combustion engines, to start. All this, combined with the reduction in the price of gasoline and the cost of production, loosened the interest in electric cars. The current environmental crisis, as well as the need for alternatives to the use of fossil fuels, reawakened the interest in the development of electric vehicles.

An EV can be defined as any road vehicle which uses, partially or totally, electricity as a source of energy. Within the currently available topologies of EVs, the hybrid (HEV), plug-in hybrid (PHEV) and battery (BEV) topologies are the ones that stand out the most. A hybrid EV uses both an electric motor and an ICE and its batteries are charged by the combustion engine or by regenerative braking. PHEVs are similar to conventional hybrids in that they have both an electric motor and internal combustion engine, except PHEV batteries can be charged by plugging into an outlet, while also offering the possibility to operate only with the electric motor, sacrificing autonomy. Finally, BEVs run exclusively on electricity via on-board batteries that are charged by plugging into an outlet or charging station. These vehicles have no combustion engine, offer longer electric driving ranges compared to PHEVs, and do not produce tailpipe emissions (though there are emissions associated with charging these vehicles).

Nowadays, these topologies can be found throughout large manufacturers' catalogs (e.g. BMW, Toyota), being that these vehicles can have performances very similar to their combustion engine counterparts [10]-[12].

The advantages of using an electric vehicle are that it is not pollutant and the cost of electricity is quite low. In addition, the electric motor is quiet thus having no

Development of Power Converters for Electric Vehicle Charging with Photovoltaics Interface
Júlio André Machado Fernandes - University of Minho

7

contribution to sound pollution. However, as it was stated earlier, its two biggest disadvantages are the high purchase cost and the limited autonomy. In the long term, as technology continues to evolve, it will be possible to circumvent these obstacles in order to finally bring balance to the energy consumption on the transport sector.

As mentioned in the previous chapter, photovoltaic energy could potentially become one of Portugal's main sources for production of electrical energy, despite the low impact that it currently has in comparison to other renewable sources. Even so, the increase in the efficiency of the panels, together with the reduction of the manufacturing cost, constitutes a good bet for energy production in the near future, in terms of profitability.

2.2. Batteries

A battery can be defined as an energy storing device that uses electrochemical reactions in order to store the energy that is given to it. Ideally, a battery can store the energy indefinitely and return it when needed.

Batteries can be classified as primary or secondary, depending on the purpose for which they are intended. A primary battery is built with the purpose of providing electrical energy only once. On the other hand, a battery is considered secondary if it can be recharged a finite amount of times. From an environmental standpoint, the latter is preferable to the former because it can be reutilized.

In terms of battery distinction, this is made taking into account its chemical composition and also the purpose for which they are assumed. For instance, a lead-acid battery, which will be approached in greater detail still in this chapter, can be used to start an engine by providing a high current for a short period of time. However, other lead-acid batteries can be used to supply UPSs, this time providing a constant current during a relatively long period of time [13].

Characteristics of Batteries

As mentioned above, a battery is an electro-chemical device capable of supplying the energy that results from an internal chemical reaction to an external electric circuit. A battery is composed of one or more cells, either parallel or series connected to obtain a required current/voltage capability. The most important electrical characteristics associated with batteries are:

- Equivalent Series Resistance (ESR) is the internal resistance present in any cell that limits the peak current that it can deliver;

8

Development of Power Converters for Electric Vehicle Charging with Photovoltaics Interface
Júlio André Machado Fernandes - University of Minho

- Amp-hour (Ah) capacity is defined as the amount of current that a battery can deliver for 1 hour before the battery voltage reaches the end-of-life point;
- C rate is a current that is numerically equal to the Ah rating of the cell. Charge and discharge currents are typically expressed in fractions or multiples of C;
- MPV (Mid-Point Voltage) is the nominal voltage of the cell, and is the voltage that is measured when the battery has discharged 50% of its total energy;
- End of Discharge Voltage (EODV) is the measured cell voltage at the end of its operating life;
- State of Charge (SoC) is the measured percentage of charge left in the battery;
- Depth of Discharge (DoD) is the inverse of SoC. It indicates the percentage of discharge of the battery;
- State of Health (SoH) is a measurement of the overall condition of the battery, considering their lifespan.

The measured terminal voltage of any battery will vary as it is charged and discharged. Figure 2.1 presents the battery charge/discharge curve [14].
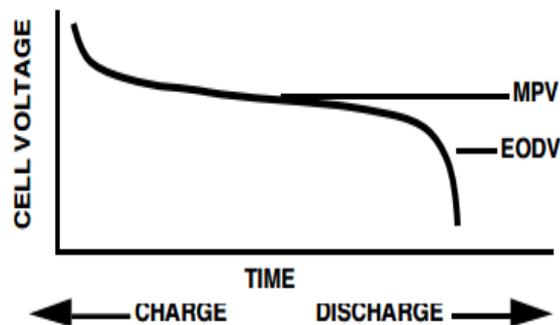
Figure 2.1 - Example of a battery's charge/discharge curve [14].

The energy density of a battery is generally expressed in two ways:

- Gravimetric energy density is a measure of how much energy a battery contains in comparison to its weight, typically expressed in Wh/kg;
- Volumetric energy density is a measure of how much energy a battery contains in comparison to its volume, typically expressed in Wh/l.

The maximum current that a battery can deliver is, as mentioned above, directly dependent on its ESR. The current flowing out of the battery must pass through the ESR, which will reduce the battery terminal voltage by an amount equal to the ESR multiplied by the load current. More importantly, the current flowing through the ESR will cause power dissipation within the battery. This can result in significant heating within the battery at high rates of discharge.

Development of Power Converters for Electric Vehicle Charging with Photovoltaics Interface
Júlio André Machado Fernandes - University of Minho

9

Self-discharge (which occurs in all batteries) determines the "shelf life" of a battery. It is highly dependent on temperature, directly proportional to the battery temperature. Another important aspect is that the discharge rate is non-linear meaning a battery which loses 30% in a month may lose 15 to 20% in the first few days [14]. Considering the electrical characteristics of a battery, the Ah capacity and the voltage present at the battery's terminals are by far the most relevant. However, the battery's temperature when charging, discharging and even when they are not being used, still needs to be taken into account, because it directly affects the battery's efficiency and SoH.

2.3. Types of Batteries used in Electric Vehicles

In EVs, the main types of batteries used are lead-acid batteries, nickel-cadmium batteries, lithium-ion batteries, lithium polymer batteries and Nickel metal hydride batteries. As such, the main features of each type of battery are presented below.

2.3.1. Lead Acid Battery

Invented by the French physician Gaston Planté in 1859, the lead acid battery was the first rechargeable battery for commercial use. Despite its advanced age, the lead acid chemistry continues to be in wide use today, and there are good reasons for its popularity. The lead acid battery is dependable and inexpensive on a cost-per-Watt base. As such, these batteries are the main choice in high power applications where the cost and robustness are of primordial importance. There are few other batteries that can deliver bulk power as cheaply as lead acid, and this makes the battery widely used to start traditional ICE vehicles, in small electric vehicles (e.g. golf cars, electric wheelchairs) and also in UPSs.

Lead acid batteries are heavy and less durable than nickel and lithium based technologies when deep-cycled. A full discharge causes strain and each discharge/charge cycle permanently robs the battery of a small amount of capacity. This loss is small while the battery is in good operating condition, but the fading increases once the performance drops to half the nominal capacity. This wear-down characteristic applies to all batteries in various degrees. Depending on the depth of discharge, lead acid for deep-cycle applications provides 200 to 300 discharge/charge cycles.

A lead acid battery can be characterized as a starter or as a deep-cycle battery. The starter battery, which is the most common type, is designed to provide a momentary

10

Development of Power Converters for Electric Vehicle Charging with Photovoltaics Interface
Júlio André Machado Fernandes - University of Minho

high power burst whereas the deep-cycle battery is built to provide continuous power for a longer period of time, allowing for a deeper discharge. From the outside, both batteries look alike, however, there are fundamental differences in design [15].

An example of a battery that uses lead acid technology and allows deep-cycling is the AGM-Type from NPower and is presented in Figure 2.2.

Figure 2.2 - AGM-Type deep-cycle lead acid battery [16].

This battery has as nominal voltage of 12 V, is able to provide 0.9 A continuously for 20 hours and, according to the manufacturer's datasheet, it can be charged with voltages ranging from 14.1 V to 14.7 V and can be cycled over 300 times [17].

Lead acid batteries should be charged in three stages, which are the constant current charge, the topping charge and, finally, the float charge. During the first stage, constant current is applied to the battery until the voltage reaches a value roughy 10% higher than the nominal voltage. In the second stage, the nominal voltage is imposed until the current diminishes to a value close to zero. Finally, the float charge will compensate for the effects of the battery's self-discharge. Figure 2.3 illustrates the different charging stages of a lead acid battery [18].
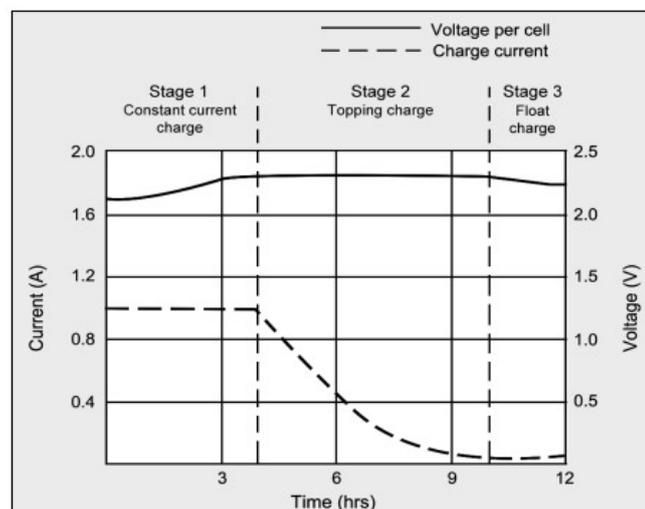
Figure 2.3 - Charging stages of a lead acid battery [18].

Development of Power Converters for Electric Vehicle Charging with Photovoltaics Interface
Júlio André Machado Fernandes - University of Minho

11

2.3.2. Nickel Cadmium Battery (NiCd)

The nickel cadmium battery is the longest running battery on the market. As such, it is an already developed and mature technology, despite not possessing a high energy density. The materials used in the construction of this type of battery are physically robust and, as such, give the battery a longer shelf life than, for example, lead-acid batteries in which the lead is actually corroded by the chemical reactions that occur in the battery. The use of nickel cadmium batteries is frequent when a long shelf life and high discharging currents are desired. It should be noted that these batteries contain toxic components and, consequently, need to be properly recycled [19].

It also should be noted that this type of battery originated the term "memory effect", which consists in the battery being able to "remember" of the amount of energy that was previously discharged. This term is still referred today to indicate the loss of capacity in nickel based batteries. As such, it is recommended to perform a full discharge to these batteries.

Regarding their charging process, NiCd batteries allow for higher charging currents than the lead acid technology previously presented. In fact, the overall efficiency of the charging process is higher for higher charge rates. The charge characteristic of a NiCd battery is depicted in Figure 2.4 [20].
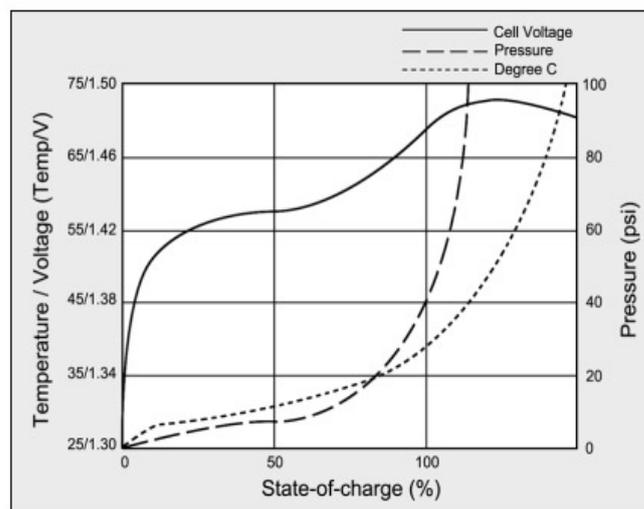
Figure 2.4 - Charging characteristics of a Nickel Cadmium battery [20].

It can be seen that, by the time the battery is charged to about 70%, the charge efficiency drops abruptly. The cells begin to generate gases, the pressure rises and the temperature increases rapidly. To reduce battery stress, some chargers lower the charge rate past the 70% mark.

12

Development of Power Converters for Electric Vehicle Charging with Photovoltaics Interface
Júlio André Machado Fernandes - University of Minho

This type of battery was used in the electric versions of the Citroën Saxo and the 1976 Alfa Romeo. An example of a battery pack comprised of NiCd batteries is presented in Figure 2.5 [21].
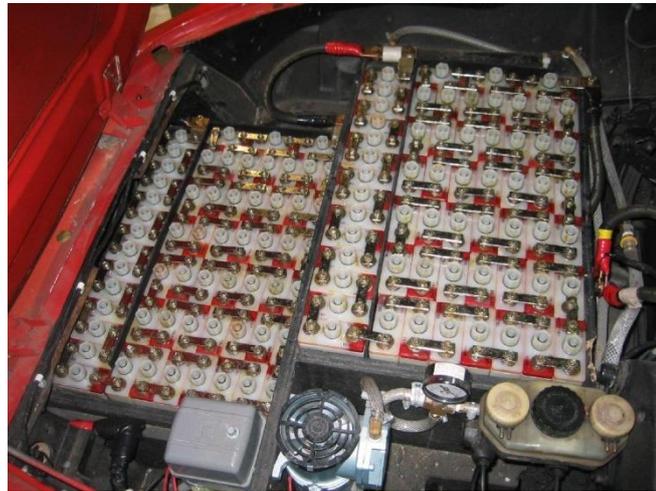
Figure 2.5 - Example of a Nickel Cadmium battery pack [22].

2.3.3. Lithium-Ion Batteries (Li-Ion)

The lithium ion batteries are rechargeable batteries, whose first prototype was developed in 1985 by the Japanese company Asahi Chemical. The first commercial battery was produced in 1991 by the Japanese company Sony. Lithium is the lightest of all metals, has the greatest electrochemical potential and provides the largest specific energy per kg. Rechargeable batteries with lithium metal on the anode could provide extraordinarily high energy densities. Furthermore, these batteries are not affected by the "memory effect" and, consequently, do not require a complete discharge before being recharged. However, this technology inspires some safety concerns. It was discovered that, on rare occasions, microscopic metal particles could come into contact with other parts of the battery cell, leading to a short circuit within the cell. In extreme cases, this could lead to the battery actually exploding which could potentially harm the user [23].

Nevertheless, this is by far the most used type of battery for consumer electronics applications and in recent years has also been widely used in EVs, due to its good relationship between energy density and density power rating. Li-ion is a low maintenance battery, an advantage that most other chemistries cannot claim, with its self-discharge being less than half when compared to nickel based technologies [24].

The use of these batteries in EV has several advantages. They can be constructed in different sizes and shapes, allowing the format of the pack to be adapted to fit areas such as the bottom of the seats or the car's central console. They are also relatively light

Development of Power Converters for Electric Vehicle Charging with Photovoltaics Interface
Júlio André Machado Fernandes - University of Minho

13

when compared with other battery technologies with the same amount of capacity. However, the shelf life of the cell, its internal resistance and the aforementioned safety issues, when they are not used correctly, are the disadvantages of this technology. Additionally, this technology tends to be more expensive than the ones previously presented. This type of battery is used in electric vehicles such as the Nissan Leaf and the BMW i3 [25].

In Figure 2.6 it is presented the lithium ion battery pack that is currently used in the BMW i3.

Figure 2.6 - Lithium ion battery pack used in the BMW i3 [26].

The charging process of a Li-Ion battery is similar to the lead acid as they both use the constant current and constant voltage charging stages. However, Li-Ion batteries require much more specific cares when being charged. While lead acid offers some flexibility in terms of voltage cut off, manufacturers of Li-ion cells are very strict on the correct setting because Li-ion has a very low tolerance to overcharge. The charge characteristic of a Li-Ion battery is presented in Figure 2.7. The charging rate for these batteries tends to be between 1 C and 2 C [27].

14

Development of Power Converters for Electric Vehicle Charging with Photovoltaics Interface
Júlio André Machado Fernandes - University of Minho
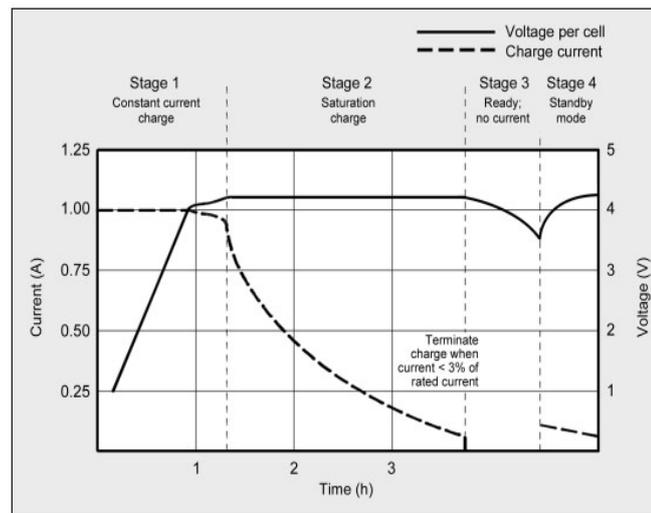
Figure 2.7 - Charging stages of a lithium-ion battery [27].

2.3.4. Lithium Polymer Batteries

The lithium polymer batteries are a cheaper version of the lithium ion battery, with a similar chemistry in terms of energy density. Due to its characteristics, these batteries may be molded into the desired shape. This allows a better use of available space, and unlike lithium ion cells that are cylindrical, these batteries are more compact because there is no wasted space within each module. Charge and discharge characteristics of Li-polymer are identical to other Li-ion systems and do not require a special charger. Safety issues are also similar in that protection circuits are needed. Gas buildup during charge can cause some prismatic and pouch cells to swell and equipment manufacturers must make allowances for expansion. An example of an EV that uses this battery technology is the Mercedes-Benz SLS AMG [25].

2.3.5. Nickel Metal Hydride Battery (NiMh)

The NiMh battery is a recent Nickel based technology that was developed with the goal of replacing the existing NiCd and also to compete with the Li-Ion technology. From a chemical point of view, the NiMh battery possesses a very similar composition to that of a NiCd battery. However, the metal hydride electrode has a higher energy density than the cadmium electrode which results in the NiMh battery having a greater storage capacity than the conventional NiCd battery. Because these batteries are based on nickel technology, they are also affected by the "memory effect" although this effect is not as pronounced as in NiCd batteries.

In terms of their shelf life, NiMh batteries last less than their NiCd counterparts in contrast offering deeper discharges. Regarding the charging process, it is identical to

Development of Power Converters for Electric Vehicle Charging with Photovoltaics Interface
Júlio André Machado Fernandes - University of Minho

15

both NiMh and NiCd batteries and, in many cases, they can even share the same charger [13].

The NiMh technology can be found in Toyota's hybrid vehicles, as shown in Figure 2.8 [24].

Figure 2.8 - Nickel metal hydride battery pack used in the Toyota Prius [28].

2.4. Comparison between Battery Technologies

The battery technology to be installed in EVs varies from case to case. When the goal is to adapt existing internal combustion vehicles, the vehicle's autonomy is not the most important factor. As such, usually one resorts to the use of lead-acid deep cycle batteries. For the same capacity these batteries are cheaper and can be installed in locations previously occupied by the previous motor, fuel tank or trunk.

Nickel-Cadmium batteries have lost importance over the years, as today these batteries are not standard in any electric vehicle. A major drawback of these batteries is the need to undertake a complete discharge, due to the "memory effect".

Lithium ion batteries are preferred by car manufacturers for pure electric and plug-in hybrid vehicles because the packs can be built with the format of the space they are meant to occupy. Additionally, lithium based batteries are not affected by the "memory effect" nor do they need exercising (a deliberate full discharge) in order to keep them in good operation conditions. The drawbacks are the need for protection circuits to prevent abuse, as well as being more expensive.

In Table 2.1, a comparison between the types of batteries previously mentioned is made [19].

16

Development of Power Converters for Electric Vehicle Charging with Photovoltaics Interface
Júlio André Machado Fernandes - University of Minho

Table 2.1 - Comparison between different battery technologies.

	Lead Acid	*Nickel Cadmium*	*Lithium Ion*	*Lithium Ion Polymer*	*Nickel Metal Hydride*
Energy Density [Wh/kg]	30-50	45-80	110-160	100-130	60-120
ESR [mΩ]	<100 (12 V pack)	100-200 (6 V pack)	150-250 (7.2 V pack)	200-300 (7.2 V pack)	200-300 (6 V pack)
Life Cycle (80% of initial capacity)	200-300	500-1000	500-1000	300-500	500-1000
Charging Time [h]	8-16	1	2-4	2-4	2-4
Overcharge Tolerance	High	Moderate	Very Low	Low	Low
Monthly Self-discharge	5%	20%	10%	10%	30%
Cell Voltage [V]	2	1.25	3.6	3.6	1.25

2.5. Battery Charging Modes

As stated earlier, the total distance that an EV can travel before needing to be recharged is a big issue. When compared to an ICE vehicle, the EV requires more recharges and the time it takes for the batteries to be completely recharged is much greater.

The International Electro technical Commission (IEC) established four charging modes. These are defined in the norm IEC 61851-1:2010 "Electric Vehicle Conductive Charging System".

In Mode 1, the EV is directly connected to the power grid using a household socket with a standard current of 10 A. It is necessary for the charger to have a protective earth system and protections against overloads and earth leaks. This charging mode has the potential to be dangerous when used in older installations and, as such, has seen its use decline recently.

In Mode 2, the vehicle is connected to the main power grid via household socket-outlets, single-phase or three-phase, with a protective earth. A protection device is built into the cable, which communicates with the EV.

Development of Power Converters for Electric Vehicle Charging with Photovoltaics Interface
Júlio André Machado Fernandes - University of Minho

17

In Mode 3, the vehicle is connected directly to the power grid via specific socket and plug and a dedicated circuit. A control and protection function is also installed permanently. This is the only charging mode that meets the applicable standards regulating electrical installations. It also allows load-shedding so that the user can choose if he wants to prioritize other household electrical or, on the contrary, optimize the EV's charging time.

In Mode 4, the electric vehicle is connected to the power grid through an external charger. Control and protection functions and the vehicle charging cable are installed permanently in the installation. This mode is especially advantageous on a long trip, where the distance is greater than the vehicle's range, as it allows charging the vehicle in 20 minutes.

For normal charges (3 kW), car manufacturers have built a battery charger into the car. Connection to the electrical grid is achieved through a charging cable. For quicker charges (22 kW, even 43 kW and more), manufacturers have chosen either to use the vehicle's built-in charger or an external charger. In Table 2.2 the various charging modes are presented, in which attributes like the charging time, current and voltage can be seen [29].

Table 2.2 - Comparison between the charging modes of an EV.

Charging time [h]	Power supply	Voltage [V]	Maximum current [A]
6-8	Single-phase (3.3 kW)	230	16
2-3	Three-phase (10 kW)	400	16
3-4	Single-phase (7 kW)	230	32
0.3-0.5	Three-phase (43 kW)	400	63
0.3-0.5	DC (50 kW)	400-500	100-125
1-2	Three-phase (24 kW)	400	32

2.6. Battery Charging Systems

Battery Charging Systems are electronic devices that perform the charging of one or more batteries simultaneously, in accordance with each battery requirements.

18

Development of Power Converters for Electric Vehicle Charging with Photovoltaics Interface
Júlio André Machado Fernandes - University of Minho

The failure to respect this regard can result in the damage of the battery or the reduction of its useful life.

When a vehicle is plugged into the power grid, theoretically it is possible to have a bidirectional flow of energy. This interactivity between the EVs and PHEVs with the power grid is expected to be one of the key technologies in the future of the Smart Grids concept. In this context, the charging or discharging process of the EV's batteries can be done in two different ways: coordinated or uncoordinated. The coordinated concept consists on the charging or discharging of the batteries according to the capabilities of the electrical grid, in real time, and the needs of the vehicle's owner. In this context, different parameters are taken into account, mainly the price of energy and the remaining energy stored in the batteries. On the other hand, in the uncoordinated concept, from the moment when the vehicle is plugged into the electrical grid the charging either starts immediately or after a fixed time delay (controlled by the user). This often can result in problems in the power grid due to the large number of vehicles to be charged, which results in a high power consumption. Nevertheless, nowadays, the batteries charging process is performed without any type of coordination between the vehicles and the power grid.

Some vehicles allow their batteries to be charged via off-board Battery Charging Systems (e.g. public charging stations), but almost every vehicle is equipped with an on-board Battery Charging System. This system is comprised of an AC-DC power converter, controlled to preserve the battery's lifespan by monitoring them during the charging and discharging process [30].

Figure 2.9 presents the different types of AC-DC power converters that can be used in EV Battery Charging Systems [31].
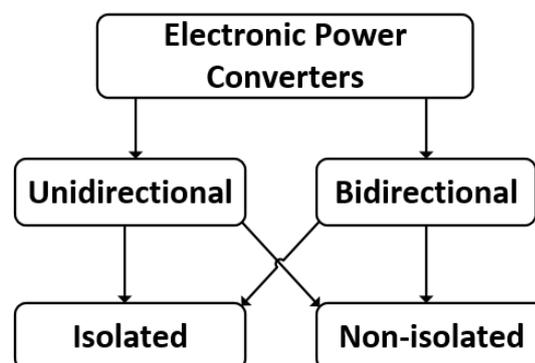
Figure 2.9 - Main categories of AC-DC power converters used in Battery Charging Systems.

The topologies for the Battery Charging Systems are most often formed by an AC-DC converter, followed by a DC-DC converter. The AC-DC converter is used to

Development of Power Converters for Electric Vehicle Charging with Photovoltaics Interface
Júlio André Machado Fernandes - University of Minho

19

rectify the AC voltage from the grid to DC and the DC-DC converter adjusts the rectified voltage to a level suitable for the batteries, also controlling the charging process [31].

Naturally, both converters can have different topologies, allow bidirectional energy flow or even have isolation between them, as shown in Figure 2.9.

Figure 2.10 shows an example of a unidirectional AC-DC converter. It is composed by four power diodes and by the capacitor filter in output, and only allows the charge of the batteries with constant voltage imposed by the maximum value of the input voltage, and without any type of voltage control [32].
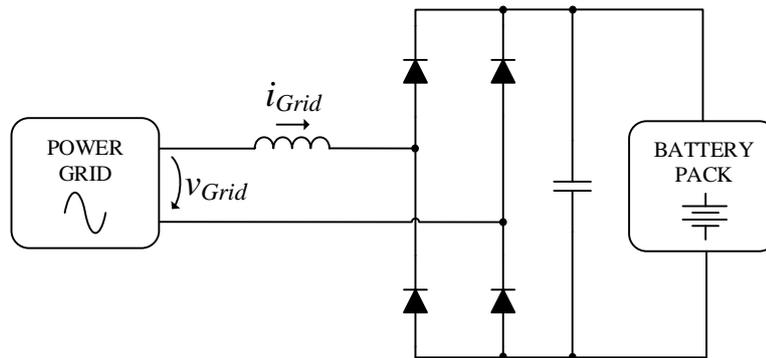
Figure 2.10 - Unidirectional AC-DC converter, without voltage and current control.

This type of converter is easy to implement, more robust and cheap. However, the fact that the output voltage, as well as the consumed current, are not controlled (therefore not sinusoidal), contribute to the degradation of the electric power quality, with high levels of harmonic distortion.

If a DC-DC boost converter is placed between the AC-DC diode converter and the battery bank, as shown in Figure 2.11, it is possible to control the output voltage and current. The boost converter also allows the consumed current to be sinusoidal with unitary power factor [32].
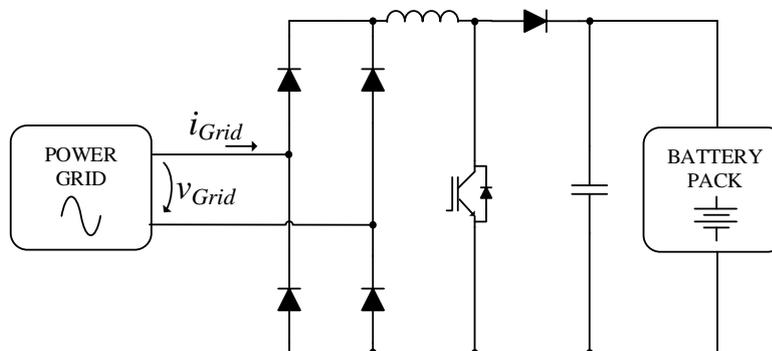
Figure 2.11 - Unidirectional AC-DC converter, with Power Factor Correction.

20

Development of Power Converters for Electric Vehicle Charging with Photovoltaics Interface
Júlio André Machado Fernandes - University of Minho

The major drawback of the circuit presented above, is that it only allows unidirectional energy flow.

In Figure 2.12, it is shown a fully controlled AC-DC converter with sinusoidal current consumption, unitary power factor and output voltage and current control. The main advantage of this topology is that it allows bidirectional energy flow which means that it is possible for the batteries to give back to the power grid some of their stored energy [31][32].
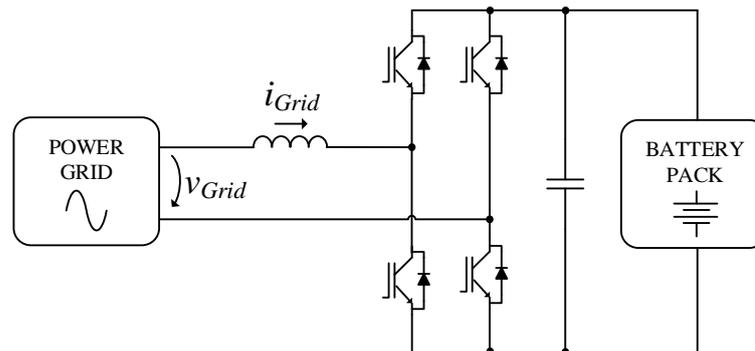
Figure 2.12 - Bidirectional AC-DC converter, with Power Factor Correction.

2.7. EV Interaction with Smart Grids

It is predictable that in the near future, in a real Smart Grid scenario, the power grid should meet the increasing demand of energy in a reliable and efficient way, maintaining the required stability and interfacing renewable energy resources, as a large network of microgrids. Such power grid scenario, with the EVs smart charging systems, will allow the communication of the vehicles with the local utilities to ensure that the batteries are charged when the electricity is cheapest and the impact of the charging systems on the grid is smallest. An example of the integration of EVs, renewable energy sources and Energy Storing Systems is depicted in Figure 2.13 [31].
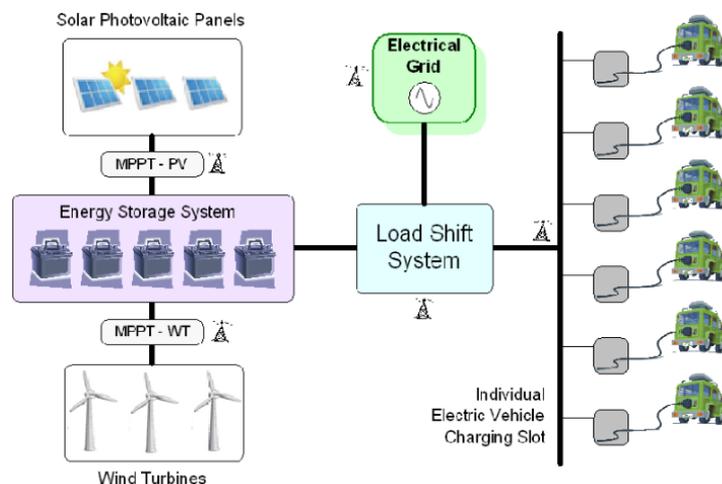
Figure 2.13 - Example of a microgrid [31].

Development of Power Converters for Electric Vehicle Charging with Photovoltaics Interface
Júlio André Machado Fernandes - University of Minho

21

Regarding the interaction between the EV's and the power grid, several concepts can be defined such as Grid-To-Vehicle (G2V), Vehicle-To-Grid (V2G) or even Vehicle-To-Home (V2H) [31].

G2V is the simplest interaction between an EV and the power grid and requires no form of communication between both systems. In this mode of interaction there only is unidirectional energy flow from the power grid to the EV, therefore, it only allows the charging of the batteries. Nowadays, it still is the most common battery charging process and will be the first main approach to the lasting integration of EVs.

In V2G the EV utilizes the stored energy in its batteries and sends it back to the power grid. Applying that premise to the future Smart Grids, the EV can deliver part of the energy stored in its batteries during periods of high demand (peak shaving) or receive energy from the grid during hours of excessive production (valley filling) [31] [33]. Peak shaving and valley filling can give electric utilities new ways to provide regulation services (e.g. keeping voltage and frequency stable) and provide spinning reserves (e.g. meet sudden demands for power) [34].

Besides the aforementioned operation modes, using a bidirectional EV battery charger based in a voltage-source converter, the EV can also be used to operate as a voltage source. The concept of V2H is somewhat identical to V2G. In this mode, the stored energy in the batteries can be used to feed other loads, typical at home. Thereby, V2H can be used to feed home loads during power outages. It can also be used to feed loads in places without connection to the power grid.

Finally, Figure 2.14 illustrates the different interaction modes described above.

G2V – Grid-To-Vehicle
V2G – Vehicle-To-Grid
V2H – Vehicle-To-Home
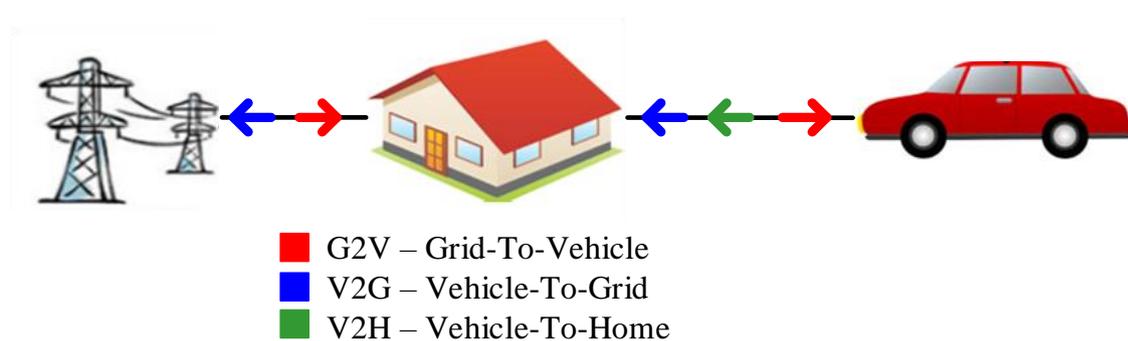
Figure 2.14 - Electric Vehicle with G2V, V2G and V2H operation modes.

2.8. Photovoltaic Panels

A photovoltaic panel is composed of several modules and each module comprising a set of photovoltaic cells, as shown in Figure 2.15. The modules can be connected in either series or parallel, depending if one wishes to increase the output voltage or current, respectively.
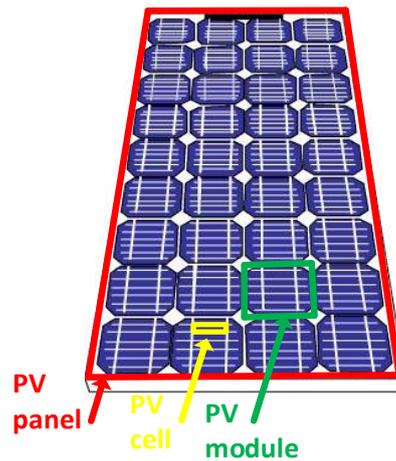
Figure 2.15 - Composition of a PV panel.

A PV module consists of a number of interconnected solar cells (typically 36 connected in series) encapsulated into a single, long-lasting, stable unit. The key purpose of encapsulating a set of electrically connected solar cells is to protect them and their interconnecting wires from the typically harsh environment in which they are used. For example, solar cells, since they are relatively thin, are prone to mechanical damage unless protected. A photovoltaic cell converts light energy from sunlight into DC electrical power. Photons, the light energy carriers in sunlight, collide with the solar panel and are absorbed by these solar cells. Each solar cell is comprised of semi conducting materials, such as silicon, which expend the absorbed electrons down the wire. These solar cells are composed of two different types of semiconductors - a P-type and an N-type - that are joined together to create a P-N junction.

In addition, the metal grid on the top surface of the solar cell and the wires interconnecting the individual solar cells may be corroded by water or water vapor. As such, the two key functions of encapsulation are to prevent mechanical damage to the solar cells and to prevent water or water vapor from corroding the electrical contacts [35].

As mentioned earlier, the process in which a photovoltaic cell converts sunlight into electricity is called the Photovoltaic Effect. In this process, the collection of light-generated carriers by the P-N junction causes a movement of electrons to the N-type side and holes to the P-type side of the junction. This process is illustrated in Figure 2.16 [36].

Development of Power Converters for Electric Vehicle Charging with Photovoltaics Interface
Júlio André Machado Fernandes - University of Minho

23
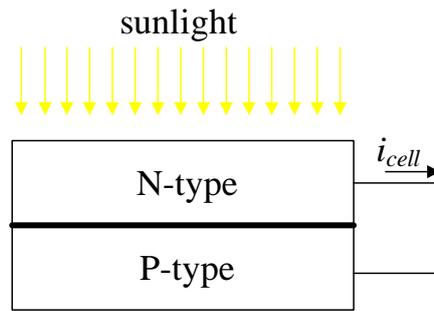
Figure 2.16 - Illustration of the Photovoltaic Effect occurring in a PV cell.

A photovoltaic cell can also be described through its equivalent electrical circuit, which is presented in Figure 2.17. The diode serves as the P-N junction and resistors Rs and Rs represent, respectively, the cell's leakage current and ESR [37].
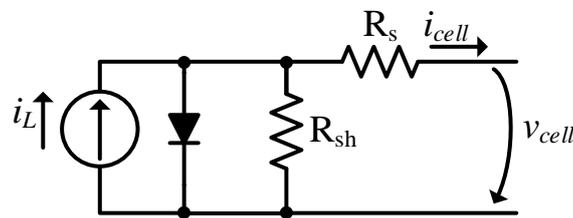
Figure 2.17 - Equivalent circuit of a solar cell.

Expression 2.1 relates the output current of a photovoltaic cell with the radiation intensity and the temperature of the cell [38]:

$$I_{cell} = I_{photo} - I_{sat} \times \left(exp \, \frac{e(V + IR_s)}{mkT_c} \right) - 1 \tag{2.1}$$

Where:

- I_{cell} is the current generated by the cell;
- I_{photo} is the photo-generated current;
- I_{sat} is the saturation current (temperature depending);
- e is the electronic charge;
- V is the voltage imposed across the cell;
- m is the idealizing factor;
- k is the Boltzmann's constant;
- T_c is the cell temperature.

While there are dozens of variations of solar cells, the two most common types are those made of crystalline silicon (both monocrystalline and polycrystalline) and those made with what is called thin film technology. Monocrystalline solar cells (Figure 2.18) are easily recognizable by their coloring. But what makes them most

Development of Power Converters for Electric Vehicle Charging with Photovoltaics Interface
Júlio André Machado Fernandes - University of Minho

24

unique is that they are considered to be made from a very pure type of silicon. In the silicon world, the more pure the alignment of the molecules, the more efficient the material is at converting sunlight into electricity. In fact, monocrystalline solar cells are the most efficient of all, with efficiencies documented at up to 20%.

Figure 2.18 - Monocrystalline solar cell [39].

Beyond being most efficient in their output of electrical power, monocrystalline solar cells are also the most space-efficient. This is logical because fewer cells are needed per unit of electrical output. In this way, solar arrays made up of monocrystalline take up the least amount of space relative to their generation intensity.

The biggest disadvantage with this type of solar cell is its price. One of the reasons monocrystalline cells are so expensive is that the four sided cutting process ends up wasting a lot of silicon, sometimes more than half. As such, from an investment standpoint, polycrystalline and thin film cells are often the preferred choice for consumers.

Polycrystalline solar cells, an example of which is illustrated in Figure 2.19, were the first cells ever introduced. Polycrystalline cells do not go through the cutting process used for monocrystalline cells. Instead, the silicon is melted and poured into a square mold, hence the square shape of polycrystalline. In this way, they're much more affordable since hardly any silicon is wasted during the manufacturing process.
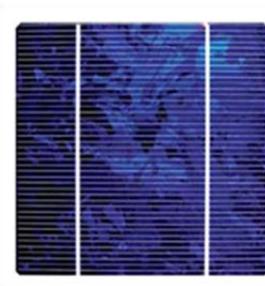
Figure 2.19 - Polycrystalline solar cell [39].

However, polycrystalline cells are less efficient than the monocrystalline ones. This is due to the fact that the material has a lower purity. Due to this reality, polycrystalline is less space-efficient, as well. One other drawback of polycrystalline is

Development of Power Converters for Electric Vehicle Charging with Photovoltaics Interface
Júlio André Machado Fernandes - University of Minho

25

that has a lower heat tolerance than monocrystalline, which means they don't perform as efficiently in high temperatures.

Thin film solar cells are characterized by the manner in which various type of semi-conducting materials (including silicon in some cases) are layered on top of one another to create a series of thin films. The major attraction of thin film technologies is their cost. Because mass production is much easier than crystalline-based modules, the cost associated with it is relatively low. The product itself is also flexible in nature, which is leading to many new applications of solar technologies in scenarios where having some type of flexible material is advantageous. Another advantage is that high heat and shading have less of a negative impact on thin film technologies. For these reasons, the thin film market continues to grow. However, thin film requires more space than other types of solar cells and also has a shorter lifespan [40].

The most used material in thin film is the amorphous silicon, as shown in Figure 2.20.

Figure 2.20 - Amorphous thin film solar cell [39].

2.9.   Maximum Power Point Tracking Algorithms

The amount of electrical energy produced by a photovoltaic cell, as well as its maximum power is dependent on two factors: the intensity of the solar radiation and the cell's own temperature. Firstly, the change of the solar radiation's intensity originates a change in the current produced by the cell. Lastly, the rise of the cell's temperature results in a reduction of the open circuit voltage.

Figure 2.21 depicts the power curve of the cell when there is a change in the intensity of the radiation and when there's a change in the cell's temperature.

(a)   (b)
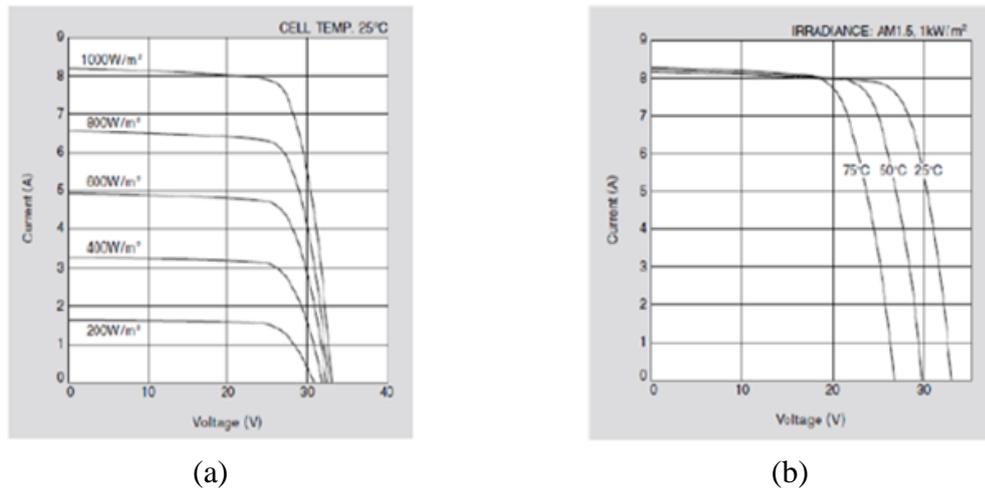
Figure 2.21 - PV panel's power curve with: (a) change in the cell's temperature; (b) change in the solar irradiance [41].

To ensure that the solar panel is always operating in its maximum power point, it is necessary to implement a Maximum Power Point Tracking (MPPT) algorithm. As such, numerous MPPT algorithms were studied in order to find out which one has the potential of producing the best results. A bibliographical review of those algorithms will be presented below.

2.9.1. Open Voltage

The Open Voltage algorithm is based on the fact that the ratio between the maximum output voltage and the open circuit voltage is almost constant. This value is independent of external conditions. This method uses between 71% and 78% of the open circuit voltage as a reference voltage. The operating principle of this method is quite simple. The voltage at the terminals of the panel is measured and compared with the reference voltage. If the voltages are equal, the panel is in the maximum power point. If the measured voltage is higher or lower than the reference voltage, the duty cycle is decremented or incremented respectively. This process is illustrated in Figure 2.22.

Development of Power Converters for Electric Vehicle Charging with Photovoltaics Interface
Júlio André Machado Fernandes - University of Minho

27
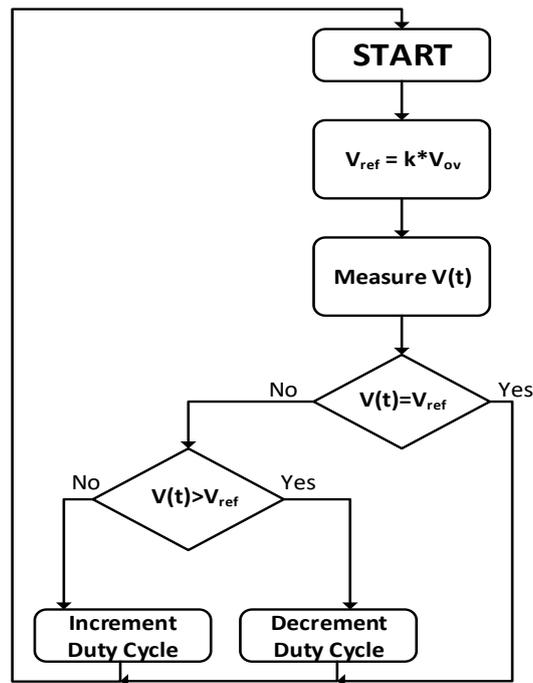
Figure 2.22 - Flowchart of the Open Voltage MPPT.

Despite being a simple, inexpensive method it is not very efficient since for each performed measurement is necessary to open the circuit, and in that instant, the extracted power from the panel is null [42] - [44].

2.9.2. Constant Current

This algorithm has an operation similar to the Open Voltage method. The operation is based on the fact that the current at the MPP is proportional to the short-circuit current. A flowchart of this method is presented in Figure 2.23.
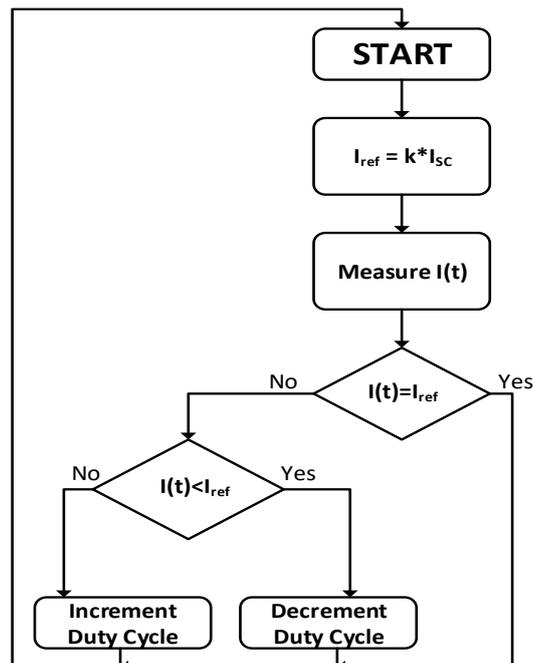
Figure 2.23 - Flowchart of the Constant Current MPPT algorithm.

This method requires the measurement of the panel's short circuit current. For that, it is mandatory the use of a switch in parallel with the PV panel. After the measurement of the short circuit current the reference current is calculated and compared to the measured output current from the PV panel. The value of duty-cycle is then incremented or decremented accordingly. Typically, values ranging from 78%-92% of the short circuit current are used as reference [43].

2.9.3. Current Sweep

In this method the I-V characteristic curve is obtained using a sweep waveform for the PV panel current. The sweep is repeated at fixed time intervals so the I-V curve is updated periodically and the MPP voltage can be determined from it at these same intervals. With this method the real MPP is obtained. On the other hand, the sweep takes certain time during which the PV panel is not providing power to the rest of the system. Furthermore, the implementation complexity is high, the convergence speed is slow and both voltage and current measurements are required [45].

2.9.4. Perturb & Observe (P&O)

This is the most used MPPT algorithm due to its ease of implementation. It works by perturbing, observing and then comparing the power generated by the panel. Figure 2.24 shows the flowchart of the P&O algorithm.
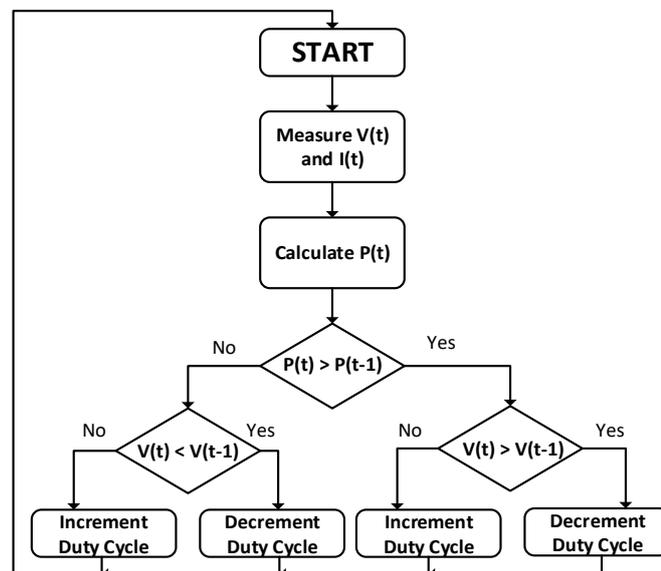
Figure 2.24 - Flowchart of the P&O MPPT algorithm.

This algorithm works by measuring the instantaneous values of the output current and voltage of the panel and calculating the instantaneous power. If the calculated PV panel power is higher or lower than the one calculated in the previous iteration, then the

Development of Power Converters for Electric Vehicle Charging with Photovoltaics Interface
Júlio André Machado Fernandes - University of Minho

29

instantaneous values of the voltages are compared. After the comparing of the voltages, the value of duty-cycle is updated accordingly.

Despite being very simple to implement, this algorithm has some disadvantages. As the system is constantly being disturbed, the panel is not always operating at maximum power point. Instead, the power generated by the panel will oscillate close to the maximum power point. The amplitude of the oscillation is determined by the magnitude of the variation of the duty cycle. Also, if the radiation intensity changes quickly, it can lead to incorrect readings, since the power curve changes [46].

2.9.5. Incremental Conductance

This method consists in using the slope of the derivative of the current with respect to the voltage in order to reach the maximum power point. This MPPT algorithm works by determining the direction of the change of the panel's voltage through the measuring and comparison of the incremental and instantaneous conductances. If the values of the two conductances are equal, then the panel is operating in its maximum power point. This can be described by the expressions below:

$$\frac{dI}{dV} = -\frac{I}{V} \tag{2.2}$$

$$\frac{dI}{dV} < -\frac{I}{V} \tag{2.3}$$

$$\frac{dI}{dV} > -\frac{I}{V} \tag{2.4}$$

As it was stated above, if expression (4.2) is verified, then the panel is working on the maximum power point. If expression (4.3) is verified, the MPP is to the left of the current point. Finally, if expression (4.4) is verified, the MPP is to the right of the current point. By using the expressions above, the controller determines the direction in which the perturbation must be made. This allows it to adapt quicker to the variations of the MPP. To facilitate the understanding of this MPPT algorithm, its flowchart can be seen in Figure 2.25.

30

Development of Power Converters for Electric Vehicle Charging with Photovoltaics Interface
Júlio André Machado Fernandes - University of Minho
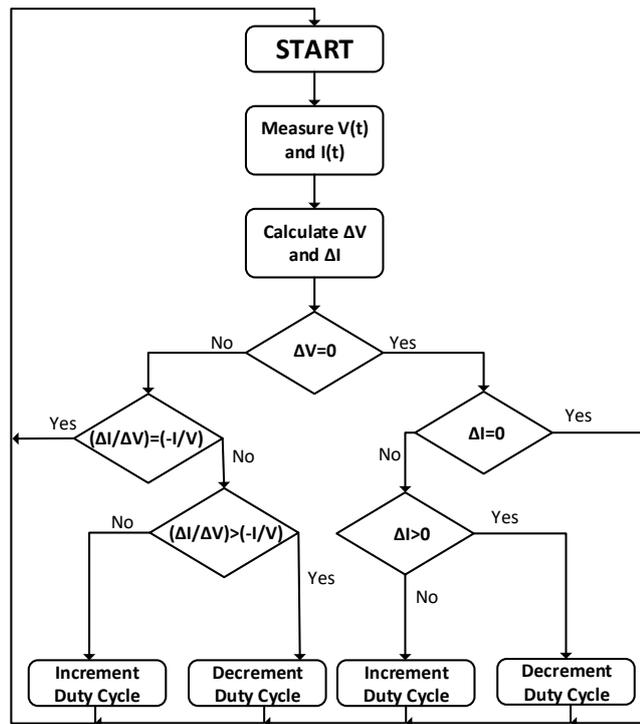
Figure 2.25 - Flowchart of the Incremental Conductance MPPT algorithm.

Despite having many similarities, the Incremental Conductance presents advantages over the P&O algorithm. One advantage of this algorithm is that it can find with more precision the MPP, minimizing the oscillation around it. Furthermore, it is also not susceptible to false readings due to rapid changes in external conditions [47].

However, similarly to the P&O it is necessary to establish a commitment relationship between the response speed to the changes in the MPP and the oscillation around it. A typical solution to this issue is to use an adaptive algorithm which gradually decreases the value of the perturbation as the MPP is approached [25].

2.9.6. Comparison between the Different MPPT Algorithms

The P&O and Incremental Conductance algorithms have a very similar mode of operation. The only differences are that in the Incremental Conductance method the controller knows which direction is the point of maximum power and stabilizes when it reaches it. This makes the Incremental Conductance method quicker to find the maximum power point. The disadvantage of the Incremental Conductance method is a slight increase in the complexity of the controller.

The open voltage method is the least complex of all, but does not guarantee the maximum power extraction. This is because apart from just making an estimate of the maximum power point, the sampling frequency of the open circuit voltage must be low in order to reduce the number of times the module is disconnected from the rest of the system. These two factors make this method not very advantageous.

Development of Power Converters for Electric Vehicle Charging with Photovoltaics Interface
Júlio André Machado Fernandes - University of Minho

31

The constant current algorithm presents the same disadvantages as the open voltage algorithm.

The current sweep method has the same disadvantages compared to the open voltage and constant current methods, with the exception that the calculated maximum power point is accurate. But because obtaining a P-V curve is a much slower process than obtaining the value of open circuit voltage, the maximum power point refresh rate must be very low or otherwise the panel could be disconnected from the system for a long time thus reducing the efficiency of the whole system.

In Table 2.3, it is shown a comparison between the MPPT algorithms mentioned above. The comparison was made taking into account aspects like the complexity of the controller, the power variation in steady state and if the disconnection of the PV panel from the system is required in order to make the necessary measurements.

Table 2.3 - Comparison between MPPT algorithms.

Algorithm	Complexity of control system	Variation of power	Disconnection required
Open Voltage	Low	None	Yes
Constant Current	Low	None	Yes
Current Sweep	Medium	None	Yes
Perturb & Observe	Low	Medium	No
Incremental Conductance	Medium	Low	No

As mentioned above, an MPPT algorithm is necessary to ensure that the PV panel always operates in its maximum power point. Obviously, this is not enough. A DC-DC converter is also necessary to vary the output voltage and current of the PV panel. Although other topologies can be used, depending on the application, a simple buck or boost topology is enough. A boost converter should be used when a voltage higher than the voltage provided by the PV panel is required. On the other hand, if a lower voltage is needed, then a buck converter should be used. Naturally, the value of the duty-cycle applied to the gate of the semiconductor will determine the value of the extracted power.

Figure 2.26 shows a boost converter connected between the PV panel and the DC-link.

32

Development of Power Converters for Electric Vehicle Charging with Photovoltaics Interface
Júlio André Machado Fernandes - University of Minho
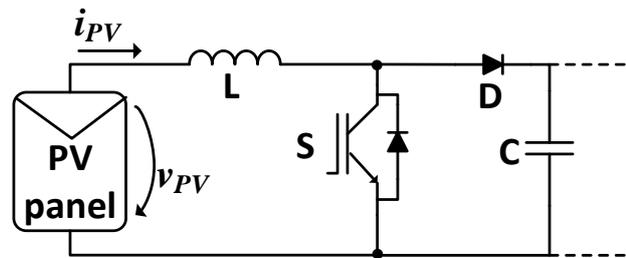
Figure 2.26 - Boost converter connected between PV panel and DC-link.

2.10. Conclusions

In this chapter, various battery technologies used in EVs were presented. A comparison between the different types of batteries used (e.g. lithium-ion) was also presented, as well as the different charging modes and the interaction modes between the EV and the electrical power grid.

A closer look was taken into the power electronics associated with Battery Charging Systems. There are many different topologies of power converters that can be used when the goal is to develop a charging system. Unidirectional converters are used when it is only necessary to charge the batteries. However, bidirectional controlled topologies offer the advantage of not only charging the batteries but also allow part of the energy stored in them to be delivered to the power grid. In the ever growing Smart Grid context, where the EVs will have the ability to communicate with the grid, this kind of topologies are being used more and more nowadays.

Currently, an EV still cannot compete against with a regular vehicle powered by an Internal Combustion Engine in terms of range and battery recharging time. Despite that, new technologies are being developed every day that, little by little, will allow the EV to get a run for its money. As of now, lithium-ion and lithium polymer batteries are the types preferred by manufacturers to install in their EVs and PHEVs. Lead acid batteries, despite being cheaper, are mostly used when an ICE vehicle is to be converted to an EV.

In addition, different charging modes were presented. As EVs need to be charged quite regularly, the charging time becomes one of the, if not the most, important aspect to consider. Nowadays is possible to charge the vehicle with powers up to 50 kW, allowing the batteries to be charged in less than 30 minutes.

Also in this chapter, a detailed look into the composition of a PV panel was made giving particular attention on how they are able to produce electricity from solar radiation. Different types of photovoltaic cells commercialized today were also presented. There are numerous more solar cell technologies, however they are either in

Development of Power Converters for Electric Vehicle Charging with Photovoltaics Interface
Júlio André Machado Fernandes - University of Minho

33

early stages of development or they are simply not economically viable. The major obstacle to this technology is the low efficiency of the photovoltaic cells available today. The highest efficiency ratio in a solar cell record was set in December, 2014, when the collaboration efforts of companies Soitec, CEA-Leti (both from France) and Fraunhofer ISE (Germany) developed a solar cell with a 46% efficiency ratio [48].

Finally in this chapter, various Maximum Power Point Tracking techniques implemented today in an effort to bridge the gap in the variations of the maximum power point were presented. This way it is ensured that the maximum power is always extracted from the PV panel. From the different MPPT algorithms studied, the Incremental Conductance offers better results when compared to the Perturb & Observe, Open Voltage, Constant Current and Current Sweep algorithms. It comes with the expense of higher complexity but makes up in quickness finding the maximum power point and stability.

34

Development of Power Converters for Electric Vehicle Charging with Photovoltaics Interface
Júlio André Machado Fernandes - University of Minho

CHAPTER 3

Power Electronics Converters for Electric Vehicle Charging Systems

3.1. Introduction

A power converter is an electronic circuit that allows changing a signal into another that may have a different frequency or amplitude. These types of converters can transform alternating current into direct current (AC-DC) or direct current into alternating current (DC-AC). In the specific case of battery chargers, with connection to the power grid, it is necessary to use an AC-DC converter in order to convert the voltage and current of the grid (AC), to a suitable voltage and current to be supplied to the batteries (DC). As was stipulated in the beginning, the integrated converter to be developed will allow for G2V and V2G operation. For this, it is mandatory to choose a topology for each type of converter that allows for a bidirectional flow of energy.

As such, some topologies of bidirectional AC-DC converters and also bidirectional DC-DC converters will be presented below.

3.2. Single-Phase Bidirectional AC-DC Converters

As mentioned above, the bidirectional AC-DC converter will convert an AC signal into a DC signal while the battery is being charged. On the other hand, it will convert a DC signal into an AC signal when the batteries return part of their energy to the power grid. The main topologies of single-phase bidirectional AC-DC converters that were studied in the scope of this Dissertation are presented.

3.2.1. Half-Bridge Converter

This topology, shown in Figure 3.1, is the simplest regarding AC-DC converters. It uses an inductor, two capacitors and two controlled semiconductors. The current i_{Grid} can be controlled, so that power factor correction can be achieved, by applying PWM signals in the gates of S1 and S2. This will force the input current to be sinusoidal and in phase with the power grid voltage.

Development of Power Converters for Electric Vehicle Charging with Photovoltaics Interface
Júlio André Machado Fernandes - University of Minho

36

When compared with other topologies, such as the Full-bridge, this one offers a simpler control aligned with fewer losses, due to the reduced number of semiconductors used. However, because it uses two capacitors on the DC-link, the input voltage must be doubled in order to achieve the required output voltage and additional control is needed to balance the voltages of the capacitors. In other words, if it is desired to obtain an output voltage of 100 V, the voltage in the DC-link must be 200 V. As such, the semiconductors used must be able to withstand higher voltage levels.
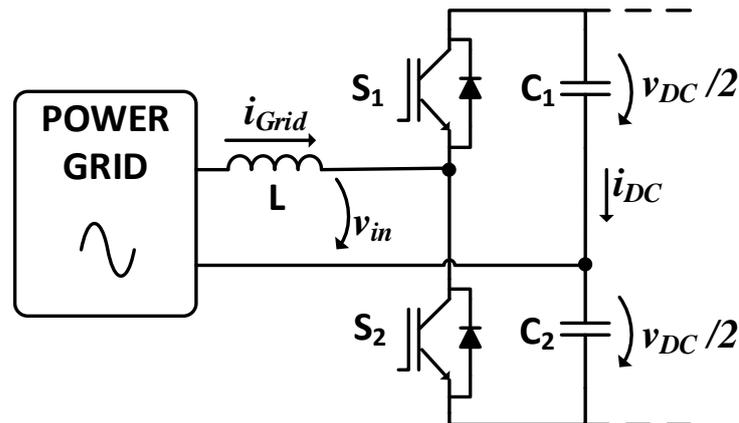
Figure 3.1 - Half Bridge bidirectional AC-DC converter.

When this converter is providing energy to the power grid, the control signals applied at the gates of S1 and S2 must be such that the current in the inductor is 180° out of phase with the grid voltage.

This topology only allows 2 voltage levels at its output ($+V_{DC}/2$ and $-V_{DC}/2$). One important aspect to note is that switches S1 and S2 cannot be turned on simultaneously. Failure to do that would result in a short circuit across the DC-link, which could imply major damage to the converter [49] [50].

3.2.2. Full-Bridge Converter

Unlike the Half-Bridge converter, which uses two power semiconductors, this topology instead makes use of four semiconductors. Despite the higher count of semiconductors, these do not have to withstand voltages as high as the Half-Bridge topology. This topology, unlike the previous, makes use of only one capacitor in the DC-link. This means that the additional control to balance the voltages is disposable.

In Figure 3.2 it is depicted the power circuit of the Full Bridge AC-DC converter.

Development of Power Converters for Electric Vehicle Charging with Photovoltaics Interface
Júlio André Machado Fernandes - University of Minho

37
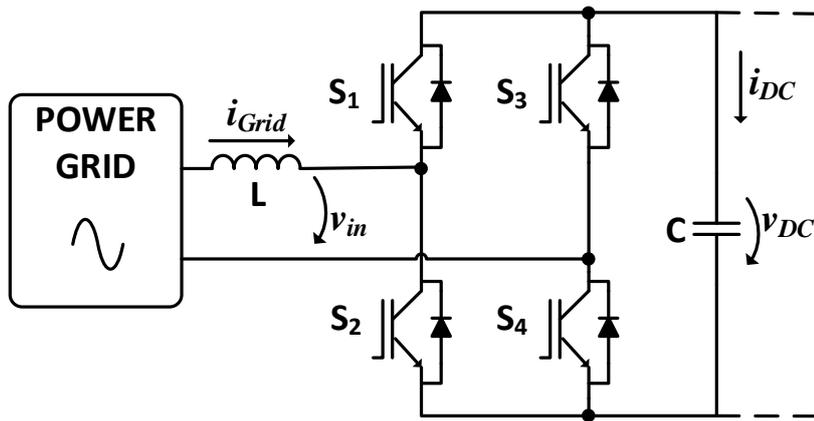
Figure 3.2 - Full-Bridge bidirectional converter.

As shown in Figure 3.2, the Full-Bridge converter consists of two legs. Like the Half-Bridge topology, the two switches of each leg are driven so that when one is switched on, the other is switched off. Unlike the topology previously presented, the Full-Bridge converter allows for 3 distinct voltages on the output ($+V_{DC}$, 0 and $-V_{DC}$). As such, the use of this topology allows for a higher power factor and lower harmonic distortion, resulting in a better overall quality of the synthesized wave [49] [51].

3.2.3. Multi-level Converter

The use of a single level topology, such as the Full-Bridge topology, in higher power applications can be troublesome, as the semiconductors will be exposed to high currents and voltages. As such, the multi-level converters, an example of which is illustrated in Figure 3.3, are used in situations when higher powers are at stake. Because more semiconductors are used, each will be subject to a lower value of voltage.
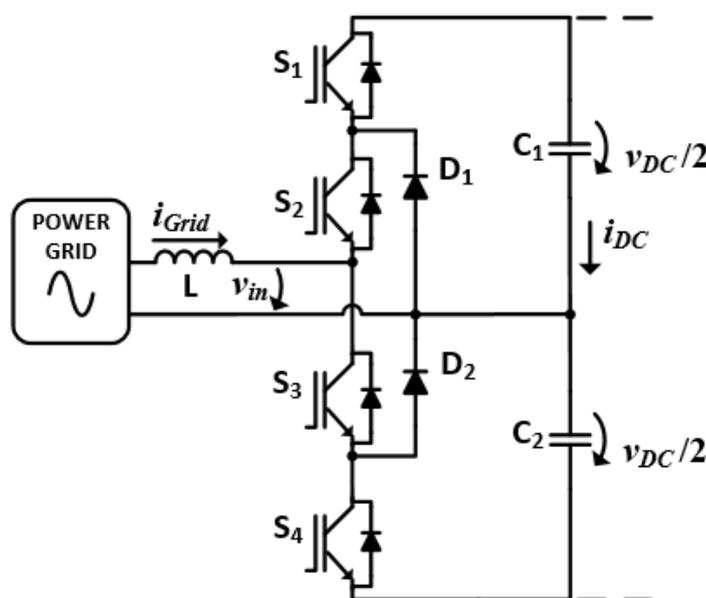
Figure 3.3 - Three-level diode clamped bidirectional AC-DC converter.

The presented topology, similarly to the Full-Bridge, allows 3 voltage levels at its output ($+V_{DC}/2$, 0 and $-V_{DC}/2$). However, more levels can be added to these converters whereby the quality of the synthesized wave is higher than in the other previously mentioned topologies. In addition, it offers the possibility of working with lower switching frequencies which leads to fewer switching losses.

One clear concern however with this topology is the added complexity and additional number of components. These two issues add to the cost and magnitude of the required control circuitry [49] [51].

3.3. Bidirectional DC-DC Converters

As mentioned earlier in this chapter, it is required the use of a bidirectional DC-DC converter to make the interface between the batteries and the rest of the system. As such, a review of the topologies of bidirectional DC-DC converters that are most frequently used in EVs will be approached below.

3.3.1. Buck-boost Converter

The buck-boost DC-DC converter has one inductor, one capacitor, and two switches with internal diodes, arranged in a Half-Bridge configuration as shown in Figure 3.4.

This converter works as a boost converter in one direction and a buck converter in the other. When the charger operates in battery charge mode, the circuit must function as a buck-converter. To activate this mode, S2 is left open as S1 is switched with a PWM signal. The reduction ratio of the voltage depends on the duty cycle of the signal applied to S1.
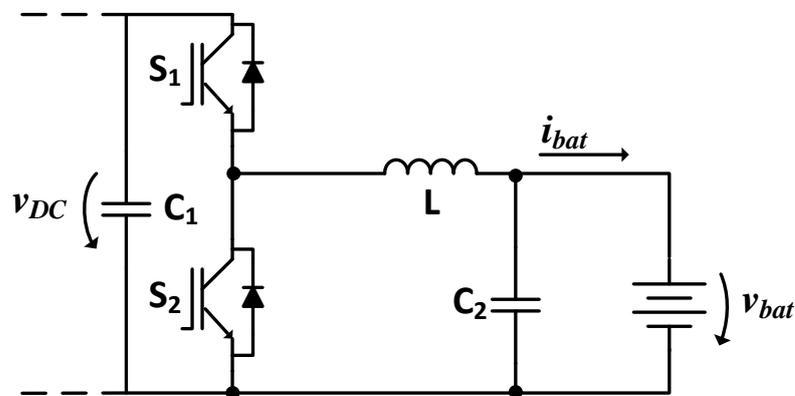
Figure 3.4 - Bidirectional Buck-boost DC-DC converter.

Development of Power Converters for Electric Vehicle Charging with Photovoltaics Interface
Júlio André Machado Fernandes - University of Minho

39

On the other hand, when the circuit is operating in battery discharge mode, S1 remains off while S2 is switched with a PWM signal. In this mode, the circuit functions as a boost converter. The need to only control two switches greatly simplifies the control circuitry required.

However, the inductors used tend to be bulky and expensive. Also, this topology only has the capability to operate either as a buck or a boost, for a given direction. This would work for most applications, but situations might arise where the functionality of a buck and boost converter is required in both directions [25] [51].

3.3.2. Dual Half-Bridge Converter

The charging of an electric vehicle's batteries is an application that may require galvanic isolation to ensure the safety of all users. Although one can achieve galvanic isolation by placing a transformer upstream of the AC-DC converter, this solution will require the use of an expensive, heavy and bulky transformer. Another solution is to utilize an isolated DC-DC converter. Isolated DC-DC converters achieve galvanic isolation by using a high-frequency transformer. These transformers are lighter and less expensive, making this a much more advantageous solution.

The Dual Half Bridge converter, presented in Figure 3.5, consists of 2 Half-Bridge AC-DC converters, connected together by a high-frequency transformer.
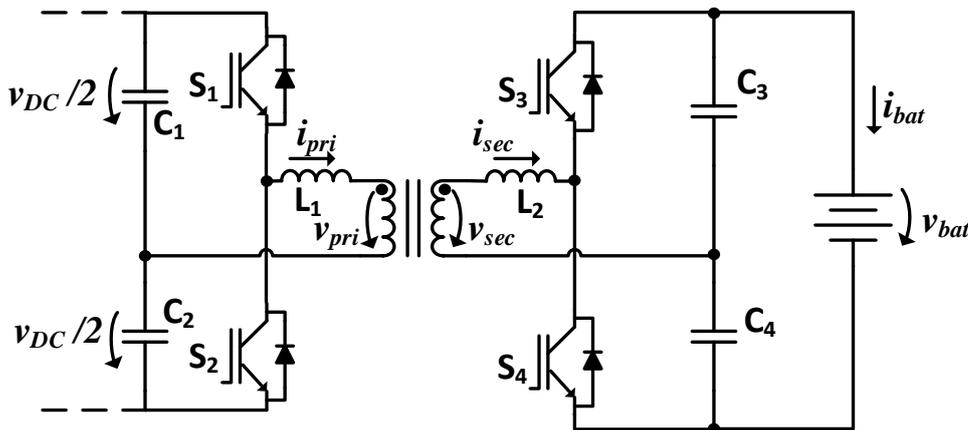
Figure 3.5 - Dual Half-Bridge bidirectional DC-DC converter.

In order to transfer the energy from one side of the transformer to the other, the phase shift technique is widely used. As such, the energy transfer occurs through the phase shift between the voltages of the primary and secondary sides of the transformer. If v_{pri} is delayed compared to v_{sec}, the energy is delivered from the secondary to the primary. In this way, the amount of transferred power relates to the value of the phase

shift and is at maximum for a phase shift of 90°. However, other factors affect the amount of transferred power, such as the switching frequency used and also the values of the auxiliary inductors *L1* and *L2* [49] [50].

3.3.3. Dual Active Bridge Converter

The schematic of the Dual Active Bridge converter is shown in Figure 3.6.
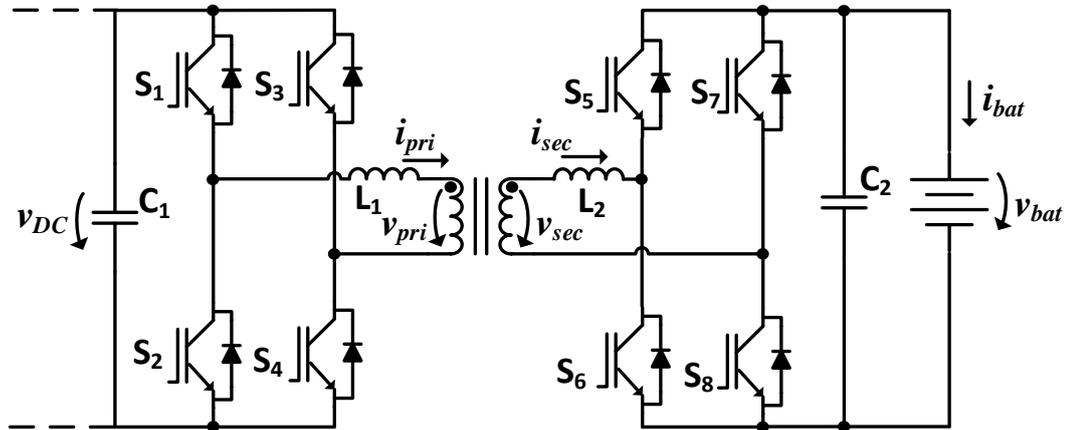
Figure 3.6 - Bidirectional Dual Active Bridge bidirectional DC-DC converter.

The Dual Active Bridge converter consists of two Full-Bridge AC-DC converters, linked together by a high-frequency transformer. When charging the batteries, the active bridge on the left side of Figure 3.6 acts as an inverter while the internal diodes of the switches on the right act as a full-bridge to rectify the AC back to DC.

When the converter runs in battery discharge mode, the bridge on the right inverts the DC current of the battery which induces an AC voltage in the left active bridge through the transformer. The internal diodes of the switches on the left hand side of Figure 3.6 act as a full-bridge to rectify the current back to DC that is usable by the bidirectional AC-DC converter. As such, the PWM signals may only be applied to one bridge at a time, the other remaining uncontrolled. The current conduction is assured by the antiparallel diodes of the semiconductors.

Similarly to the Dual Half-Bridge converter, the phase shift technique can also be employed in this topology.

The topology presented makes use of 8 semiconductors. This of course translates into a bigger size, complexity and overall cost of the converter, when compared with other topologies such as the Buck-boost and the Dual Half Bridge. Nevertheless, because it offers galvanic isolation, it is commonly used in high power applications [25] [49] [51].

Development of Power Converters for Electric Vehicle Charging with Photovoltaics Interface
Júlio André Machado Fernandes - University of Minho

41

3.4. Sinusoidal Pulse Width Modulation

In order to control the switching of the semiconductors and, consequently, the output signal of the AC-DC converter, it is necessary to implement a modulation technique.

In this regard, Sinusoidal Pulse Width Modulation (SPWM) is one technique of Pulse Width Modulation (PWM) which is highly utilized in AC-DC converters. The SPWM is a familiar modulation technique in the field of Power Electronics in which a high frequency triangular carrier signal is compared with a sinusoidal reference signal. The frequency of the triangular carrier will determine the switching frequency of the power semiconductors. On the other hand, the sinusoidal reference consists on the desired output to be synthesized being that the frequency of this signal will determine the frequency of the synthesized wave. The number of pulses per cycle is decided by the ratio of the triangular carrier frequency to that of modulating sinusoidal frequency. This ratio is called Modulation ratio (M_R) and is given by the expression [52]:

$$M_R = \frac{f_{tri}}{f_{mod}}$$
(3.1)

Where,

- M_R is the Modulation ratio;

- f_{tri} is the frequency of the triangular carrier wave;

- f_{mod} is the frequency of the modulating wave.

Figure 3.7 shows a working example of the SPWM technique, where the carrier, reference and output voltage waves are all represented.
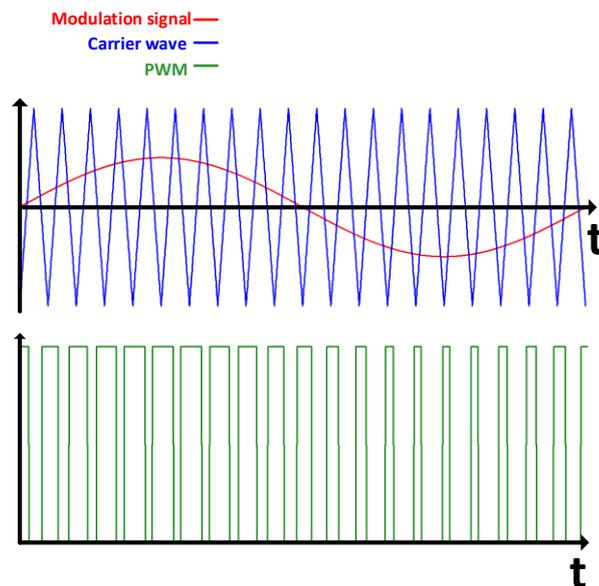
Figure 3.7 - Synthesis of the output signal in the SPWM technique.

Through the analysis of Figure 3.7, it can be seen that the output voltage has only two states. These are the result of the comparing between the reference and the carrier waves and translate to the operation states of the power semiconductors. A high level on the output signal means that the semiconductor is on (i.e. closed), and a low level means that the semiconductor is off (i.e. open). It is verified that the output signal will be high when the value of the reference is greater than the carrier wave and low when the opposite occurs. This is the basic principle of pulse width modulation where a signal is synthesized based on the duty cycle variation while maintaining the frequency constant. The SPWM is a particular case of this type of modulation. Nevertheless, there are variants of the SPWM, which will be presented next [53].

3.4.1. Bipolar SPWM

The basic idea behind the Bipolar SPWM is shown in Figure 3.8. A comparator is used to compare the reference signal with the triangular carrier signal, thus producing the bipolar switching signal.
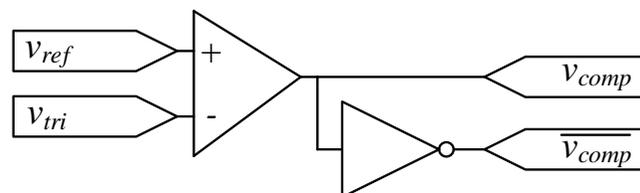
Figure 3.8 - Generation of the command signals by the bipolar SPWM modulation.

The signals v_{comp} and $\overline{v_{comp}}$ correspond to the command signals to be applied to the power semiconductors, whereby the output of the comparator has a waveform equal to that of the output voltage of the converter. In Figure 3.9 are presented the typical

Development of Power Converters for Electric Vehicle Charging with Photovoltaics Interface
Júlio André Machado Fernandes - University of Minho

43

waveforms for the bipolar SPWM. The variable v_{out} represents the output voltage of the converter. It can be seen that the width of the output signal will vary its average value in each instant [54] [55].
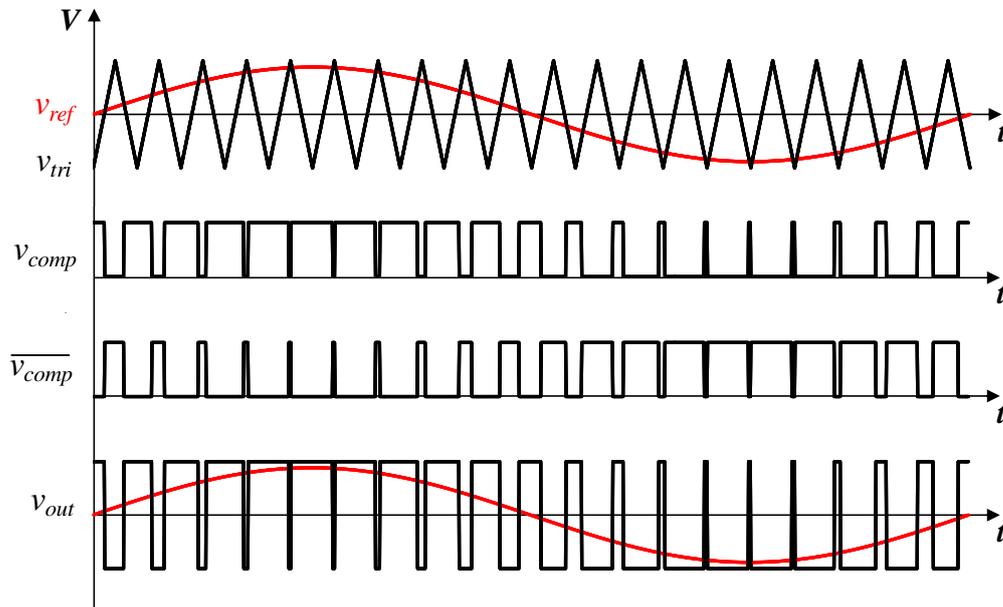
Figure 3.9 - Synthesized signal by the bipolar SPWM modulation.

This technique can be applied to both Half-Bridge and Full-Hridge topologies, however the generated signal has a relatively low quality.

3.4.2. Unipolar SPWM

In this scheme, the triangular carrier is compared with two reference signals. These signals consist of the same sinusoidal reference from the bipolar SPWM, with the addition of a second sinusoidal signal 180° out of phase with the first one. This time two comparisons are made which result in 4 different command signals, as shown in Figure 3.10 [54].
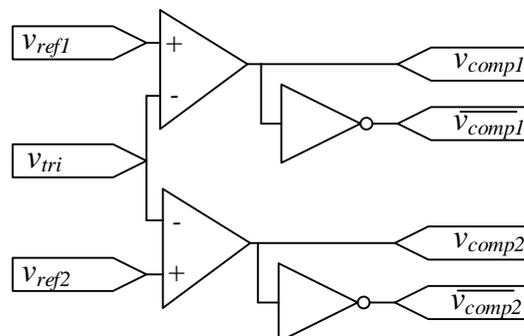
Figure 3.10 - Generation of the command signals by the unipolar SPWM modulation.

The use of unipolar SPWM allows for a better quality of the output signal. This is possible due to the fact that this switching scheme generates 3 voltage levels on the

44

Development of Power Converters for Electric Vehicle Charging with Photovoltaics Interface
Júlio André Machado Fernandes - University of Minho

output of the converter. The effective switching frequency, seen by the load, is doubled and the voltage pulse amplitude is halved. Due to this, the harmonic content of the output voltage waveform is reduced when compared to the bipolar modulation. Also, because the frequency of the output signal is twice the switching frequency, more compact passive filters can be used. Figure 3.11 shows the typical waveforms for the unipolar SPWM [54] [55].
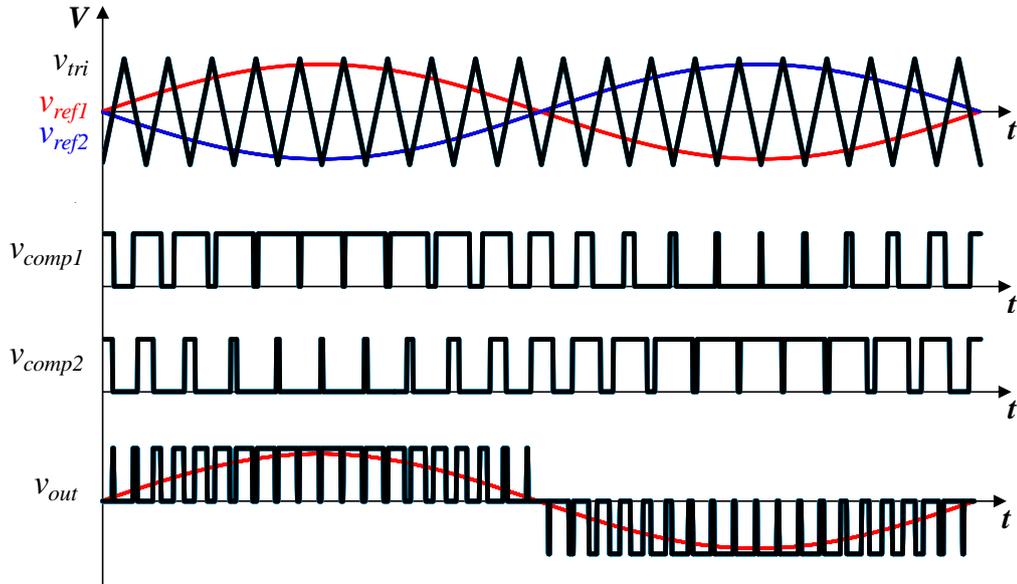
Figure 3.11 - Synthesized signal by the unipolar SPWM modulation.

It should be noted that, due to the insufficient number of power semiconductors in relation to the number of command signals at hand, this technique cannot be used in a Half-Bridge topology.

3.5. Current Control Techniques

Among multiple functions of grid connected systems, the current control plays one of the most important roles. The performance of the complete system largely depends on the quality of the applied current control strategy. There are a vast number of current control strategies, each one with applications in different areas such as Active Power Filters or UPSs.

In the case of VSI AC-DC converters, these control strategies work by keeping the output current of the converter as close as possible from a calculated reference current. The control strategies can be described as linear (e.g. PI control) or non-linear (e.g. hysteresis control), depending on whether the error compensation and voltage modulation are separated. The harmonic content of the output current and, therefore, its quality is directly affected by the quality of the applied current control technique [56].

Development of Power Converters for Electric Vehicle Charging with Photovoltaics Interface
Júlio André Machado Fernandes - University of Minho

45

3.5.1. Hysteresis Current Control

In this control technique, a hysteresis band is defined for the reference current and it is compared with the output current error. If the error is below the lower limit of the hysteresis band the inverter switches to a high state and switches back to low once the error is greater than the higher limit of the hysteresis band. Figure 3.12 shows an implementation example of a hysteresis current controller in which the reference current, the output current and the output signal of the comparator are all presented [57].
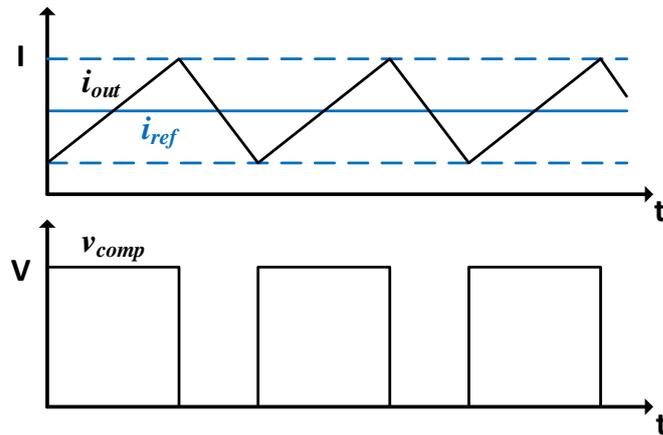
Figure 3.12 - Hysteresis current control waveforms.

The hysteresis modulation for power electronic converters is attractive in many different applications because of its unmatched dynamic response and wide command tracking bandwidth. However, one of its major drawbacks is the fact that the switching frequency is not constant nor is it limited to a maximum value. Resonance problems can arise from these variable switching frequencies and, in addition, the switching losses limit this controller to low power levels [58].

3.5.2. Periodic Sampling Current Control

This current control technique is simple to implement and robust. It is very similar to the hysteresis current control, comparing the reference with the output current at a constant sampling frequency. This technique can be easily implemented on a DSC or also using a flip-flop D, as shown in Figure 3.13. The result of the comparison between the reference current and the actual output current of the converter is connected to the input of the flip-flop and a square-wave is connected to the clock input, in order to define the maximum switching frequency.
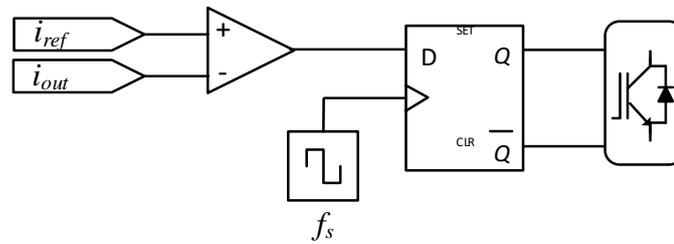
Figure 3.13 - Implementation of the Periodic Sampling current control.

Nevertheless, just like the hysteresis controller, this technique has the disadvantage of not guaranteeing a fixed switching frequency and only a maximum switching frequency (half of the sampling frequency) can be defined [59].

3.5.3. PI Current Control

In this control technique, the reference current is also compared with the output current of the converter. The resulting error is fed into a Proportional Integral (PI) controller. The output of the PI controller will be the reference signal for the SPWM, resulting in the command signal to be applied to the power semiconductors. A block diagram with the implementation of this current control technique is presented in Figure 3.14 [60] [61].
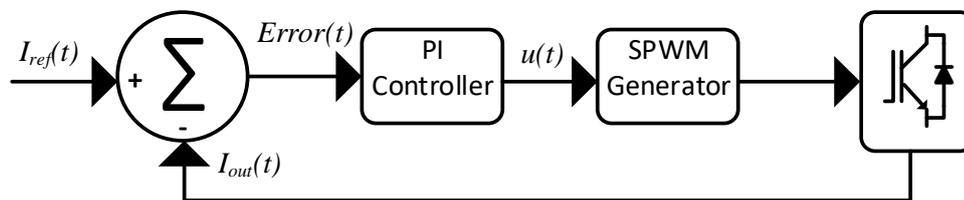
Figure 3.14 - Implementation of the PI current control.

A PI current control strategy allows for a fixed switching frequency, resulting in known harmonics. This is particularly helpful when it comes to the design of the passive filters.

However, one of the drawbacks of this control technique is the fact that it doesn't react quickly to sudden changes in the current. This is due to a delay between the reference and the output currents, which is typical in this control strategy. In addition, it is also necessary the readjustment of the proportional and integral gains whenever it is desired to synthesize different currents or when the load changes [57].

3.5.4. Predictive Current Control

This is a technique that uses the electric model of the system to predict the next stage that of the converter in order to eliminate de error between the produced and the current reference.

Development of Power Converters for Electric Vehicle Charging with Photovoltaics Interface
Júlio André Machado Fernandes - University of Minho

47

Figure 3.15 shows the typical predictive control model for a grid-tie VSI [61].
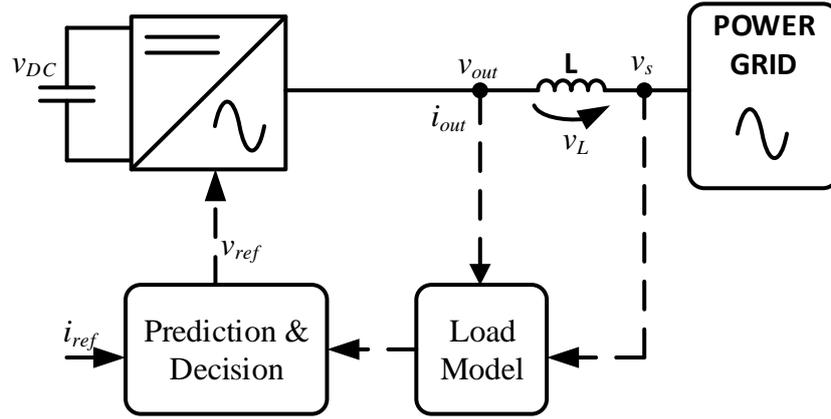
Figure 3.15 - Predictive control model for a grid-tie VSI.

Taking into account the model presented in Figure 3.15, the output voltage of the converter (v_{out}) must be equal to the sum of the voltage in the inductor (v_L) with the voltage of the connection point of the system (v_s), as presented in expression (3.2).

$$v_{out} = v_L + v_s \tag{3.2}$$

Ignoring the inductor's ESR, expression (3.3) is obtained by substituting v_L for the inductor's voltage/current characteristic.

$$v_{out} = L\frac{di_{out}}{dt} + v_s \tag{3.3}$$

Similarly to other control techniques previously presented, in this type of control the error of the current (i_{error}) between the reference current (i_{ref}) and the synthesized current (i_{out}) is calculated. The resulting error is given by expression (3.4).

$$i_{error} = i_{ref} - i_{out} \tag{3.4}$$

The current i_{out} in (3.3) can be replaced by its value in (3.4), resulting in expression (3.5).

$$L\frac{di_{error}}{dt} = L\frac{di_{ref}}{dt} + v_s - v_{out} \tag{3.5}$$

By using a high sampling frequency, the variation of the error derivative is almost linear. Assuming that i_{out} has a low ripple value, it is considered that the increase of the error in the current is equal to the instantaneous value of i_{error}. As such, expression (3.5) can be rewritten into expression (3.6), in which T_s represents the sampling period and Δi_{ref} represents the variation of the reference current.

$$L\frac{i_{error}}{T_s} = L\frac{\Delta i_{ref}}{T_s} + v_s - v_{out} \tag{3.6}$$

The voltage applied to the inductor has to be symmetrical to the calculated value, in order to annul the error of the current. The voltage produced by the converter is given by expression (3.7). As such, the value of v_{out} will be the reference voltage (v_{ref}) used in the SPWM modulation.

$$v_{out} = v_s + L\frac{\Delta i_{ref}}{T_s} + L\frac{i_{error}}{T_s}$$ (3.7)

To make these calculations in a digital controller it is necessary the discretization of the equations, resulting in (3.8).

$$v_{ref}[k] = v_s[k] + \frac{L}{T_s}(i_{ref}[k] - i_{ref}[k-1] + i_{error}[k])$$ (3.8)

The final expression to the implementation of the predictive current control is obtained by substituting the term i_{error}, as shown in expression (3.9).

$$v_{ref}[k] = v_s[k] + \frac{L}{T_s}(2\,i_{ref}[k] - i_{ref}[k-1] - i_{out}[k])$$ (3.9)

In similarity to the PI current control, the predictive control constitutes a linear type of control, because the voltage modulation is separated from the error compensation. Therefore, this control allows the converter to operate at fixed switching frequency. However, the predictive control has a faster response to variations in the reference thus having a better performance in terms of THD. Another advantage of this control is that it does not require the adjustment of gains, which is a drawback in a PI type control.

On the other hand, the predictive current control is sensitive to errors in the determined system parameters or to possible changes in them. For instance, in a real operating situation, the value of L changes according to the frequency and also the current that flows through it. As such, this variation will lead to parameter errors in the predictive control model [49] [61].

3.6. Conclusions

One of the goals of this dissertation is to develop a Battery Charging System capable of allowing bidirectional power flow (i.e. charging and discharging of the batteries). As so, in this chapter were presented numerous topologies of bidirectional AC-DC and DC-DC converters that were considered as a possible solution. An analysis was made in terms of number of components, size, efficiency and control complexity.

Development of Power Converters for Electric Vehicle Charging with Photovoltaics Interface
Júlio André Machado Fernandes - University of Minho

49

The power electronics area has also been subject to various developments over the past years, allowing for higher powers, faster switching frequencies and smaller losses (meaning higher efficiencies). Those breakthroughs had made major contributions in the recent development of lighter, more economic Battery Charging Systems (BCS). The possible solutions presented in this chapter all guarantee that the goals that were proposed for this BCS are fulfilled.

Also in this chapter the Sinusoidal Pulse Width Modulation (SPWM) was discussed. As mentioned before, this switching technique is largely applied in AC-DC converters and the unipolar SPWM presents better results than the bipolar SPWM.

Finally, a number of current control techniques used in VSIs were listed. They range from non-linear (e.g. hysteresis current control), which provide a variable switching frequency, to linear (e.g. PI current control), which provide a fixed switching frequency.

Of all the current control strategies that were studied, it was concluded that the ones who provided a fixed switching frequency presented better results in terms of harmonic distortion and the overall quality of the synthesized current.

50

Development of Power Converters for Electric Vehicle Charging with Photovoltaics Interface
Júlio André Machado Fernandes - University of Minho

CHAPTER 4

Simulation of the Electric Vehicle Charging System

4.1. Introduction

In Power Electronics, a good implementation of a control system is as much important as the choice of the topology to adopt for the system. As such, it is necessary to model and analyze all converters used as to choose the right control strategy for each one. In this chapter the overall development and modeling of the power converters that were used to make the proposed Battery Charging System will be presented. The chosen topologies will also be presented as well as the control algorithms used for each converter.

Nowadays, the use of simulation tools when developing Power Electronics converters has become vital. These tools allow us to study the behavior of the entire system, in function of different components, topologies and control algorithms with total safety. Furthermore, the use of simulation software allows preventing modeling errors, greatly improving the cost of the final solution. As such, for the development of the power converters, the simulations were carried out using the simulation software PSIM and the results of which are presented along this chapter.

4.2. Modeling and Control of the Bidirectional AC-DC Converter

For the bidirectional AC-DC converter, the Full-Bridge topology was chosen as shown in Figure 4.1. In this particular case, the load represents the rest of the system's converters seen from the DC-link.
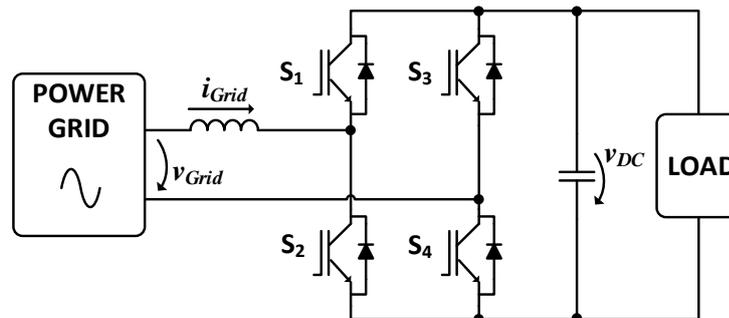
Figure 4.1 - Full-Bridge bidirectional AC-DC converter used in the proposed system.

Development of Power Converters for Electric Vehicle Charging with Photovoltaics Interface
Júlio André Machado Fernandes - University of Minho

52

As mentioned before, the switches on each leg of the converter must be complementary to each other. For example, if S1 is on then S2 must be off (the same applies to S3 and S4) to avoid short-circuiting the DC-link.

The control strategy applied to this converter is responsible by regulating the DC-link voltage to 400 V and the converter's input or output current. If the converter is working as a rectifier, the input current should be sinusoidal and in phase with the grid voltage. On the other hand, if the converter is working as a grid-tied inverter, the output current should be sinusoidal and 180° out of phase with the grid voltage. For this particular case, different control strategies were studied such as the ones proposed in [62] and [63]. The final decision was to implement a PI controller as proposed in [62], which is shown in Figure 4.2. More specifically, it uses a PI controller to regulate the DC-link voltage and another to control the output current.
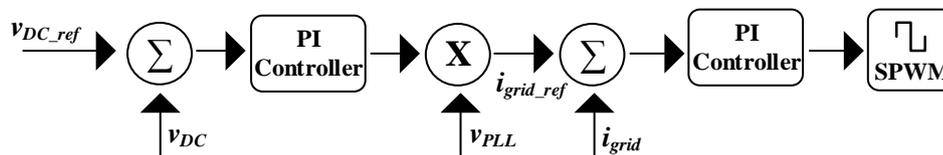
Figure 4.2 - Block diagram of the AC-DC converter controller.

For the controller to work properly, it is necessary to read the instantaneous values of the DC-link voltage (v_{DC}) and grid current (i_{Grid}). The first PI controller is responsible for stabilizing the DC-link voltage by calculating the amplitude of the reference grid current. The output is multiplied by the instantaneous value of the PLL algorithm to generate a sinusoidal signal which is the reference for the grid current (i_{Grid_ref}). It should be noted that the grid voltage also needs to be measured for the functioning of the PLL algorithm, but was left out of Figure 4.2 for purposes of simplification. Nevertheless, the PLL algorithm will be described in detail in a more appropriate section.

The second PI controller is used to maintain the measured grid current (i_{Grid}) within the reference. Lastly, the output of the second PI controller will be the reference signal used in the SPWM modulation.

4.3. Modeling and Control of the Bidirectional DC-DC Converter

For the bidirectional DC-DC converter responsible for the interface of the batteries with the rest of the system, the buck-boost topology was chosen and it is presented in Figure 4.3. When the batteries are being charged, the converter operates as a buck converter with S6 being always blocked. On the other hand, when delivering the

energy stored in the batteries to the grid, it switches to a boost mode of operation with S5 being always blocked.
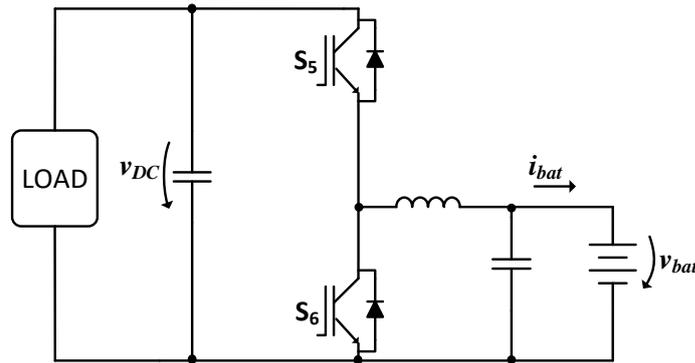
Figure 4.3 - Buck-boost bidirectional converter selected for the proposed system.

When the bidirectional DC-DC converter is working in buck mode, that is, the batteries are being charged, it is necessary to separate the control strategies depending on which stage of the charging process the battery is currently in. If the battery is in the constant current stage, the control strategy is shown in Figure 4.4. Once again, it makes use of a PI controller to force the current to follow the reference.
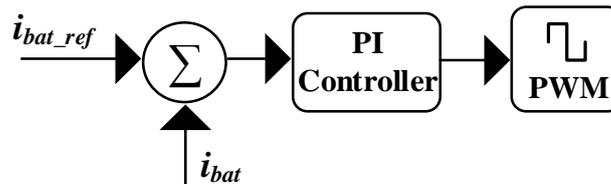
Figure 4.4 - Control algorithm for the Constant Current stage of charging.

However, if the battery is in the constant voltage stage, the controller needs to keep the battery voltage constant so the current slowly decreases. A block diagram of the controller for this case is presented in Figure 4.5.
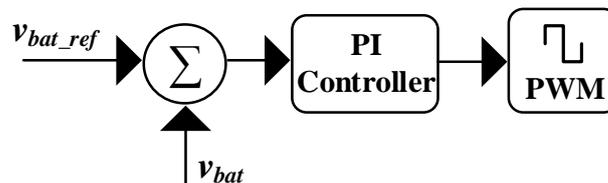
Figure 4.5 - Control algorithm for the Constant Voltage stage of charging.

Finally, if the battery is discharging its energy, it is intended that the discharging power remains constant. For that the same control algorithm showed in Figure 4.4 was used, with the difference in that the reference current is calculated in accordance with the battery voltage, meaning that the reference current should be such that the discharging power remains constant, despite the voltage of the battery decreasing. One important thing to note is that the DC-DC converter is only responsible for controlling

the charging or discharging of the batteries. As such, the DC-link voltage is maintained at 400 V by the AC-DC converter.

4.4. Modeling and Control of the DC-DC Boost Converter

For the DC-DC converter making the interface between the PV array and the rest of the system, it is not required a bidirectional power flow. That said, the decision was to choose the same topology as above. As explained, the energy will only flow from the PV array to the batteries or the grid. As such, the semiconductor S7 (buck) will be permanently open, with the current flowing through its freewheel diode, as shown in Figure 4.6.
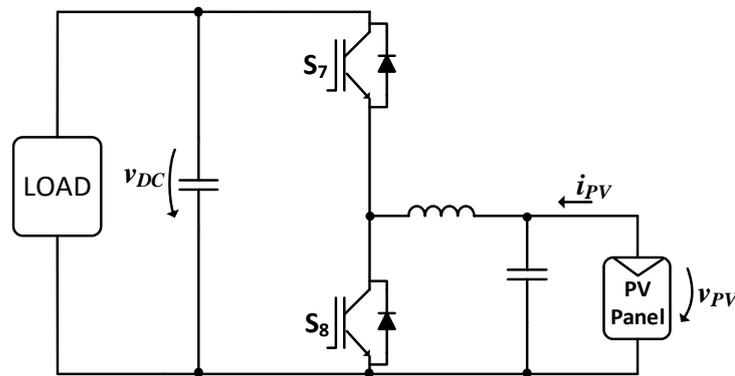
Figure 4.6 - DC-DC boost converter used in the proposed system.

This converter is only responsible for extracting the maximum power from the PV array at all times. For that, the control algorithm applied to this converter is the Incremental Conductance MPPT algorithm, explained in detail in the previous chapter.

The choice of this MPPT algorithm is due to the fact that, from all algorithms studied, this was the one that theoretically would produce the best results. The MPPT will calculate the point of maximum power and adjust the value of the duty cycle of the converter, as shown in Figure 4.7.
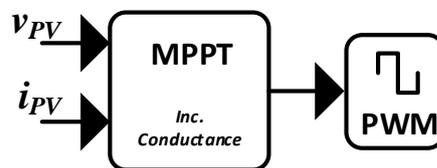
Figure 4.7 - Control algorithm for the DC-DC boost converter.

4.5. Simulations of the Proposed System

The next step on the development of the project was to validate all the different topologies and control strategies chosen for each of the 3 converters that comprise this battery charging system. This was achieved by using the simulation software PSIM.

Development of Power Converters for Electric Vehicle Charging with Photovoltaics Interface
Júlio André Machado Fernandes - University of Minho

55

This tool allows us to see the behavior of the entire system under various conditions of operation. In addition to that, it is also possible to write the code for the control algorithms in C language, which is a huge help when programming the DSC later on.

Before starting the simulations it was necessary to establish the entire system's specifications, which are presented in Table 4.1. This is extremely important because there are a number of different components, like the passive filters for the converters, which still need to be modeled.

Table 4.1 - Specifications of the system to be developed.

Nominal power	3 kW
Grid voltage RMS value	230 V
Nominal grid current	13 A
Grid frequency	50 Hz
DC-link voltage	400 V
Battery bank capacity	10 kWh
Battery bank nominal voltage	240 V
Battery bank voltage when discharged	210 V
Battery bank voltage when charged	290 V
Battery bank nominal charging current	10 A
Battery bank maximum charging current	13 A
Battery bank nominal discharging power	1.5 kW

Firstly, each converter was simulated independently and, after validating its functioning, the 3 converters were simulated simultaneously. The look of the entire system can be seen in Figure 4.8.
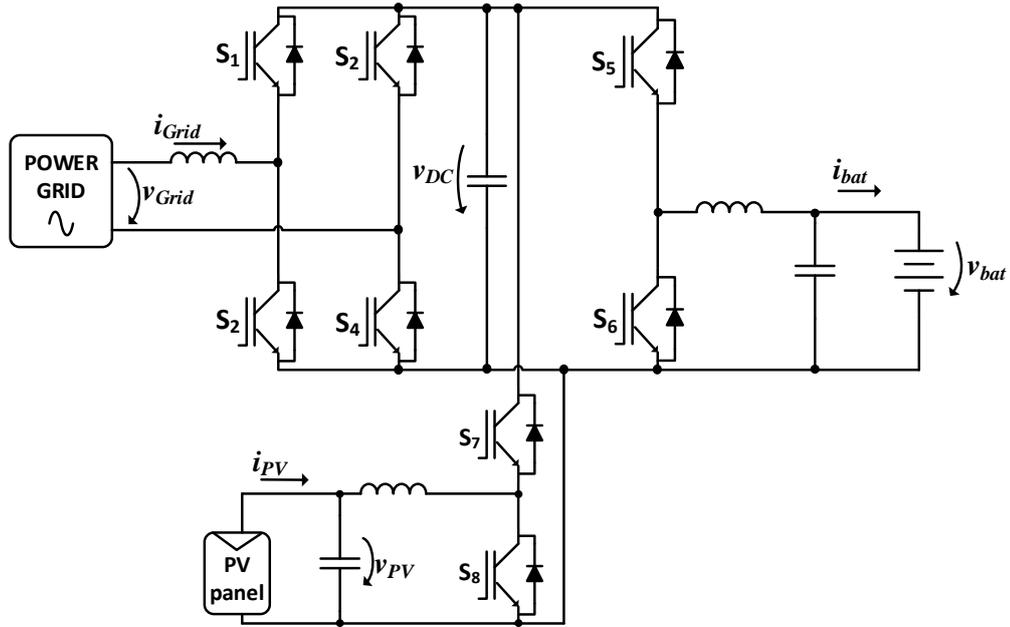
Figure 4.8 - Circuit schematic of the proposed system.

Once again, to summarize, the system is comprised of a Full-Bridge AC-DC converter which will make the interface to the power grid, a bidirectional buck-boost converter which will be responsible for controlling the charge and discharge processes of the battery pack and a DC-DC boost converter which will be responsible for interfacing the PV array with the rest of the system, while also ensuring that the PV panel is working in its MPP.

4.5.1. Modeling of the Passive Elements of the AC-DC Converter

The DC-link of a bidirectional AC-DC converter must be able to store a considerable amount of energy. In addition, it is necessary that the voltage ripple is not too high so as not to affect the correct operation of the converter. For the DC-link capacitor modeling, expression (4.1) was used [25].

$$P = 4 \times f_{grid} \times C(V_{dc} - (V_{dc}^2 - (V_{dc} - \Delta V_{dc})^2)) \tag{4.1}$$

Where:

- P is the nominal power of the converter [W];

- f_{grid} is the frequency of the grid voltage [Hz];

- C is the value of the DC-link capacitor [F];

- V_{dc} is the nominal voltage of the DC-link [V];

- ΔV_{dc} is the desired voltage ripple of the DC-link [V];

Development of Power Converters for Electric Vehicle Charging with Photovoltaics Interface
Júlio André Machado Fernandes - University of Minho

57

The converter was designed to work with a nominal power of 3 kW. As previously mentioned, the desired voltage on the DC-link is 400 V, with a voltage ripple of 5 V. Rearranging equation (4.1), the value of C can be calculated:

$$C = \frac{3000}{4 \times 50 \times (400^2 - (400-5)^2)} = 3.77 \text{ mF} \tag{4.2}$$

For the modeling of the inductor that will make the interface between the power grid and the rest of the system, certain factors need to be taken into account. As such, equation (4.3) can be used to determine the value of said inductor [57] [64]:

$$L_f = \frac{V_{dc}}{4 \times f_s \times \Delta I_L} \tag{4.3}$$

Where:

- L_f is the value of the inductor [H];

- V_{dc} is the nominal voltage of the DC-link [V];

- f_s is the switching frequency of the converter [Hz];

- ΔI_L is the desired ripple of the grid current [V];

As it was mentioned before, the nominal voltage of the DC-link is 400 V. By using a 20 kHz switching frequency with unipolar modulation, the actual switching frequency, as seen by the load, doubles. Finally, stipulating 0.5 A as the desired ripple in the current we have:

$$L_f = \frac{400}{4 \times 40000 \times 0.5} = 5 \text{ mH} \tag{4.4}$$

4.5.2. Modeling of the Battery Bank

As mentioned earlier, batteries store energy in the form of chemical energy, and so, it becomes necessary to define an electrical model in order to make possible the correct simulation of the charge and discharge processes.

As such, to simulate the EV's battery bank, a battery's equivalent Thévenin model was used [65]. The model, presented in Figure 4.9, is simple enough yet sufficient to simulate the application at hand. It is comprised by an ideal DC voltage source, a series resistor and a parallel RC circuit. The response of the RC circuit during charging and discharging can simulate the dynamic behavior of the battery.

The capacitor C_{bat} represents the battery's energy storing capacity, R_s represents the battery's series resistance, R_{dis} represents the battery's self-discharge effect and, finally, V_{bat_min} the battery's voltage when it's fully discharged.

Despite this, the model used does not account for variations of the resistors due to temperature and SoC. The model assumes that V_{bat_min} has a constant relationship with the SoC and the ohmic resistance doesn't change during charging and discharging [66].
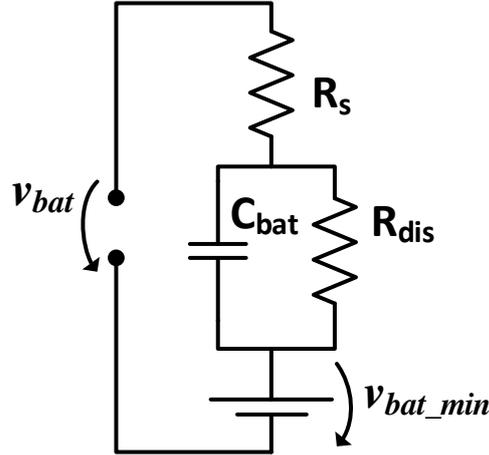
Figure 4.9 - Battery Thévenin equivalent model.

Considering the total capacity of the battery pack to be 10 kWh and the voltage when fully charged and discharged to be 290 V and 210 V, respectively, the value of the capacitor *C* can be calculate using the following expression [25]:

$$C = \frac{Ebat \times 3600 \times 1000 \times 2}{(Vmax^2 - Vmin^2)} \qquad (4.5)$$

Where:

• *C* is the value of the capacitor [F];

• *E* is the total energy capacity of the battery [kWh];

• V_{max} is the battery voltage when fully charged [V];

• V_{min} is the battery voltage when fully discharged [V].

Substituting the above values in the expression, the value of *C* is:

$$C = \frac{10 \times 3600 \times 1000 \times 2}{(290^2 - 210^2)} = 1800 \text{ F} \qquad (4.6)$$

Naturally, it would be impossible to run a simulation with a capacitance of such high value because of the time it would take for any variation in the battery voltage to be noticed. For that reason, a 1.8 F capacitor was used.

Development of Power Converters for Electric Vehicle Charging with Photovoltaics Interface
Júlio André Machado Fernandes - University of Minho

59

4.5.3. Modeling of the Passive Elements of the Buck-boost Converter

The inductor for this converter was modeled resorting to an application note from Texas Instruments in which the following equations are used to calculate the power stage of the buck-boost converter [67] [68].The minimum value for the inductor is:

$$L_f = \frac{V_{out} \times (V_{in\_max} - V_{out})}{k \times f_s \times V_{in\_max} \times I} \tag{4.7}$$

Where:

- L_f is the value of the inductor [H];

- V_{out} is the desired output voltage [V];

- V_{in_max} is the maximum input voltage [V];

- k is an estimated coefficient that represents the amount of inductor ripple current relative to the maximum output current;

- f_s is the switching frequency of the converter [Hz];

- I is the desired maximum current [A].

For the coefficient k, [67] recommends a value between 0.2 and 0.4. Considering the voltage from the DC-link as the input voltage and 290 V as the maximum output voltage, the value of the inductor can be calculated.

$$L_f = \frac{290 \times (400 - 290)}{0.2 \times 20000 \times 400 \times 13} = 1.21 \text{ mH} \tag{4.8}$$

For the capacitor that will make the other half of the passive LC filter of this converter, the following equation was used:

$$C_f = \frac{D_{max} \times I}{f_s \times \Delta V} \tag{4.9}$$

Where:

- C_f is the value of the capacitor [F];

- f_s is the switching frequency of the converter [Hz];

- I is the desired maximum current [A];

- D_{max} is the maximum value of duty-cycle;

- ΔV is the desired voltage ripple [V].

60

Development of Power Converters for Electric Vehicle Charging with Photovoltaics Interface
Júlio André Machado Fernandes - University of Minho

The value of duty-cycle, for protection reasons, was limited to 90%. For a voltage ripple of 2 V, we have:

$$C_f = \frac{0.9 \times 20}{20000 \times 2} = 292.5 \text{ uF} \tag{4.10}$$

4.5.4. Modeling of the PV array

Although the system to be developed wasn't designed for any specific model of a PV panel, PSIM provides a utility tool in which real datasheet parameters from the manufacturers can be inserted and the tool automatically calculates the simulation parameters to be placed inside the Solar Module. As such, the model chosen was the KD215GX from Kyocera, shown in Figure 4.10.

Figure 4.10 - Kyocera KD215GX PV panel [69].

The datasheet parameters can be found in PSIM's examples library. In Figure 4.11 are presented its I-V and P-V curves.

(a)   (b)
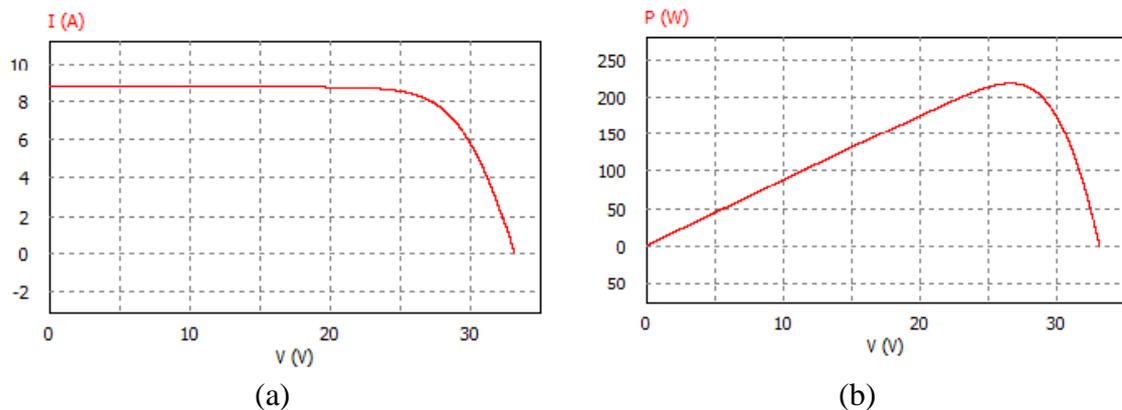
Figure 4.11 - Kyocera KD215GX PV panel's: (a) I-V curve; (b) P-V curve.

Each panel has a maximum power of 215 W. In order to boost the output voltage, the number of panels was multiplied by 7. In reality, this is equivalent to connecting

Development of Power Converters for Electric Vehicle Charging with Photovoltaics Interface
Júlio André Machado Fernandes - University of Minho

61

7 panels in series. As such, a maximum total of roughly 1.5 kW can be extracted from the PV panel with an intensity of 1000 W/m^2 and a reference temperature of 25 °C [69].

4.5.5. Modeling of the Passive Elements of the Boost Converter

The modeling of the passive LC filter used in the boost converter responsible for extracting the maximum power from the PV array was also based on an application note from Texas Instruments [70]. The following equation can be used to determine the minimum value of the inductor:

$$L_f = \frac{V_{in} \times (V_{out} - V_{in})}{\Delta I \times f_s \times V_{out}} \tag{4.11}$$

$$\Delta I = \frac{k \times I_{out\_max} \times V_{out}}{V_{in}} \tag{4.12}$$

Given that the PV array, when working with at maximum power, will have a voltage of around 187 V and a current of 8.23 A, the minimum value of the inductor is:

$$\Delta I = \frac{0.2 \times 8.23 \times 400}{187} = 3.5 \text{ A} \tag{4.13}$$

$$L_f = \frac{187 \times (400 - 187)}{3.5 \times 20000 \times 400} = 1.42 \text{ mH} \tag{4.14}$$

4.5.6. Microcontroller Implementation

To simulate the behavior of a microcontroller in PSIM, the C Block was used. This function block allows the user to program in C language, thus simulating an actual microcontroller. More than one C Block can be used in the same simulation. This is useful because it is possible to use one C Block for each controller, ultimately making it easier to find any problems code related. Figure 4.12 shows the different controllers implemented in PSIM using the C Block To the inputs are connected the measurements from the sensors and the outputs are the command variables that will be used to generate the PWM signals to be applied to the gates of the semiconductors. The sampling frequency was set at 20 kHz by using the Zero-Order-Hold block.

```
37    Vgrid=in[0];
38    Igrid=in[1];
39
40    // DC-LINK REGULATION
41    kp_dc=0.0005;
42    ki_dc=(0.00675);
43
44        Vdc_erro=(400)-Vdc;
45        Vdc_soma_erro+=Vdc_erro;
46
47
48        Ireg=kp_dc*Vdc_erro + ki_dc*Vdc_soma_erro;
49
50        Iref = Ireg*Vgrid;
51
52  /*  if(Iref > 40) Iref =40;
53        else if(Iref<40) Iref=40;
54  -*/
55        If_erro = Iref-Igrid;
56
57        DT - Tf orro:
```
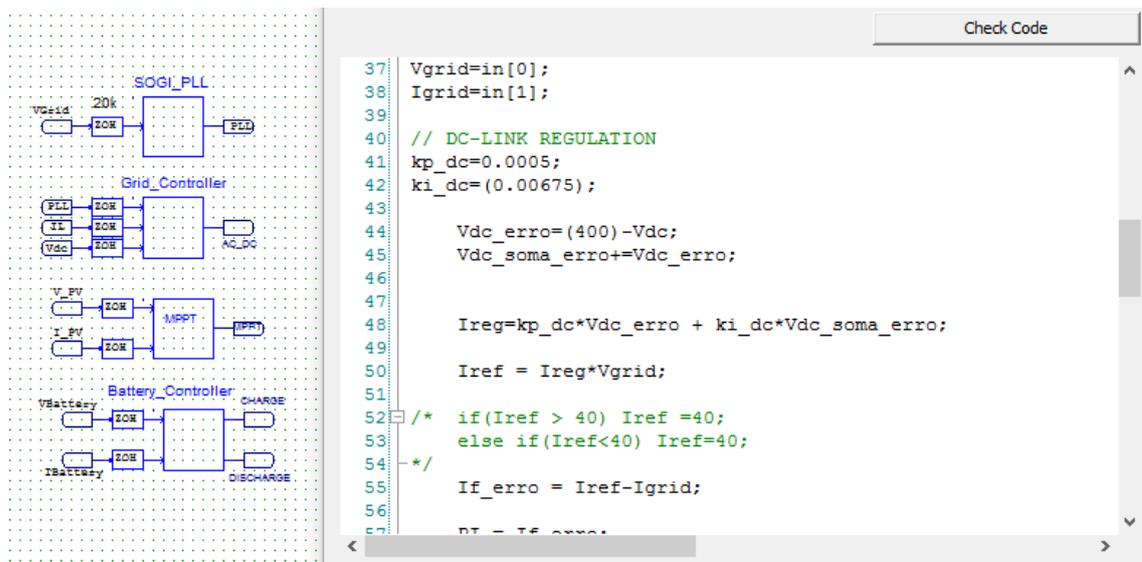
Figure 4.12 - Digital controllers of the converters implemented in PSIM using the C Block.

The frequency of the PWM used was also 20 kHz for every converter. For the AC-DC converter, unipolar SPWM modulation was used. The signals are applied to the gates of the switches S1-S4. For the bidirectional DC-DC converter each semiconductor has a different control signal. When discharging the batteries, the PWM signal is applied to the gate of S6 (S5 is blocked). When charging the batteries, the PWM signal is applied to the gate of S5 (S6 is blocked). Finally, for the unidirectional DC-DC converter, as shown in Figure 4.13, the PWM signal is applied to the gate of S8, with S7 always working as a diode (always blocked).
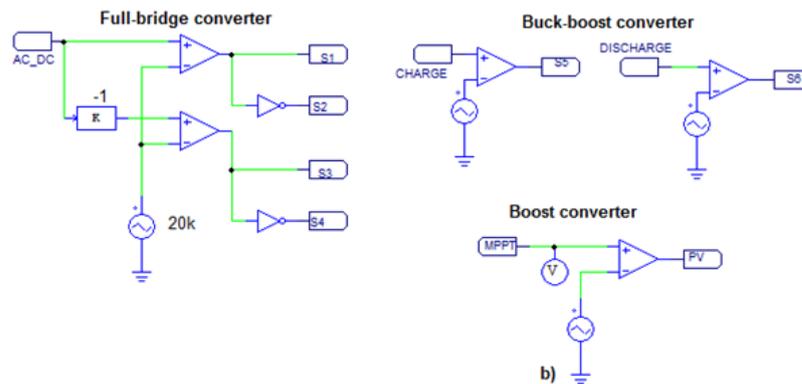
Figure 4.13 - PWM generators for the converters in PSIM.

4.6. Simulation Results of the Proposed System

With all the necessary elements modeled, it was possible to finally simulate the system to be developed and validate the different topologies and control strategies that were employed. As such, the results of the simulations will be presented and analyzed below.

Development of Power Converters for Electric Vehicle Charging with Photovoltaics Interface
Júlio André Machado Fernandes - University of Minho

63

4.6.1. Phase Locked Loop (PLL)

For the correct operation of the Full-Bridge AC-DC converter, which will be connected to the power grid, it is necessary to have a synchronization mechanism with the grid voltage. That can be achieved by making use of a PLL. A PLL is a closed loop in which an oscillator is controlled to follow the phase of an external signal. The quality of the implementation, naturally, affects the performance of the converter's control system. In this case, a Second Order Generalized Integrator (SOGI) PLL, as proposed in [71] and whose block diagram is shown Figure 4.14, was used.
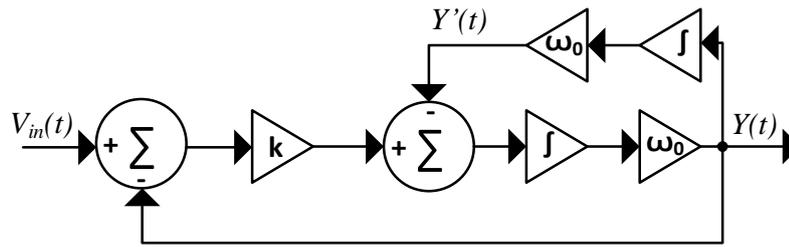
Figure 4.14 - Block diagram of the SOGI PLL.

The outputs of the SOGI PLL are two orthogonal signals (Y and Y'), meaning that the signals have a 90° phase shift between them. As such, the value of the signal's peak amplitude of the fundamental can be calculated using the following expression:

$$V_{1\_Grid\_pk} = \sqrt{Y(t)^2 + Y'(t)^2} \tag{4.15}$$

From there, the RMS value of the fundamental can be calculated by using the expression:

$$V_{1\_Grid\_RMS} = \frac{V_{1\_Grid\_pk}}{\sqrt{2}} \tag{4.16}$$

The proposed PLL algorithm was simulated in PSIM in which the responses to various disturbances were tested. The simulation results are presented in Figure 4.15, in which the waveforms of the grid voltage and the generated output from the PLL can be seen.
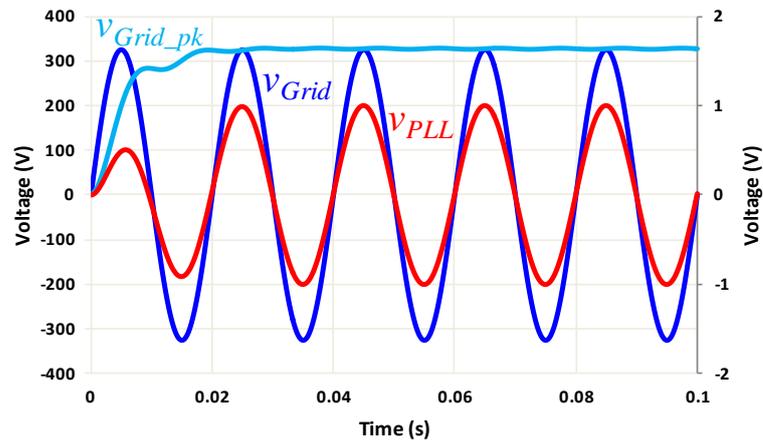
Figure 4.15 - Grid voltage and PLL output simulation results.

It can be seen that after no more than two cycles of the grid voltage the synchronization is established. However these results were obtained with an ideal sinusoidal input voltage, without harmonic distortion. As such, the PLL algorithm was also simulated in a more realistic scenario with the presence of harmonics in the grid voltage. The results are shown in Figure 4.16.
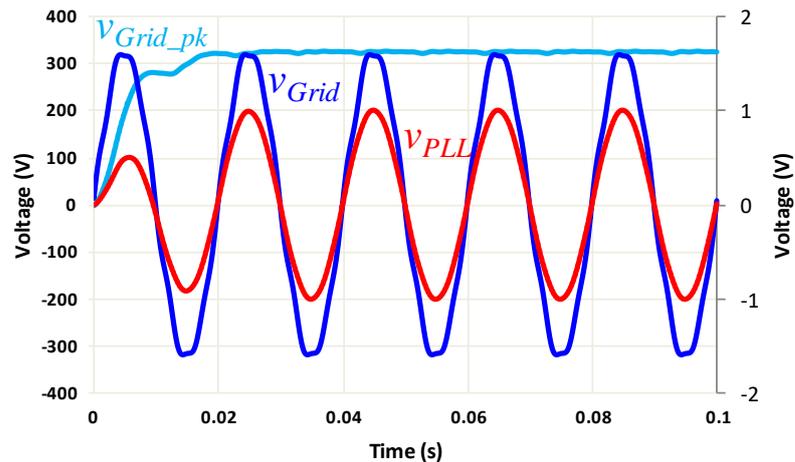
Figure 4.16 - PLL response to the presence of harmonic distortion in the input signal.

Figure 4.16 allows concluding that the algorithm can successfully generate a sinusoidal signal despite the input signal being distorted. In reality, the grid voltage can have variations of up to 10% of its nominal value (230 V) and the frequency has a 1% tolerance in regard of the nominal value (50 Hz). As such, a simulation was made in which the goal was to see the behavior of the PLL when the fundamental frequency of the grid voltage was diverted in 1% from 50 Hz, which is an admissible value. In addition to that, a voltage sag was provoked. The results are presented in Figure 4.17 and it can be seen that these deviations do not compromise the performance of the algorithm.

Development of Power Converters for Electric Vehicle Charging with Photovoltaics Interface
Júlio André Machado Fernandes - University of Minho

65
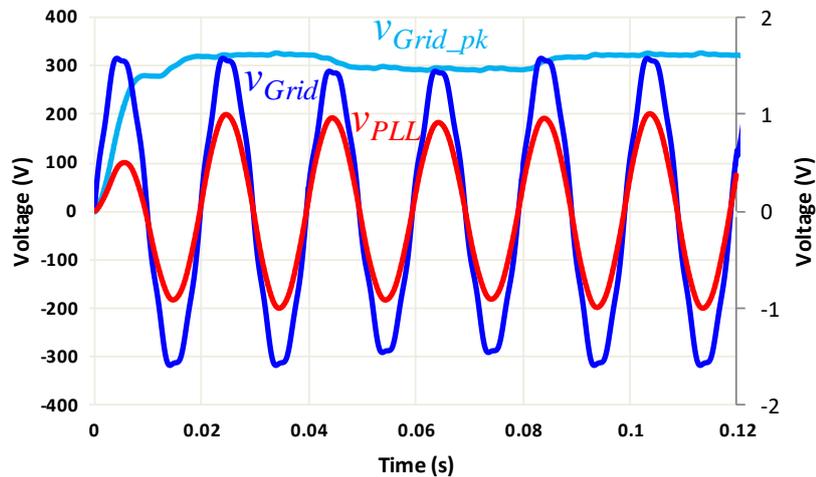
Figure 4.17 - PLL response to a fundamental frequency of 50.5 Hz and a voltage sag.

These deviations seen in the grid voltage amplitude are mainly caused by the connection and/or disconnection of loads from the power grid. However, due to the line impedance, these voltage fluctuations can originate a phase shift on the voltage. To simulate this, a 50° phase shift was introduced on the grid voltage. Figure 4.18 shows the resulting waveforms in which it can be seen that the PLL algorithm successfully synchronizes with the grid voltage despite the phase shift.
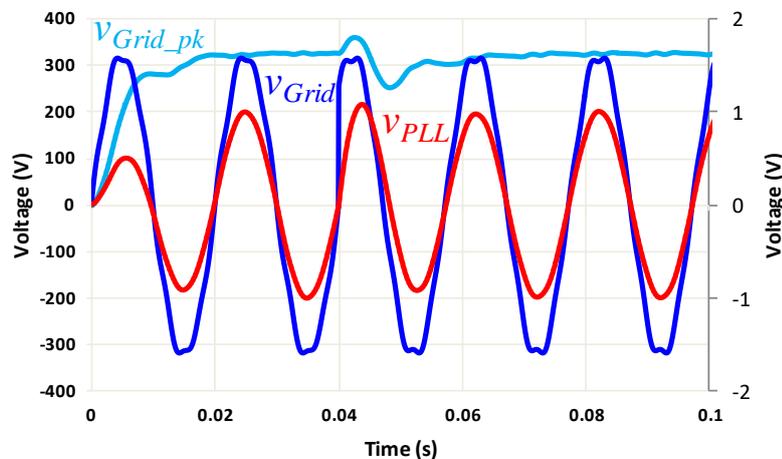
Figure 4.18 - PLL response to a phase shift of the grid voltage.

4.6.2. Bidirectional Buck-Boost Converter Simulations

As it was previously mentioned, the bidirectional buck-boost converter is responsible for controlling the battery charge and discharge processes. As mentioned before, when it is intended to charge the batteries, the converter will operate in buck mode, stepping down the DC-link voltage to a level suitable for the batteries. In Figure 4.19, it is shown the simulated circuit when the converter is working in buck mode.
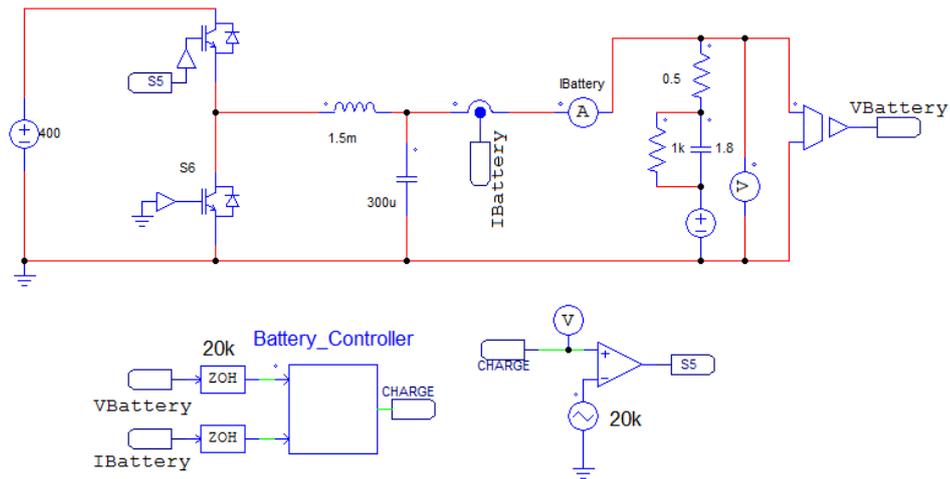
Figure 4.19 - PSIM implementation of the bidirectional buck-boost converter in buck mode.

In this case it was intended to charge the batteries with a constant current of 10 A. The battery pack is initially charged with 65 V (v_{bat} = 275 V) and the DC source in the DC-link represents the AC-DC converter maintaining a constant 400 V. The results were positive and are presented in Figure 4.20. From the analysis of the figure it's possible to conclude that the batteries are in fact being charged, given the rise in the battery's voltage, with a constant current of 10 A. Also, the transition between the constant current and constant voltage charging methods is evident. In this case, it can be seen that the voltage at the batteries' terminals are kept constant while the current slowly decreases.
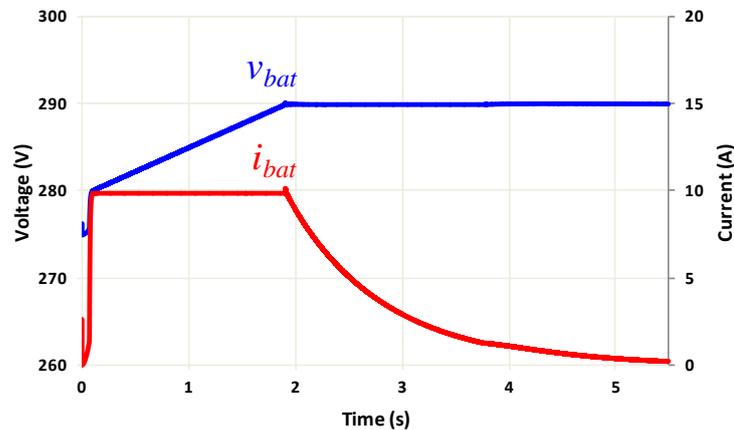
Figure 4.20 - Battery voltage (v_{bat}) and current (i_{bat}) during constant current and constant voltage charge.

If a closer look is taken into the battery current, it can be seen that the charging current is practically constant. This is achieved by the use of the passive filters previously calculated.

Development of Power Converters for Electric Vehicle Charging with Photovoltaics Interface
Júlio André Machado Fernandes - University of Minho

67
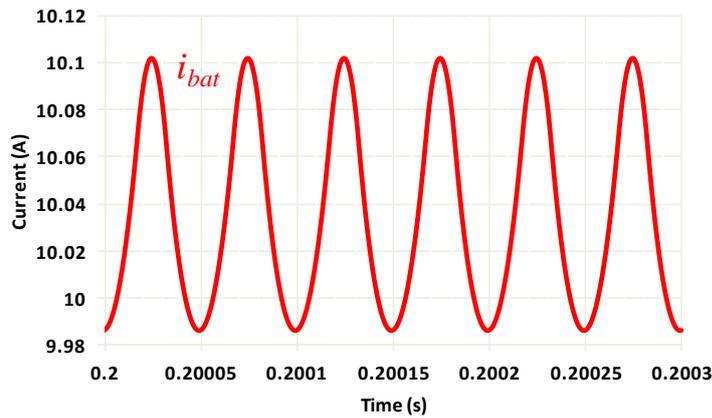
Figure 4.21 - Battery current ripple during charge.

To simulate the boost mode of operation, that is, when the batteries are being discharged, was used in PSIM the schematic presented in Figure 4.22. In this case, the battery pack is initially fully charged (V_{bat} = 290 V) and it was intended to discharge it with a constant power of 1.5 kW. The controller should be able to adapt the value of the reference current in order to compensate the decreasing of the battery voltage, thus maintaining a constant discharge power. In this case, the capacitor that represents the battery capacity was changed to 200 mF. The reason for that lies in the fact that with a 1.8 F capacitor, as it was its calculated value, it would take much time before the voltage would decrease low enough to notice any changes in the discharging current.
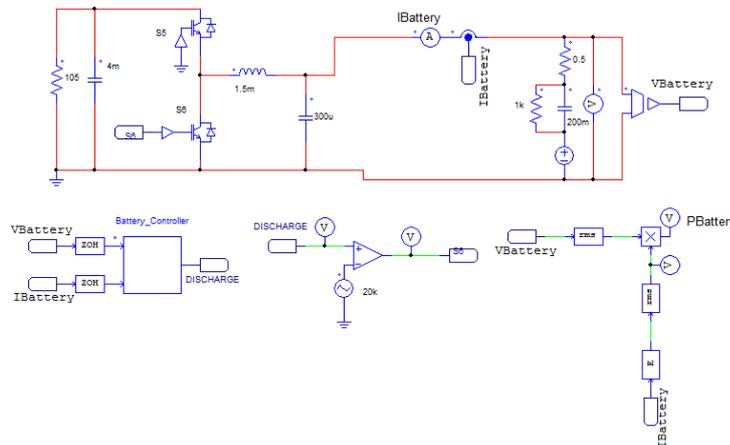
Figure 4.22 - PSIM implementation of the bidirectional buck-boost converter in boost mode.

The results of the simulation are presented in Figure 4.23 and Figure 4.24. In the first figure, it can be seen that the batteries are effectively being discharged as the voltage at their terminals starts to decrease. The discharge current tends to rise (in absolute value) in order to make up for the decrease of the voltage.
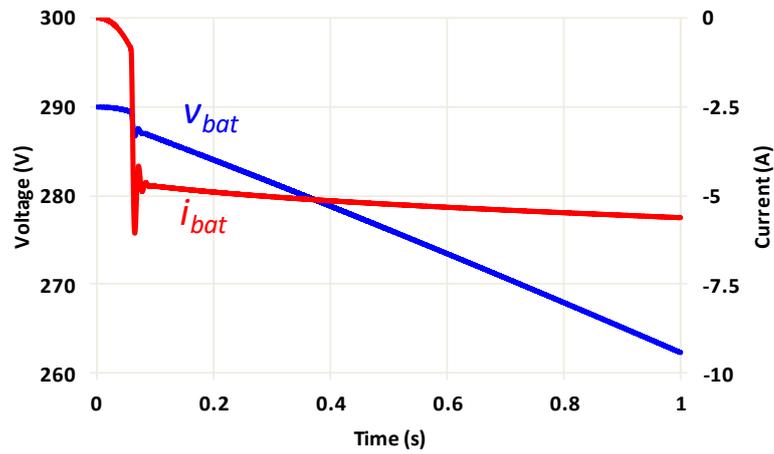
Figure 4.23 - Battery voltage (v_{bat}) and current (i_{bat}) during constant power discharge.

Figure 4.24 shows the average value of the measured power of the battery. It can be seen that the discharge power is kept constant at 1.5 kW.
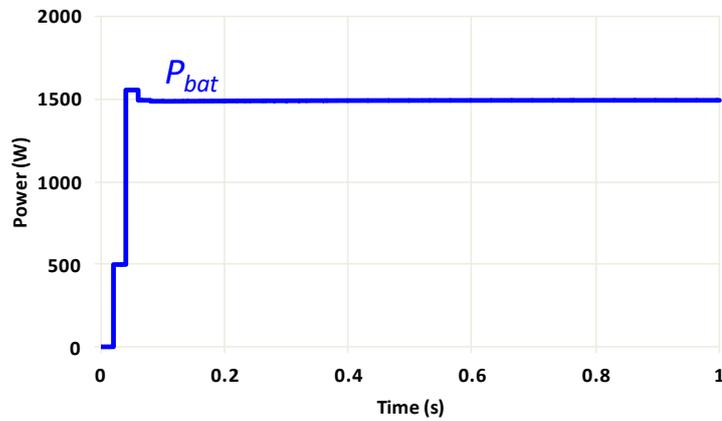
Figure 4.24 - Average value of the discharge battery power (P_{bat}).

Finally, in Figure 4.25, a closer look at the battery current is taken. Like in the buck mode of operation, the discharging current is kept practically constant, with a ripple of 0.1 A.
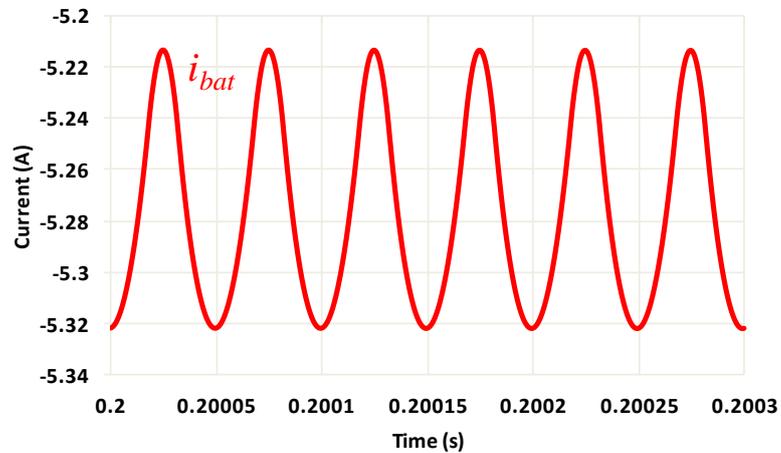
Figure 4.25 - Battery current ripple during discharge.

Development of Power Converters for Electric Vehicle Charging with Photovoltaics Interface
Júlio André Machado Fernandes - University of Minho

69

4.6.3. Boost Converter Simulations

In Figure 4.26 it is presented the PSIM implementation of the boost converter responsible for extracting the maximum power from the PV array. As it was mentioned previously, the PV module selected for the simulation was the Kyocera KD215GX with 7 panels connected in series.
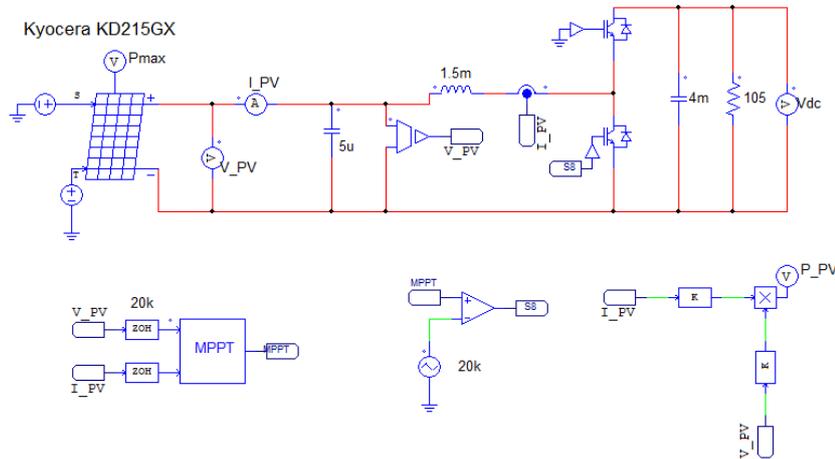
Figure 4.26 - PSIM implementation of the boost converter.

Initially, the simulations were made with a constant value of radiation of 1000 W/m^2 and a reference module temperature of 25 °C. The extracted power from the PV array can be seen in Figure 4.27.

(a)

(b)
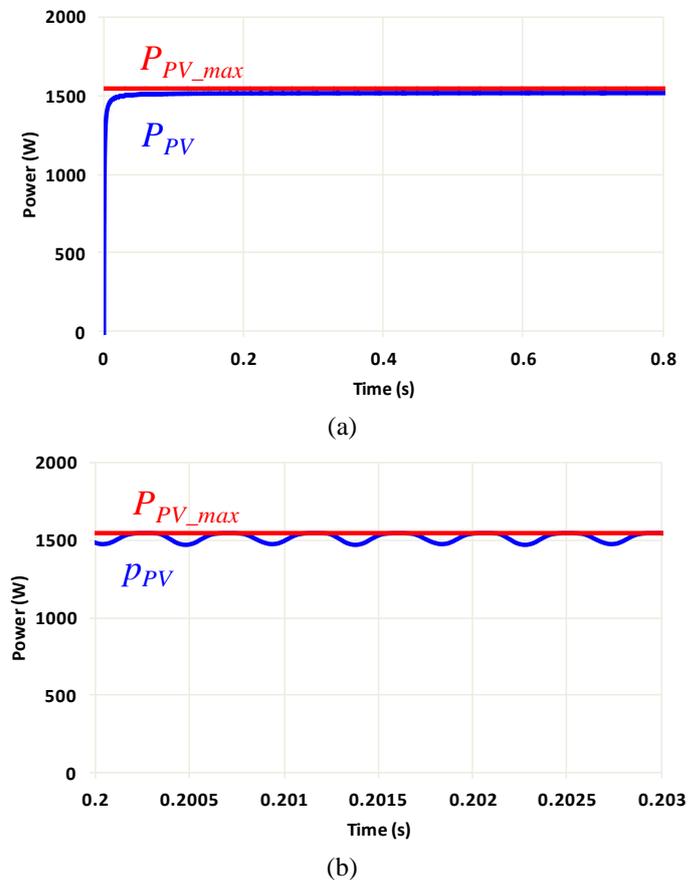
Figure 4.27 - Extracted power from the PV array: (a) Average power (P_{PV}); (b) Instantaneous power (p_{PV}).

The analysis of the above waveforms allows concluding that, for a constant value of radiation, the MPPT controller quickly finds the maximum power point. To note, the oscillation around the MPP is mitigated due to the passive LC filter that was designed earlier in this chapter. However, it is impossible to completely eliminate this oscillation, due to the nature of the utilized MPPT algorithm. In an effort to simulate real life conditions, the value of the intensity of solar radiation was varied over time. This simulates the different times of day where the amount of sun light that hits the PV array is not constant. The MPPT algorithm should adapt to the change and quickly find the new maximum power point. The results of the simulation are presented in Figure 4.28, in which the response of the MPPT controller to the variations of solar irradiance can be seen.
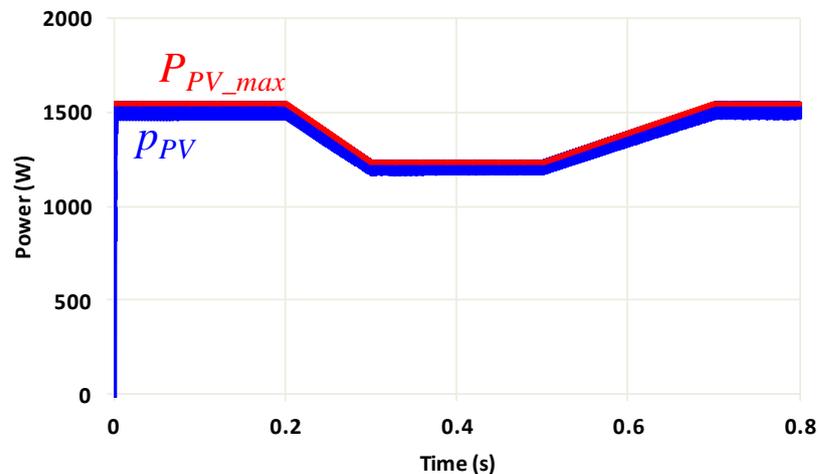
Figure 4.28 – Extracted power from the PV array (p_{PV}) in response to variations of solar radiation.

It can be seen that the control system quickly adapts to the change in radiation and the power extracted from the PV array is very close to the maximum power available. It is important to note that in reality the variations of maximum power (i.e. solar radiation) are not as abrupt as the ones that were simulated. However these simulations provide useful information regarding the controller's response time.

4.6.4. AC-DC Converter Simulations

As mentioned in previous chapters, the AC-DC Full-Bridge converter is responsible for making the interface between the power grid and the rest of the system. This converter was designed for a power of 3 kW and will work as a rectifier when charging the batteries and as a VSI when receiving energy from both the battery and the PV array. The PSIM implementation of this converter, as a rectifier, is shown in Figure 4.29.

Development of Power Converters for Electric Vehicle Charging with Photovoltaics Interface
Júlio André Machado Fernandes - University of Minho

71
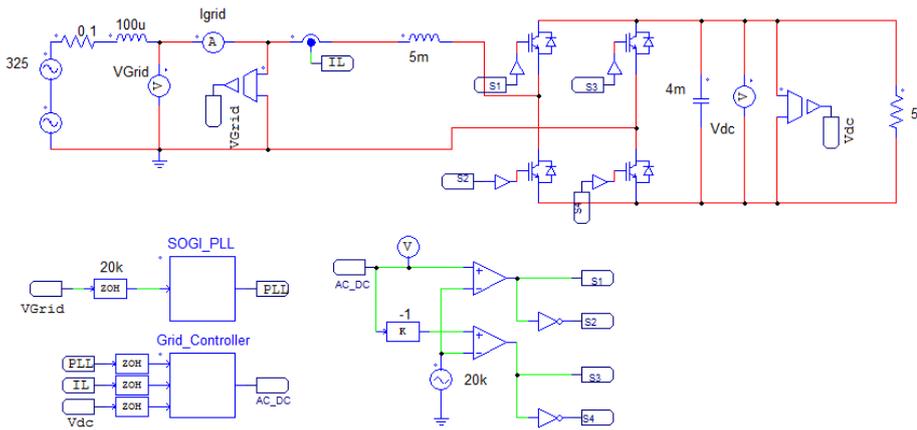
Figure 4.29 - PSIM implementation of the AC-DC converter, in rectifier mode.

The results of the simulations are presented in Figure 4.30. It is intended for the grid current to remain sinusoidal and in phase with the voltage and also for the DC-link voltage to be regulated around 400 V, with a low value of ripple. Harmonics were introduced in the grid voltage to make the simulation as close as possible of real life conditions.

(a)

(b)
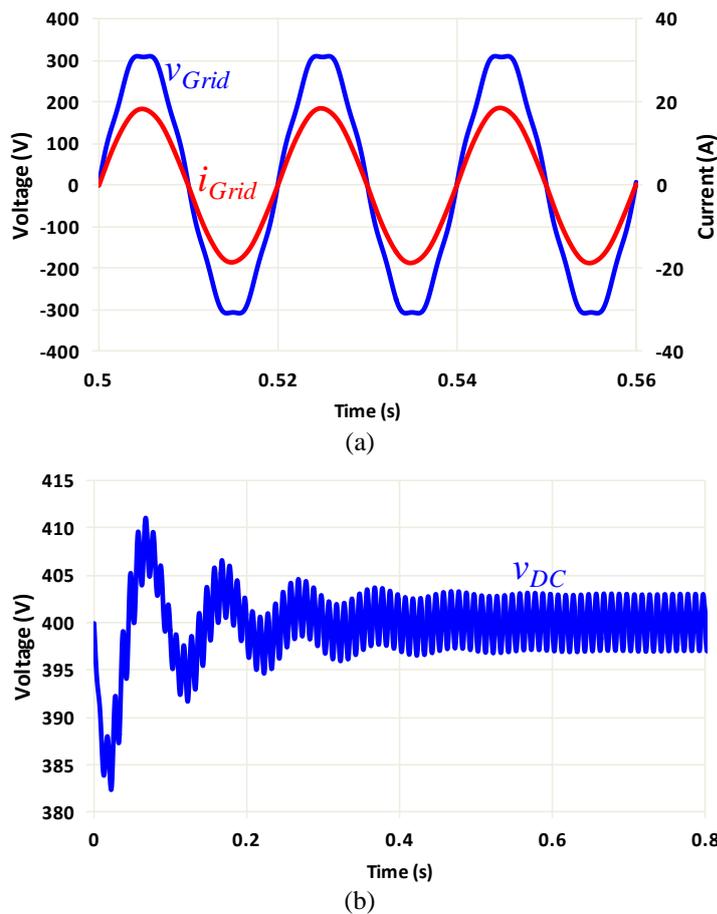
Figure 4.30 - Simulation results of the AC-DC operating as a rectifier: (a) Grid voltage (v_{Grid}) and current (i_{Grid}); (b) DC-link voltage (V_{DC}).

It can be seen that the current is sinusoidal, despite the voltage being distorted, and in phase with the latter. The current has a low TDH value, with a measured value of

1.3% which is a reasonable value. The RMS value of the current is 12.8 A which means the load is drawing 2.94 kW from the grid. Also the DC-link is kept constant at 400 V with a voltage ripple of 3 V.

To simulate the converter working as a VSI, the schematic shown in Figure 4.31 was used. In this particular case, the converter is working without being coupled to the power grid, supplying a 3 kW load.
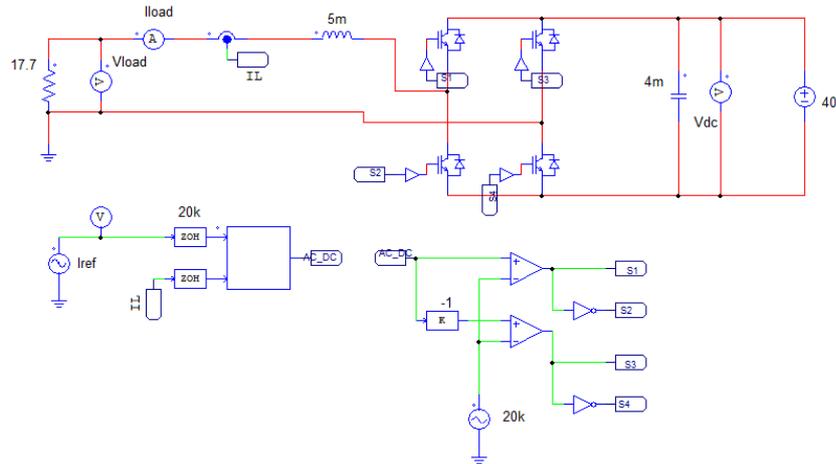
Figure 4.31 - PSIM implementation of the AC-DC converter in VSI mode.

It is clear from the analysis of Figure 4.31 that in this case, as the converter is operating off-grid, the PLL algorithm cannot be used. The solution is to implement in the DSC a sinusoidal signal which will act as the reference current. In this case, in order to simplify the simulation, a sinusoidal voltage source was used instead. The results of the simulation are presented in Figure 4.32. It is intended for the current to be sinusoidal but, this time it should be 180° out of phase with the voltage, as the energy is flowing from the DC-link to the load.
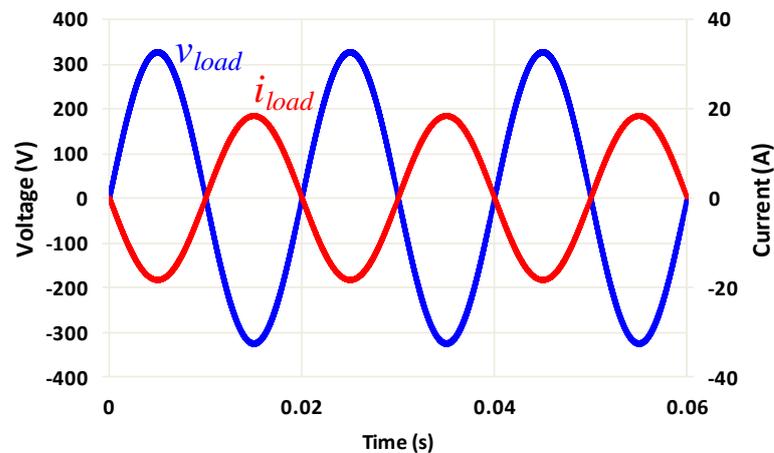
Figure 4.32 – Load voltage (v_{load}) and current (i_{load}) when the AC-DC converter is operating as an off-grid VSI.

Development of Power Converters for Electric Vehicle Charging with Photovoltaics Interface
Júlio André Machado Fernandes - University of Minho

73

As it can be seen, the current delivered to the resistive load is sinusoidal with a RMS value of 13 A and the load voltage has a RMS value of 230 V, which translates into an active power of 3 kW being delivered to the load.

The last simulation made was with the converter now operating as a grid tied VSI. This simulates the mode when the energy will be injected into the power grid. Once again, grid synchronization is essential and harmonics were added to the grid voltage. The simulated circuit is shown in Figure 4.33.
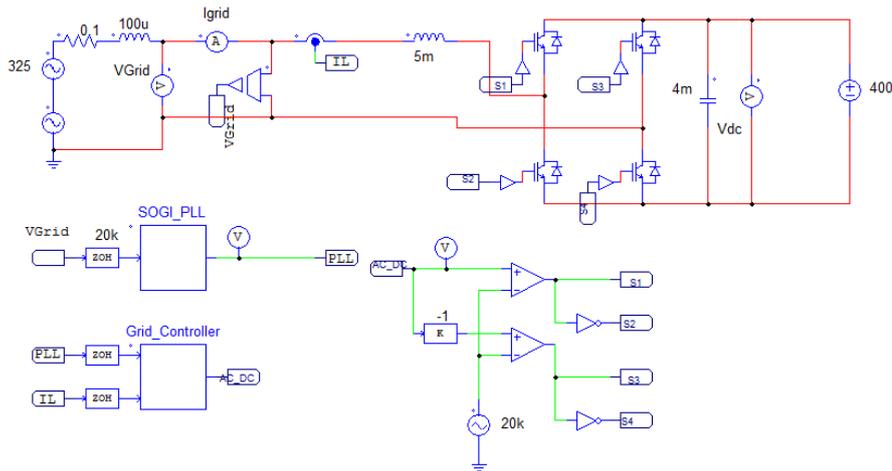
Figure 4.33 - PSIM implementation of the AC-DC converter working as a grid tied VSI.

It is desired that the current flowing through the inductor will be sinusoidal and in phase opposition with the grid voltage. The results of the simulation can be seen in Figure 4.34, where the waveforms of the grid voltage, current and also the reference current are shown. It can be seen that despite the harmonic distortion present in the voltage, the current is sinusoidal with a value of THD of 1.4%. Also the RMS value of the current is 12.9 A, which means that a total power of almost 3 kW is being injected into the grid.
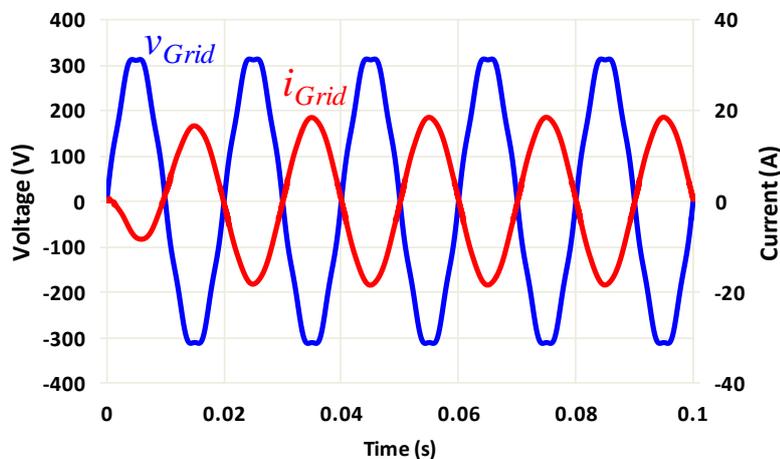
Figure 4.34 - Grid voltage (v_{Grid}) and current (i_{Grid}) when the AC-DC converter is operating as a grid tied VSI.

74

Development of Power Converters for Electric Vehicle Charging with Photovoltaics Interface
Júlio André Machado Fernandes - University of Minho

4.6.5. PV to Grid Simulation Results

So far, each of the converters that make this Battery Charging System was simulated individually and all of them have been validated. As such, the next step was to simulate all of the converters working together. In Figure 4.35 it is shown the PSIM implementation in which the power extracted from the PV array will be injected into the grid. This also simulates a situation in which no EV is connected to the system so all the power from the PV array should go to the power grid.
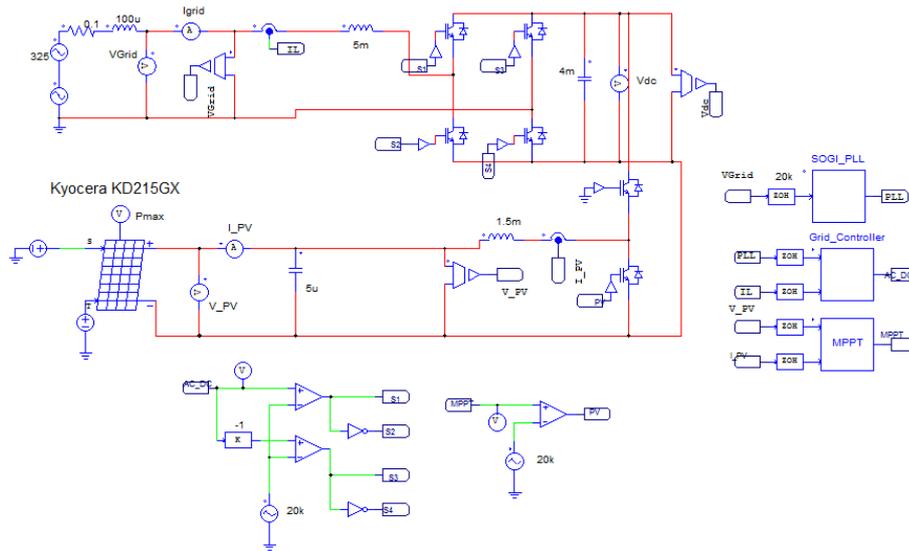
Figure 4.35 - PSIM implementation of the PV to grid operation.

As mentioned above, the MPPT algorithm should extract the maximum power from the PV array and the energy should be injected into the power grid. For that, it is desired a sinusoidal current in the power grid side, in phase opposition with the voltage. The results are presented in Figure 4.36 and Figure 4.37. In Figure 4.36, the waveforms for the grid current and voltage are shown.
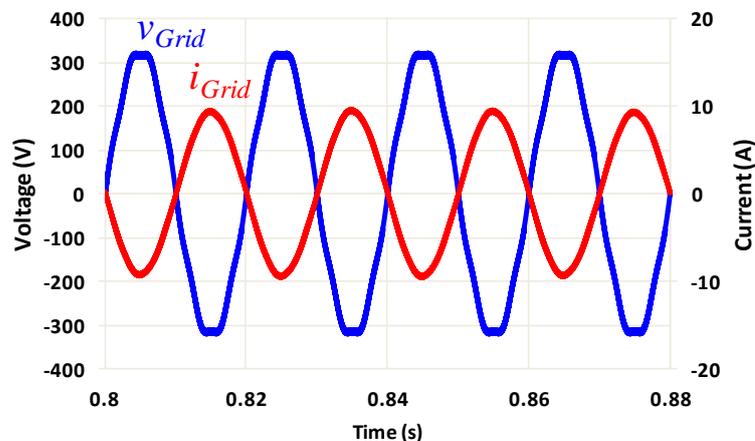
Figure 4.36 - Grid voltage (v_{Grid}) and grid current (i_{Grid}) during PV to grid operation.

Development of Power Converters for Electric Vehicle Charging with Photovoltaics Interface
Júlio André Machado Fernandes - University of Minho

75

As expected, the current is 180° out of phase with the voltage confirming that energy is being injected into the grid. Figure 4.37 shows the extracted power from the PV array and also the evolution of the DC-link voltage over time.
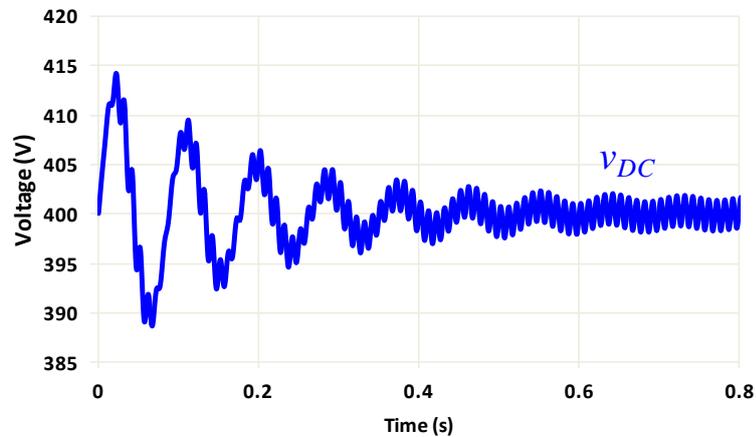
(a)
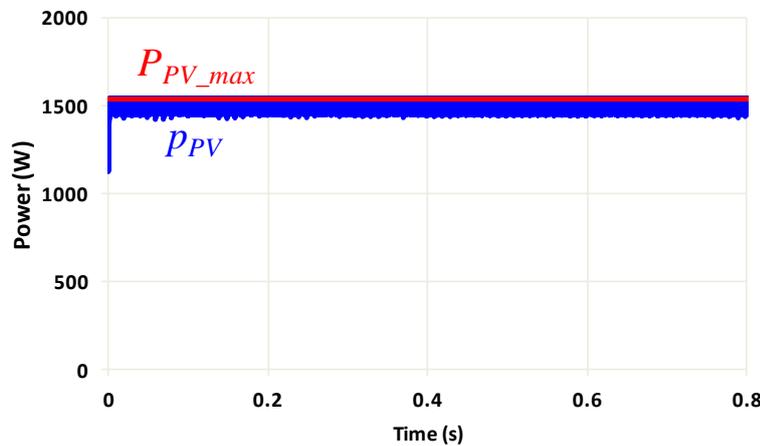
(b)

Figure 4.37 - Simulation results of the PV to Grid operation: (a) DC-link voltage (v_{DC}); (b) extracted power (p_{PV}) and maximum power (P_{PV}).

It can be seen that the controller also successfully regulates the DC-link voltage around 400 V and the energy extracted from the PV array is injected into the power grid. It is important to note that a portion of the power generated by the PV array is used for the regulation of the DC-link.

4.6.6. Complete System Simulations

The last step of the whole simulation process was to simulate the entire proposed system in which the 3 previously simulated converters all work together. The PSIM implementation of the complete system can be seen in Figure 4.38.
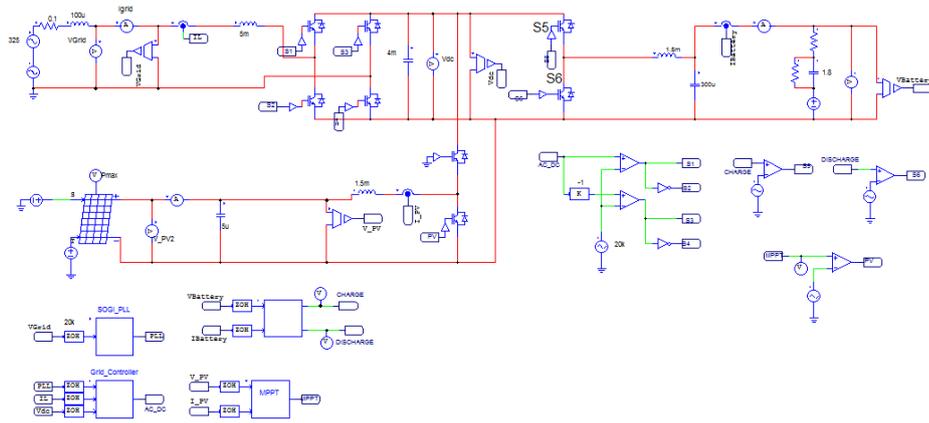
Figure 4.38 - PSIM implementation of the Battery Charging System.

In this stage simulations were made for a variety of operation modes under different circumstances. Firstly, the Vehicle-To-Grid (V2G) mode was simulated. In this mode, both the PV array and the batteries, inject energy into the grid. The batteries are initially fully charged (V_{bat} = 290 V) and the PV array can generate a maximum power of 1.5 kW, considering the values of intensity of solar radiation and cell temperature used (1000 W/m^2 and 25 °C, respectively). The batteries will be discharged with a constant power of 1.5 kW, which means that a total power of 3 kW should be injected into the power grid. The waveforms resulting from the simulation are shown in Figure 4.39 and Figure 4.40.
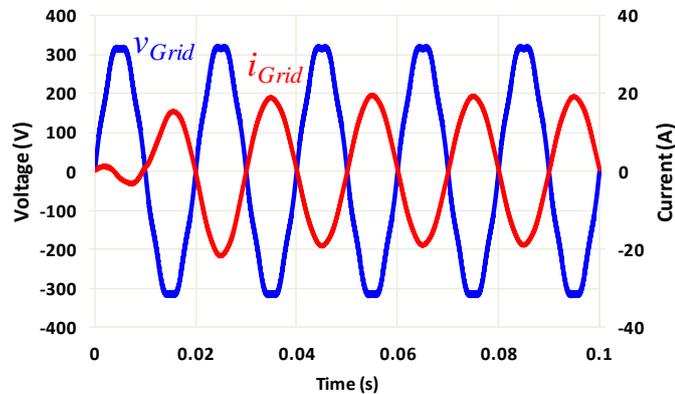

(a)
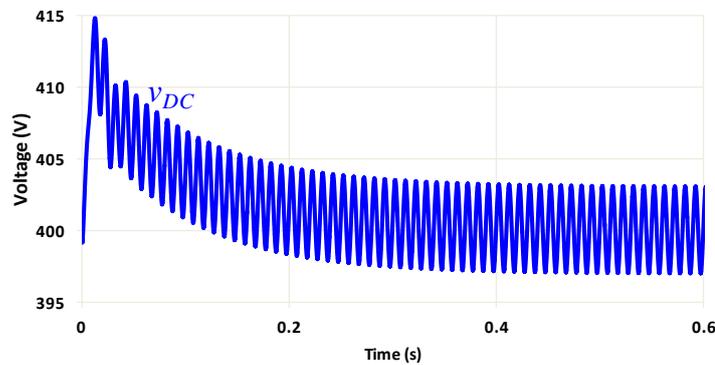
(b)

Figure 4.39 - Simulations results of the V2G operation: (a) Grid voltage (v_{Grid}) and current (i_{Grid}); (b) DC--link voltage (v_{DC}).

Development of Power Converters for Electric Vehicle Charging with Photovoltaics Interface
Júlio André Machado Fernandes - University of Minho

77
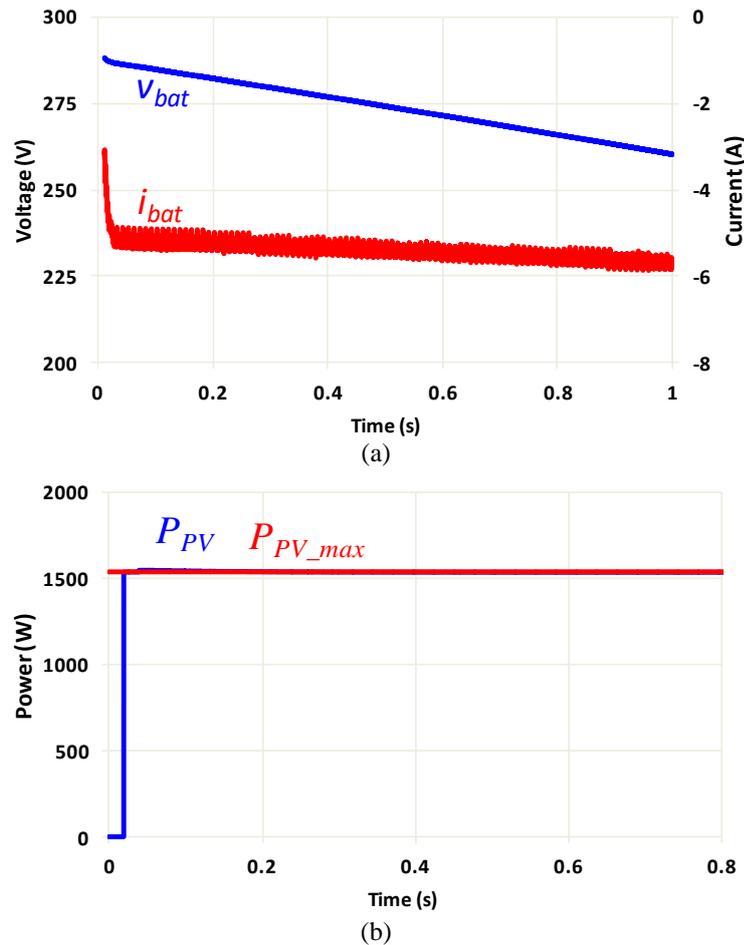
Figure 4.40 - Simulation results of the V2G operation: (a) Battery voltage (v_{bat}) and current (i_{bat}); (b) Average values of the maximum power (P_{PV_max}) and extracted power (P_{PV}) from the PV array.

The resulting waveforms show that, during V2G operation, the batteries are indeed discharged. The discharging current slowly increases (in absolute value) to maintain a constant discharging power and it is practically constant with a measured ripple of 0.3 A. Due to the oscillations of the DC-link voltage, the battery current acquires a ripple component at 100 Hz with an amplitude of almost 0.1 A. In addition, the battery current also possesses the ripple component at 20 kHz, which is the switching frequency. Regardless, the obtained results are satisfactory. Also, it can be seen that the MPPT controller is working correctly, extracting the maximum power available throughout the simulation time.

Considering the Grid-to-Vehicle mode of operation, this mode can be divided into two distinct situations- on one hand, if the PV array can't generate enough power to charge the batteries, then the remaining power should be drawn from the grid. On the other hand, in a situation where the intensity of solar radiation is such that the power extracted from the PV array is higher than the one required charging the batteries, the PV array should charge the batteries and inject the exceeding energy into the grid. As such, the first simulations were made considering the first case above

mentioned. The battery pack is initially fully discharged (v_{bat} = 210 V) and, like in past simulations, it is intended to charge it with a constant current of 10 A. The value of solar radiation used for this particular case was 1000 W/m^2 which means that the current is around 8.2 A. Considering this, it is expected that the grid provide assistance to the charging process by delivering the rest of the power needed to charge the batteries within the specified conditions. The simulation results are displayed in Figure 4.41.
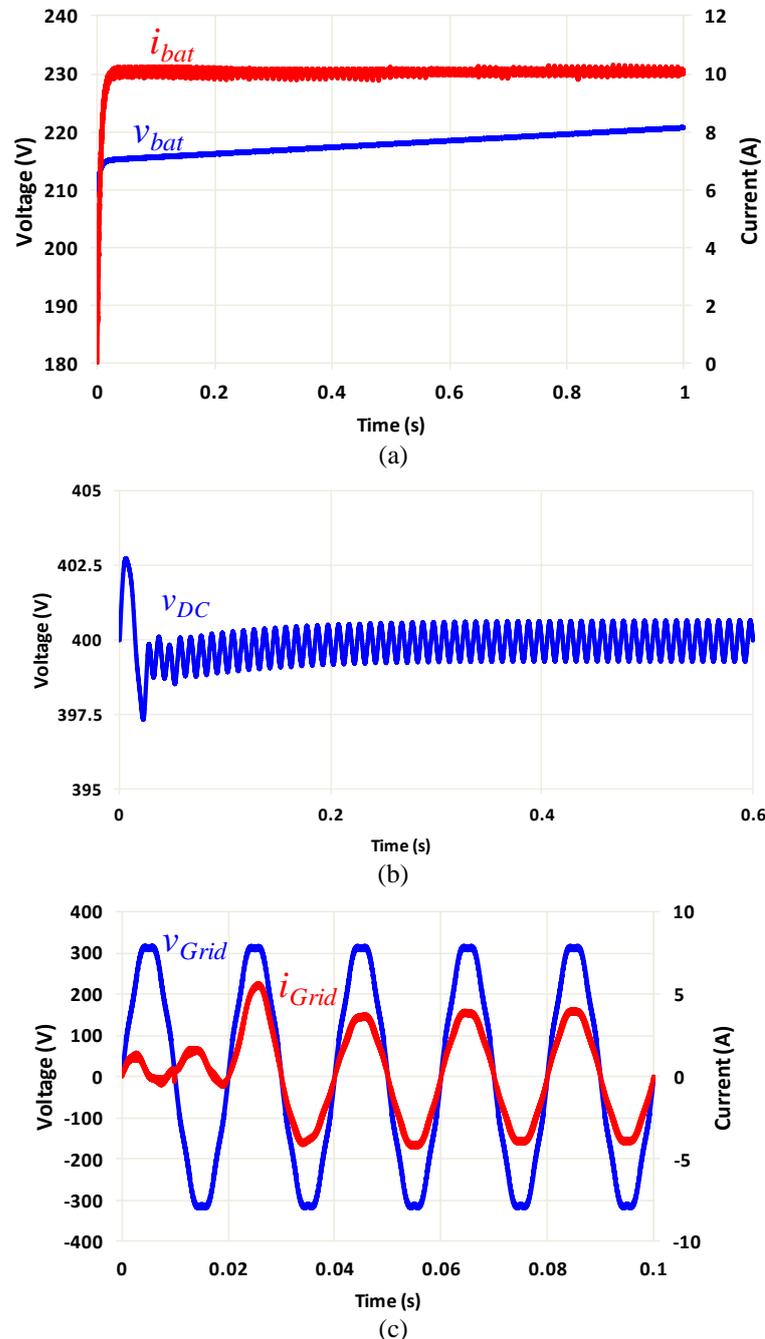
Figure 4.41 - Simulation results of the G2V operation, with 1000 W/m2 of solar irradiance: (a) Battery voltage (v_{bat}) and current (i_{bat}); (b) DC-link voltage (v_{DC}); (c) Grid voltage (v_{Grid}) and current (i_{Grid}).

Through the analysis of the waveforms shown in Figure 4.41 it is possible to conclude that the batteries are being successfully charged with a constant current of 10 A.

Development of Power Converters for Electric Vehicle Charging with Photovoltaics Interface
Júlio André Machado Fernandes - University of Minho

79

Furthermore, the charging current is again practically constant and the voltage at the batteries' terminals is steadily increasing. It should also be noted that the PV array is operating at its MPP but it is not enough to perform the battery charge on its own. As such, the grid assists the charging process, supplying roughly 3 A to the batteries. Finally, the measured value of THD in the grid current is 3.5% and the total power factor is 0.99. The increase in the value of THD is due to the fact that it is harder for the controller to synthesize lower values of current because with a small fundamental value of current, even small harmonic currents can originate high values of THD. A comparison between the different powers is illustrated in Figure 4.42.
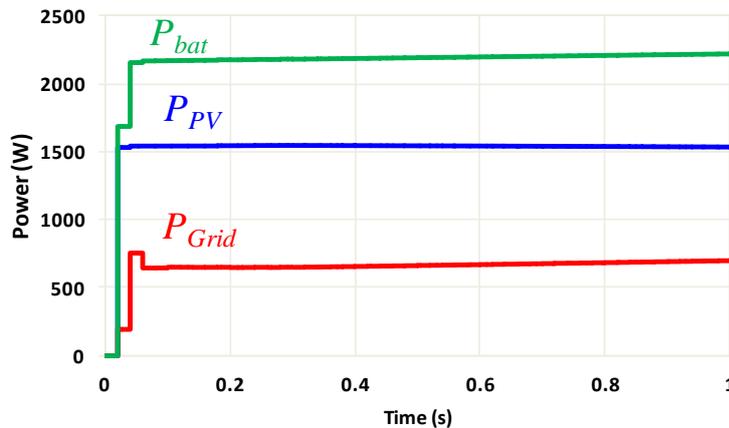
Figure 4.42 - Average values of the PV array power (P_{PV}), grid power (P_{Grid}) and battery power (P_{bat}), during G2V operation with 1000 W/m^2 of solar radiation.

Considering the case when the PV array is generating an extra amount of power, the same simulation parameters as above were used. In that regard, the goal of the simulation was to complete the charging of the batteries with a constant current. Once the batteries entered the constant voltage stage, with the charging current slowly decreasing, it would be possible to verify if the surplus energy produced by the PV panel would be delivered to the power grid. The results are shown in Figure 4.43 and Figure 4.44, respectively.
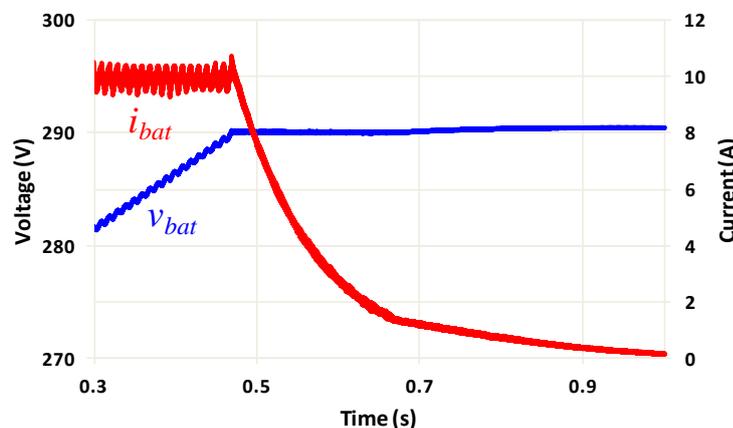
Figure 4.43 - Battery voltage (*vbat*) and current (*ibat*) in G2V during the transition between charge stages.
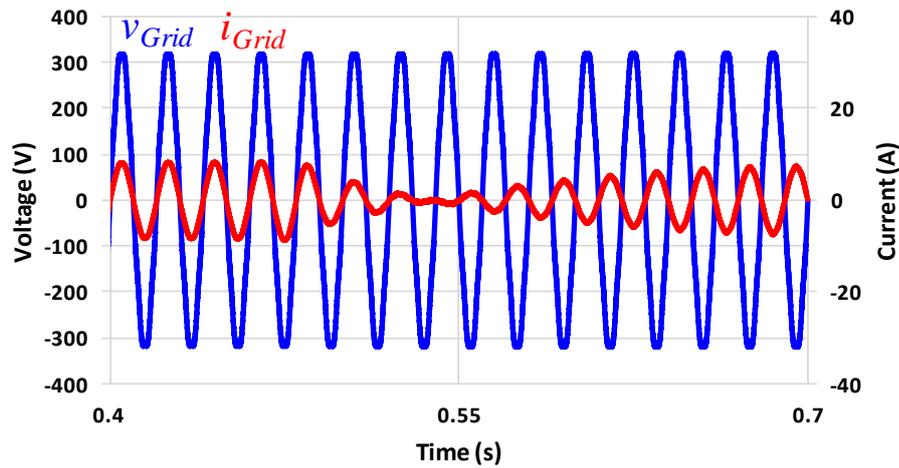
Figure 4.44 - Grid voltage (v_{Grid}) and current (i_{Grid}) in G2V during the transition between charge stages.

Once again the results obtained were positive. While the batteries are in the constant current stage, it can be seen that the power grid is assisting the charging process. As the batteries start to require less current, Figure 4.44 shows that the surplus energy produced by the PV is delivered to the power grid. The grid current has a THD value of 3.1% and the power factor is practically unitary. A closer look at the powers that come into play is shown in Figure 4.45.
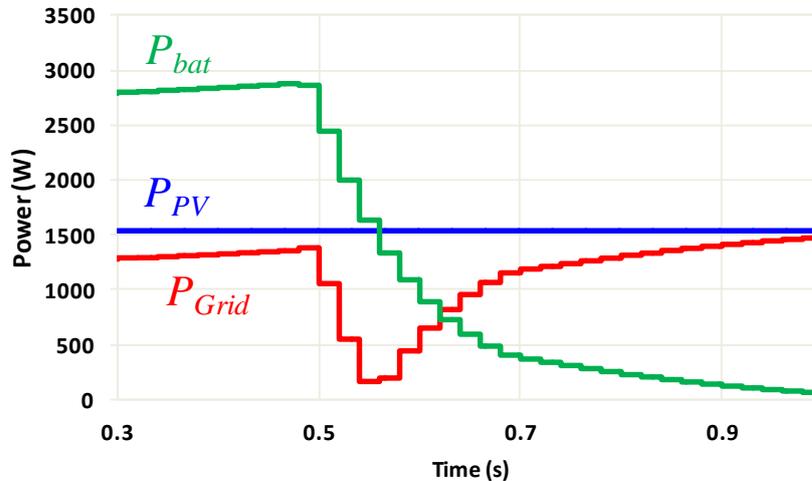
Figure 4.45 - Average values of the PV array power (P_{PV}), grid power (P_{Grid}) and battery power (P_{bat}) in G2V during the transition between charge stages

4.7. Conclusions

In this chapter, an analysis was made to each one of the converters selected for the implementation of the proposed BCS. The chosen topologies and control strategies for said converters were presented and justified, along with the modeling of the main parameters such as the passive filters.

Development of Power Converters for Electric Vehicle Charging with Photovoltaics Interface
Júlio André Machado Fernandes - University of Minho

81

The circuits in the PSIM simulation software were presented. These models allowed simulating the behavior of the various elements present in the solution such as, the batteries, the PV or the power grid. The main aim of the simulations was to validate the control algorithms and also the topologies chosen. The simulations were carried through to the early stages of development. This way it was possible to make the simulations as closer to reality as possible. In order to have a more detailed analysis of the system, each converter was initially simulated independently thus allowing the admeasurement of partial results such as the DC-link voltage regulation and current control.

The PLL algorithm was simulated under different circumstances. The synchronization was tested with a distorted voltage on the power grid side and also with frequency variations of above 1% of the fundamental (50 Hz). It was shown that the proposed algorithm would quickly achieve the synchronization and would also generate a sinusoidal output signal. Furthermore, the obtained results were also positive even when Power Quality Disturbances such as voltage sags and harmonic distortion were introduced to the system.

The simulation results of the bidirectional Full-Bridge AC-DC converter prove the viability of the PI controller implemented. When working as a rectifier, the DC-link voltage is kept at 400 V with a small value of ripple. The grid current is sinusoidal with low harmonic distortion and is in phase with the power grid voltage. On the other hand, when working as a VSI, all of the previous statements are verified, the difference being that the grid current will be 180° out of phase with the voltage, confirming that the energy is being delivered to the grid.

After that, the charging and discharging of the batteries was simulated. For this, the Thévenin equivalent model of a battery was used which, despite not contemplating all the aspects of a real battery, is still viable to be used in the simulation. It was shown that the batteries were successfully charged with a constant current and discharged with a constant power and that the batteries' current was kept practically constant, due to the passive filters utilized.

Additionally, the simulation results of the unidirectional boost converter used to make the interface between the PV array and the rest of the system show that the implemented MPPT algorithm works properly. It was shown that, even with variations in the maximum power that the PV panel can produce, the control system adapts and continues to extract the maximum available power. More importantly, the charging of the batteries directly from the PV array was verified.

82

Development of Power Converters for Electric Vehicle Charging with Photovoltaics Interface
Júlio André Machado Fernandes - University of Minho

Finally, the complete system was simulated operating in V2G and G2V modes. It was verified that, during V2G operation, the energy coming from the batteries along with the PV array was injected into the power grid. On the other hand, when working in G2V, the obtained results show that during times when the intensity of radiation is high enough, the PV array would simultaneously charge the batteries and inject the surplus of energy production into the power grid. It was also verified that in situations with low levels of solar radiation, the grid would assist the PV array in the charging process.

Development of Power Converters for Electric Vehicle Charging with Photovoltaics Interface
Júlio André Machado Fernandes - University of Minho

83

Development of Power Converters for Electric Vehicle Charging with Photovoltaics Interface
Júlio André Machado Fernandes - University of Minho

84

CHAPTER 5

Development of the Electric Vehicle Charging System Prototype

5.1. Introduction

In this chapter the different stages taken during the implementation of the converter will be explained in detail.

The system to be implemented can be divided in two main categories, the control system and the power stage. For each, all the different components used and implemented will be presented such as the semiconductors (power stage) and the microprocessor (control system).

5.2. Control System

The control system is mainly responsible for assuring the correct functioning of the power converters. For that to be possible, different voltage and current sensors must be used in order to monitor the variables needed for the control algorithm. Those analog variables are then converted into digital values by the DSC's (Digital Signal Controller) internal Analog to Digital Converter (ADC). Lastly, the DSC processes those variables and generates the proper PWM signals which are then applied to the gates of the semiconductors.

5.2.1. Hall Effect Voltage Sensors

For the correct operation of the system, it is necessary to know the instantaneous values of certain voltages namely the grid voltage, the DC-link voltage, the battery voltage and the voltage across the terminals of the PV panel. Given that these voltages are relatively high, it is necessary to use components that can successfully acquire each value of voltage and transpose them to level that can be read by the DSC's ADC, without risking its integrity. The solution is to use Hall Effect voltage sensors which allow for galvanic isolation between the power stage and the control system.

Development of Power Converters for Electric Vehicle Charging with Photovoltaics Interface
Júlio André Machado Fernandes - University of Minho

85

In Figure 5.1 it is presented a picture of the voltage sensor used, the LV 25-P. It allows measurements up to 500 V, which is more than enough for the proposed system. Also the LV 25-P internal schematic is presented in Figure 5.2.

Figure 5.1 - LV 25-P Voltage Transducer used in the power converter prototype [72].
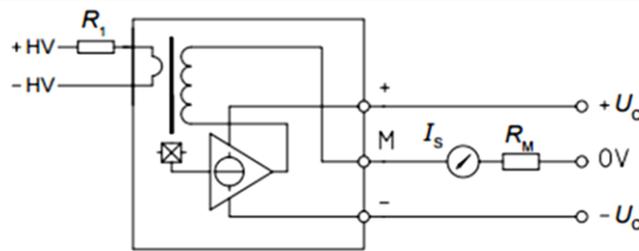
Figure 5.2 - LV 25-P schematic [72].

According to the manufacturer's datasheet, the resistor R_1 should be calculated so that the nominal voltage to be measured corresponds to a primary current of 10 mA, never exceeding 14 mA. The resistor R_M should be calculated so that the peak of the voltage at its terminals doesn't exceed the maximum input voltage allowed by the ADC (3.3 V).

The equations (5.1), (5.2) and (5.3) translate the behavior of the sensor and are used to calculate R_1 and R_M [72].

$$I_P = \frac{V_P}{R_1} \tag{5.1}$$

$$I_S = 2.5 I_P \tag{5.2}$$

$$V_M = R_M \times I_S \tag{5.3}$$

Where:

- V_p is the nominal voltage in the primary [V];
- I_p is the nominal current in the primary [A];
- I_s is the nominal current in the secondary [A];
- V_M is the measured voltage across R_M [V].

As it was mentioned previously, there are 4 different voltages that need to be measured. Considering the sensor used to measure the voltage of the grid, knowing that the nominal value of the voltage is 230 V, the sensor was modeled considering a nominal voltage of 300 V. The value of R_1 can be calculated as such:

$$R_1 = \frac{300}{10 * 10^{-3}} = 30 \text{ k}\Omega \tag{5.4}$$

The total power dissipated by the resistor will be:

$$P = R_1 \times I_P^2 \tag{5.5}$$

$$P = 30 \text{ k} \times (10 * 10^{-3})^2 = 3 \text{ W} \tag{5.6}$$

The resistor R_M can be calculated using:

$$I_S = 2.5 \times 10 * 10^{-3} = 25 \text{ mA} \tag{5.7}$$

$$R_M = \frac{V_M}{I_S} = \frac{3}{25 * 10^{-3}} = 120 \text{ }\Omega \tag{5.8}$$

$$P = 120 \times (25 * 10^{-3})^2 = 75 \text{ mW} \tag{5.9}$$

For measuring the voltage of the batteries, considering their voltage to be 290 V when fully charged, the sensor was modeled for a nominal primary voltage of 350 V. As such:

$$R_1 = \frac{350}{10 * 10^{-3}} = 35 \text{ k}\Omega \tag{5.10}$$

$$P = 35 \text{ k} \times (10 * 10^{-3})^2 = 3.5 \text{ W} \tag{5.11}$$

The same values calculated above were used for the PV panel, as the values of voltage to be measured are of the same scale.

Because there weren't any voltage sensors available in the lab at the time, a pre-existing and already assembled board was used. Its main application was to measure the phase voltages of three-phase systems so it could be adapted to this particular system. In Figure 5.3 it is presented the voltage sensor board utilized for the control system.

Development of Power Converters for Electric Vehicle Charging with Photovoltaics Interface
Júlio André Machado Fernandes - University of Minho

87
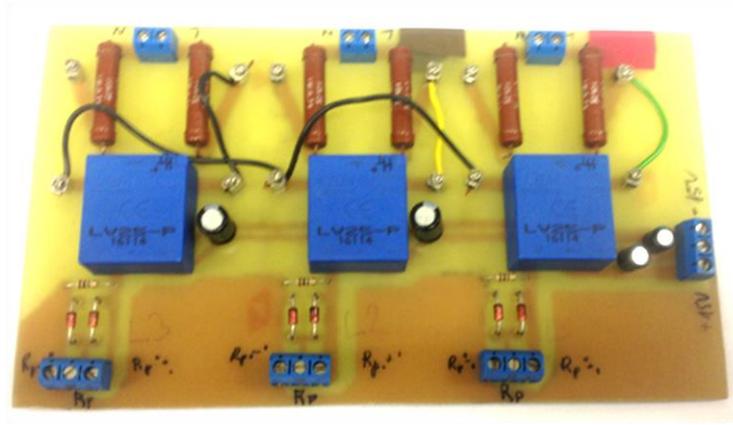
Figure 5.3 - Voltage sensor board used in the power converter prototype.

It should be noted that on Figure 5.3 there are only 3 voltage sensors. That is due to the fact that the converter module used, which will be explained later in this chapter, already had a built-in voltage sensor. That sensor was used to measure the DC-link voltage so this board was used to measure the remaining voltages (i.e. grid, battery and PV panel).

5.2.2. Hall Effect Current Sensors

Apart from measuring the voltages, it is also necessary for the control system to know the instantaneous values of three currents: the grid current, the battery current and the PV panel current. Once again, Hall Effect current sensors were used. In these kind of sensors, the conductor where the current to be measured flows goes through the sensor and acts like the primary. That way, galvanic isolation is achieved. More specifically, the current sensor used was the LA 55-P and it is presented in Figure 5.4.
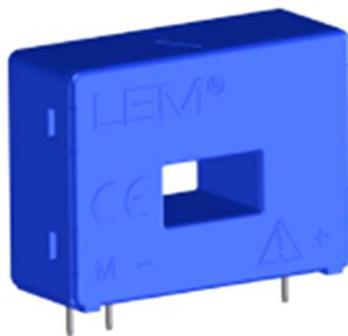
Figure 5.4 - Current Transducer LA 55-P used in the power converter prototype [73].

The nominal RMS current on the primary RMS is 50 A but currents ranging from ± 70 A can be measured. The sensor is supplied with a bipolar voltage of ± 15 V. The resistor R_M connected between M and GND is calculated in order that the output

voltage V_M does not exceed the maximum value supported by ADC. The LA 55-P internal schematic is shown in Figure 5.5.
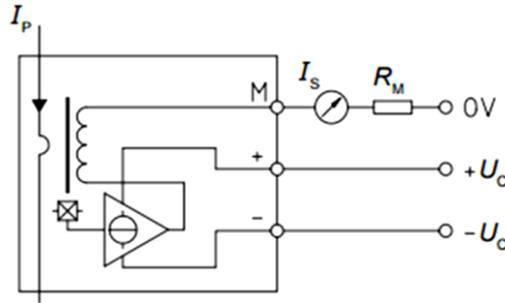
Figure 5.5 - LA 55-P internal schematic [73].

The equations (5.12) and (5.13) translate the behavior of the sensor and are used to calculate R_M [73].

$$I_S = \frac{I_P}{1000} \tag{5.12}$$

$$V_M = I_S \times R_M \tag{5.13}$$

Next, by using the above equations, the calculations made for R_M are presented. It was decided that the sensor circuit should be designed for 50 A. That would allow the sensors to be used in future applications and also minimize reading errors.

$$I_S = \frac{50}{1000} = 50 \text{ mA} \tag{5.14}$$

For safety reasons, considering the maximum voltage the ADC can read to be 3 V, R_M can be calculated using:

$$R_M = \frac{3}{50 * 10^{-3}} = 60 \ \Omega \tag{5.15}$$

Two 30 Ω resistors connected in series were used. The total power dissipated by them is:

$$P = 30 \times (50 * 10^{-3})^2 + 30 \times (50 * 10^{-3})^2 = 150 \text{ mW} \tag{5.16}$$

5.2.3. Signal Conditioning Board

As mentioned before, the sensors can measure the values of the different variables that are necessary to the control of the proposed system. For the DSC to be able to read these values, it is necessary to use an ADC. Since there are variables that have both positive and negative values (e.g. grid voltage) and the ADC used can only read values from 0 V to 3.3 V, it was necessary to develop a signal conditioning board capable of adjusting the values to a level suitable for the ADC.

Development of Power Converters for Electric Vehicle Charging with Photovoltaics Interface
Júlio André Machado Fernandes - University of Minho

89

In Figure 5.6 a schematic of the circuit for the signal conditioning is presented.
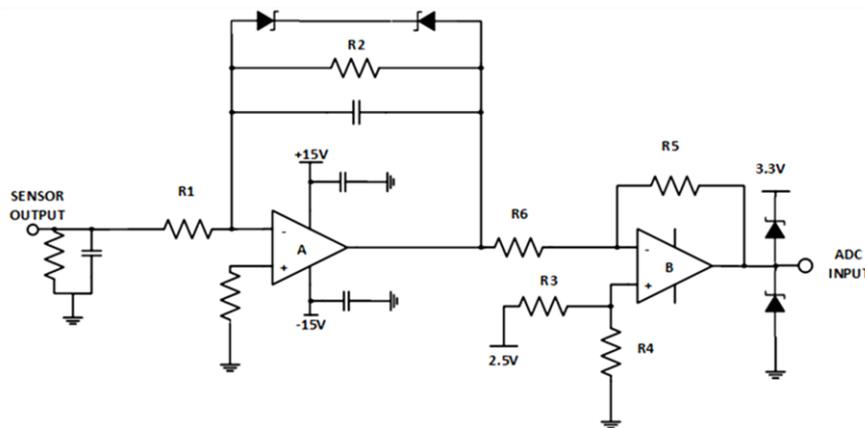
Figure 5.6 - Signal conditioning board circuit schematic.

The circuit presented in Figure 5.6 makes use of two operational amplifiers (Amp-Op) in two inverting configurations. For instance, the signal output from the grid voltage sensor will be positive or negative. That signal cannot be fed directly into the ADC because it can only read positive values up to 3.3 V. So the signal needs to be shifted and to be centered ideally on 1.5 V.

The resistor's R_1 and R_2 values were 10 kΩ and 20 kΩ, respectively. That means that the gain in the first amplifier is -2. The resistors R_3 and R_4 are of equal values so the voltage present in the inputs of the second amplifier is 1.25 V.

An output signal of 2.5 V from the sensor will result in -5 V on the output of the first amplifier. If the input of the second amplifier has 1.25 V, it means that the voltage drop across R_6, which has a value of 36 kΩ, is -6.25 V. Applying the Ohm's Law, the current flowing through R_6 and R_5 is 173 µA. That translates into a voltage drop of -0.9 V across R_5. In that case, the voltage on the output of the second amplifier will be 1.25 + 0.9 = 2.15 V. Alternatively, if the voltage on the output of the first amplifier is 5 V, the output of the second amplifier will be 0.75 V.

The implemented circuit board can be seen in Figure 5.7. To achieve the 2.5 V reference the programmable shunt regulator TL431 was used. It has a programmable output voltage that goes up to 36 V and it can be used for either positive or negative voltage reference [74].

For the amplifiers, two TL072 Amp-Ops were used. These devices feature high slew rates, low-input bias, low offset currents, and low offset-voltage temperature coefficient [75].
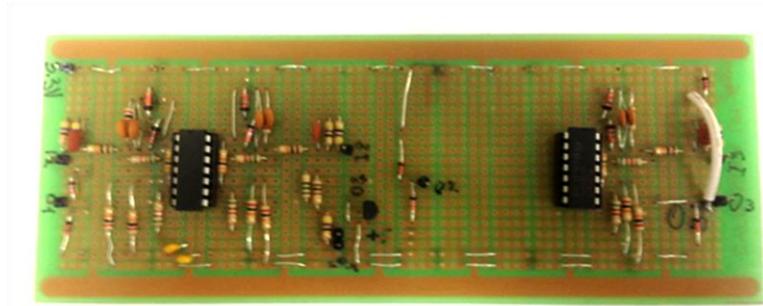
Figure 5.7 - Signal conditioning board used in the power converter prototype.

5.2.4. Digital Signal Controller (DSC)

The control algorithms were implemented using the Digital Signal Controller (DSC) TMS320F28335 from Texas Instruments. The DSC has the following characteristics:

- 32-bit CPU with maximum clock frequency of 150 MHz;

- 16-bit word on-chip flash memory with 256 k;

- 18 PWM outputs (6 main outputs, 6 high resolution outputs and 6 auxiliary outputs);

- 16 ADC channels with 12-bit resolution and conversion time of 80ns;

- 3 32-bit timers;

- 16-bit word SRAM with 34 k.

The DSC used is included in the TMS320F28335 controlCARD, shown in Figure 5.8, a board containing some peripherals required for the DSC's correct functioning such as the oscillator, pull-up resistors and decoupling capacitors. This board features 100-pin DIMM for interface, so it should be connected to a connector of the same type. Texas Instruments also offers a docking station in which the controlCARD is connected, shown in Figure 5.9 [18] [76].
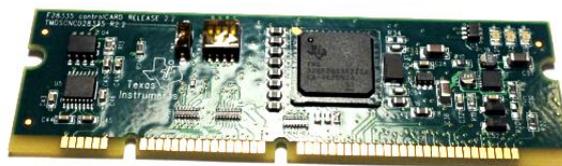
Figure 5.8 - TI F28335 controlCARD.

Development of Power Converters for Electric Vehicle Charging with Photovoltaics Interface
Júlio André Machado Fernandes - University of Minho

91
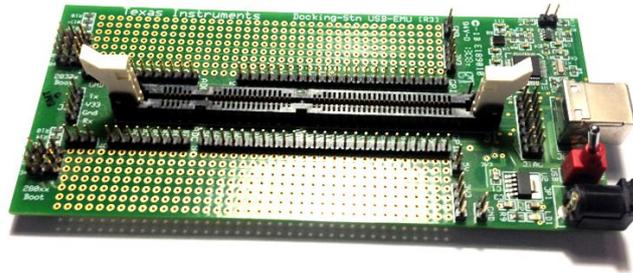
Figure 5.9 - TI F28335 docking station.

For the programming of the DSC, Texas provides an integrated development environment called Code Composer Studio (CCS). This program allows the user to implement the control system in C language and comes with several libraries with specific functions for the DSC used.

5.2.5. Command Board

For security reasons, it is not advisable for the PWM signals coming from the DSC to be directly connected to the driver circuit. As such, a command board was developed in the lab with the goal of interfacing the DSC and the driver circuit. This board will be responsible for elevating the PWM's voltage level (0 V and 3.3 V) to one suitable to be supplied to the driver circuit of the IGBT module. To achieve that, two SN 74LV07 and one SN 74HCT540 were used. The SN74LV06 is a hex buffer with open-drain outputs and the 74HCT540 is an 8-bit inverting buffer/line driver with 3-state outputs [77] [78]. The schematic of this circuit can be seen in Figure 5.10. Another important feature of this board is the ability to control the switching of the IGBTs. In other words, the switching will only take place if an *enable* signal is given.
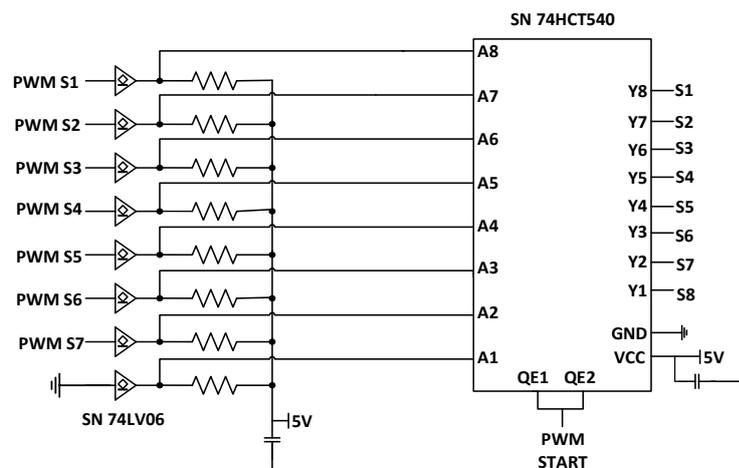
Figure 5.10 - Command board circuit schematic.

As seen in Figure 5.10, the different PWM signals coming from the DSC are fed to the first inverting buffer and then to the second one. An output of 0 V – 5 V is

92

Development of Power Converters for Electric Vehicle Charging with Photovoltaics Interface
Júlio André Machado Fernandes - University of Minho

expected, instead of the DSCs 0 V – 3.3 V. The assembled board can be seen in Figure 5.11.
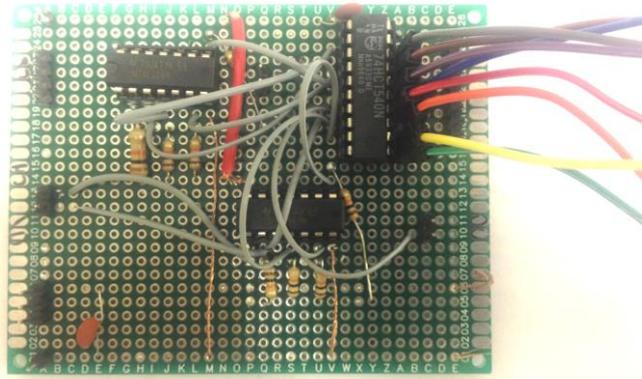
Figure 5.11 - Command board used in the power converter prototype.

5.2.6. Power Supply

To supply the voltage sensors as well as the current sensors, the signal conditioning board and the command board, a T-60C power supply from MeanWell was used with a rated power of 62.5 W. It offers three different outputs: a +5 V, 5 A; a +15 V, 2 A; and a -15 V, 0.5 V. It also is fitted with a protection against short-circuits, overloads and over voltages. A picture of the power supply can be seen in Figure 5.12 [79].

Figure 5.12 - T-60C power supply used in the power converter prototype.

5.3. Power Stage

As of now, all the different components from the control system were introduced and explained in detail.

As mentioned in the previous chapter, the topology chosen for the AC-DC converter (i.e. grid converter) was the Full-Bridge, for the DC-DC bidirectional converter (i.e. battery converter) the topology chosen was the bidirectional buck-boost

Development of Power Converters for Electric Vehicle Charging with Photovoltaics Interface
Júlio André Machado Fernandes - University of Minho

93

and, finally, the boost topology was chosen for the unidirectional DC-DC converter (i.e. PV converter). Next, the different elements from the power stage (e.g. IGBT module) will be described.

5.3.1. IGBT Module

In order to make good use of the resources available, two existing lab converter modules P3G from *PowerSys* were used. This module is presented in Figure 5.13 and already has a built-in driver circuit, DC-link capacitor and DC-link voltage sensor [80].

Figure 5.13 - PowerSys P3G lab converter module used in the power converter prototype.

This lab converter module has a nominal power of 1 kW and supports DC-link voltages up to 450 V. The value of capacitance in the DC-link is 2200 µF.

Each converter module used also has a built-in pre-charge resistor, controlled by a relay. This is very important because when the converter is connected to the power grid, the DC-link initially appears as a short circuit to the grid, which results in high currents while it isn't pre-charged.

Another feature is the presence of snubber capacitors, whose importance will be described in more detail next and also the presence of a fault detection mechanism that, in case something happens that could potentially put the integrity of the converter module at risk, it immediately blocks all IGBTs and activates a LED to let the user know of the fault. One final advantage to the use of this converter module is that, due to its open design, important control signals like the gate signals of the semiconductors can be easily monitored.

Given that each converter module is comprised of 3 converter legs, the use of a second module was required. That said, from the first module the IGBTs 1 to 4 were selected for the AC-DC converter, IGBTs 5 and 6 for the DC-DC bidirectional

converter and IGBTs 1 and 2 from the second module were selected for the DC-DC boost converter.

The DC-link is composed by two sets of three 1500 µF, 450 V electrolytic capacitors (an example of which can be seen in Figure 5.14) connected in parallel. Each set is connected in series, so it makes up for a total capacitance of 2200 µF.

As described previously, back in the simulations, the value of the capacitance of the DC-link capacitor was 4000 µF (4 mF). By connecting both converter modules, the resulting value of the DC-link capacitance is 4400 µF, instead of 2200 µF.

Figure 5.14 - Electrolytic capacitor (2200 µF, 450 V).

In an application note [81], Semikron recommends the use of snubber capacitors directly connected to the IGBT module terminals, which are connected themselves to the DC-link. The snubbers are small, absorbing energy circuits used to eliminate voltage spikes caused by inductances present in the circuits when a switch, whether mechanical or solid-state, opens. The purpose of the snubber is to provide an alternative path for the current flowing through the circuit. The use of snubber circuits offer numerous advantages such as the mitigation of voltage spikes on switches, preventing their degradation; transferring the semiconductor switching losses to a resistor and reducing the emission of electromagnetic noise [82] [83]. Figure 5.15 shows the voltage waveform of an IGBT, during turn-off, with and without the use of a snubber.

(a)   (b)
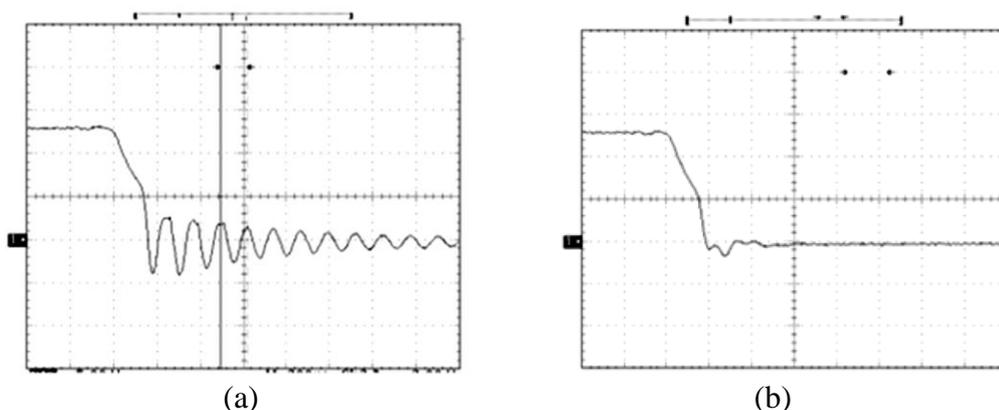
Figure 5.15 - IGBT v_{CE} voltage: (a) without snubber; (b) with snubber [82].

Development of Power Converters for Electric Vehicle Charging with Photovoltaics Interface
Júlio André Machado Fernandes - University of Minho

95

5.3.2. Power Converter Inductors

For the AC-DC converter inductor, an existing 6.7 mH inductor from the lab was used. The inductor can be seen in Figure 5.16.
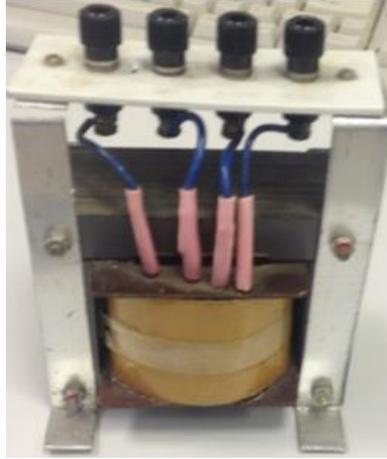
Figure 5.16 - Inductor used for the AC-DC converter.

Originally, the modeling and implementation of both inductors for the remaining DC-DC converters was planned. There are many different types of magnetic material used for the inductor cores. Ferrite materials have much higher permeability and so require fewer turns to obtain a given inductance. As such, the number of turns needed for a desired value of inductance is given by [84]:

$$N = 1000 \times \sqrt{\frac{L}{A_L}} \tag{5.17}$$

Where:

- L is the value of inductance expressed in mH;

- N is the number of turns;

- A_L is the inductance rating, expressed in mH/1000*N. This parameter is specific for each core and its value is expressed in the manufacturer's datasheet.

However, later it was decided to use two 2.7 mH inductors that already existed in the lab. This inductor can be seen in Figure 5.17.

Figure 5.17 - Inductor used for the DC-DC converters.

5.3.3. Battery Bank

For the battery bank, two lead-acid batteries from MW Power were used. Each battery has a nominal voltage of 12 V and 40 Ah. They were connected in series as to make up 24 V and 960 Wh of energy that can be stored. In Table 5.1, some characteristics from this battery are presented. The most important ones to note are the nominal voltage, the maximum charging current, the maximum discharging current and the maximum charging voltage. Finally, Figure 5.18 shows the two batteries used connected in series [85].

Table 5.1 - Technical specifications of the MW 40-12 battery.

Characteristic	*Nominal Value*	*Unit*
Voltage	12	V
Capacity	40	Ah
Maximum Discharge Current	510 (5 sec)	A
Maximum Charge Current	13	A
Maximum Charge Voltage	15	V
ESR	7.8	mΩ
Charge Temperatures	-20 to 50	°C
Discharge Temperatures	-20 to 50	°C
Weight	13.3	kg
Dimensions	198x171x166	mm

Figure 5.18 - MW 40-12 batteries used in the power converter prototype.

Development of Power Converters for Electric Vehicle Charging with Photovoltaics Interface
Júlio André Machado Fernandes - University of Minho

97

5.4. Conclusions

In this chapter, the various components for the Battery Charging System to be developed were presented. Firstly, the whole control system was presented, with the voltage and current sensors, the command board, the signal conditioning board and the DSC being explained in detail. Also, the power supply used to power the control system was presented. The control system was followed by the power stage in which the IGBT modules, the DC-link capacitors, the inductors and the batteries used were shown.

One major drawback that was encountered was with the PCBs. Although it was initially intended for all circuits to be designed and converted into PCBs, the fact was that it wasn't possible to fabricate them in the university in which this project was developed and also the time it would take is not compatible with the project timeline. Furthermore, the inherent costs of making the boards somewhere else, led to the decision of using the prototyping boards that were initially assembled to validate each board. Of course this had a major impact on the final look of the entire system, but nonetheless, it is noteworthy that apart from the voltage sensors, each board was developed and tested from scratch.

98

Development of Power Converters for Electric Vehicle Charging with Photovoltaics Interface
Júlio André Machado Fernandes - University of Minho

CHAPTER 6

Experimental Results of the Electric Vehicle Charging System

6.1. Introduction

In this chapter the experimental results that were obtained during the tests made to the Battery Charging System will be presented.

As mentioned in earlier chapters of this dissertation, this project for the development and implementation of a Battery Charging System with an interface for renewable energies was made in the context of a mobility program (Erasmus+). As such, everything that was presented so far was developed on the receiving institution, Uniwersytet Zielonogórski (University of Zielona Góra) in Poland. By the time the mobility period ended, the Vehicle-To-Grid mode and the MPPT control algorithm were not validated.

Fortunately, the opportunity emerged to migrate the developed system to an existing hardware in the GEPE laboratory, back at University of Minho. This hardware was developed by Doctor Vítor Monteiro within the scope of his PhD. thesis and it is shown in Figure 6.1. As such, in an effort to maintain the coherence throughout this dissertation, all of the tests that were made abroad were again performed along with the ones that were not validated in time. The experimental results that will be presented were all obtained in the migrated hardware. For consistency reasons, the results that were obtained during the mobility period can be found in the appendix.

The DSC in which the control algorithms were implemented was the same as the one described in the previous chapter. However, new equipment was used namely an external ADC and a DAC (Digital to Analog Converter) hence the reason they will be presented in this chapter instead.

Development of Power Converters for Electric Vehicle Charging with Photovoltaics Interface
Júlio André Machado Fernandes - University of Minho

100

Figure 6.1 - Integrated converter to which the project was migrated.

As mentioned above, an external ADC was used in detriment of the DSC's internal 16 channel ADC. The external 8 channel ADC used was the model MAX1320 from Maxim. It has a 14-bit resolution and supports bipolar inputs which represent the main advantage in comparison with the DSC's internal ADC. The communication with the DSC is then made via a parallel interface.

With the intent of visualizing the internal variables of the DSC, such as the PLL, in real time, a PCB with a DAC developed in GEPE was used. This board allows SPI communication with the DSC allowing the variables of the control algorithms to be seen on an oscilloscope. The model of the DAC used was the TLV5610 from Texas Instruments and it can be seen in Figure 6.2.
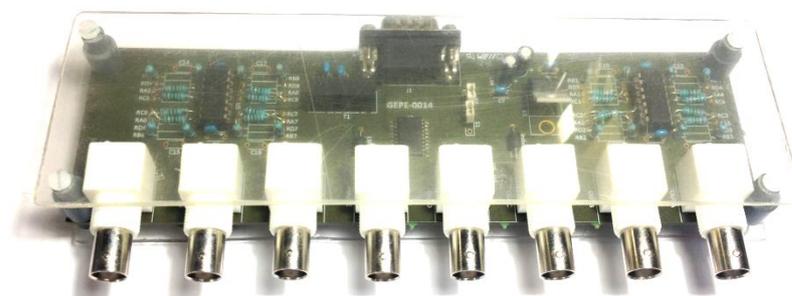
Figure 6.2 - PCB developed in GEPE in which the DAC is inserted.

Finally, it is important to note that the topologies of the converters also did not suffer any changes.

Development of Power Converters for Electric Vehicle Charging with Photovoltaics Interface
Júlio André Machado Fernandes - University of Minho

101

6.2. Experimental Results of the PLL Algorithm

To assess the performance of the PLL algorithm only the use of a voltage sensor was required. As such, this experimental test could be performed with the nominal voltage of the grid without risk of damage to the converter. By using the DAC described in the previous section the output signal of the PLL algorithm was monitored. The results of the synchronization of the PLL with the grid voltage are presented below. It should be noted that the PLL controller is turned on at the 10 ms mark.
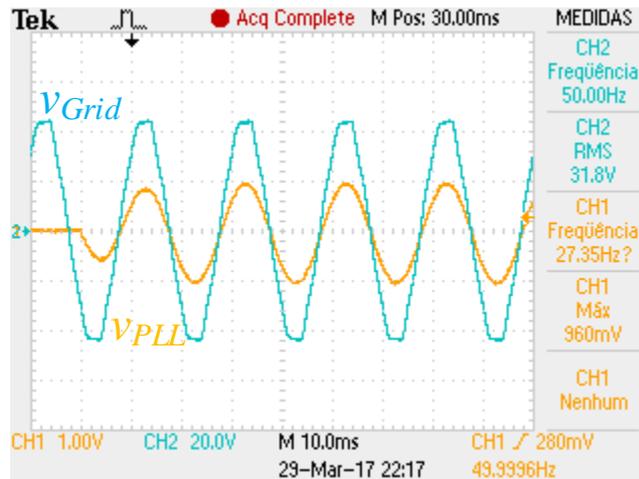
Figure 6.3 - Synchronization of the PLL output (CH1: 1 V/div) with the grid voltage (CH2: 20 V/div).

Figure 6.3 shows that the implemented PLL (v_{PLL}) is able to synchronize the output in less than one cycle of the grid voltage (v_{Grid}). More importantly, once in steady-state, the algorithm is able to synthesize a sinusoidal signal from a distorted input. This fact is further evidenced by the steady-state results of the PLL that are displayed in Figure 6.4.
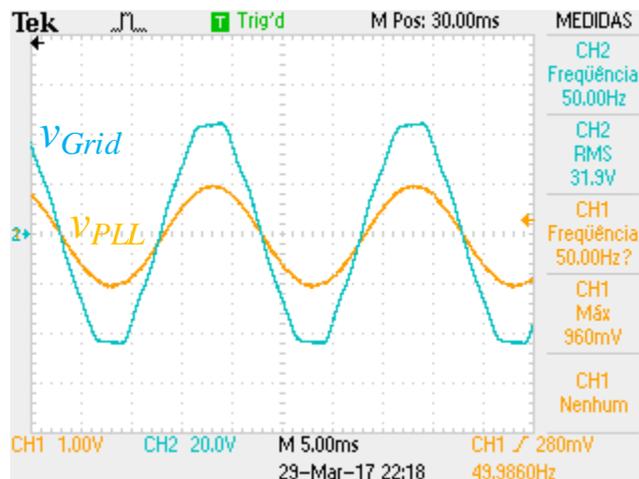
Figure 6.4 - Steady-state results of the synchronization of the PLL (CH1: 1 V/div) with the grid voltage (CH2: 20 V/div).

6.3. Experimental Results of the AC-DC Converter

Figure 6.5 shows the power circuit used to assess the operation of the AC-DC converter as a VSI. Initially, the system was disconnected from the power grid thus working as an off-grid VSI. The values of *R, L* and *C* are, respectively, 8 Ω, 3 mH and 5 mF.
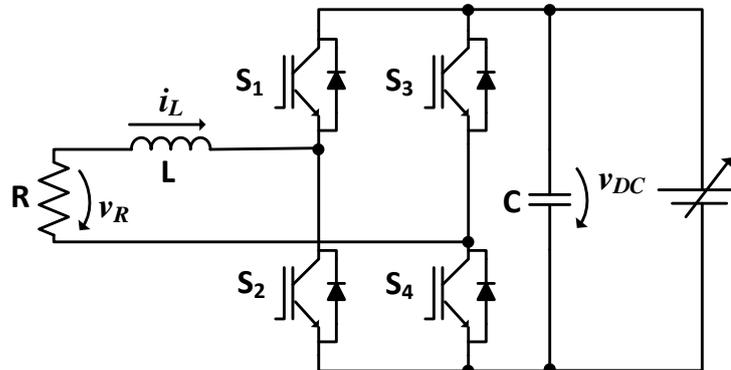
Figure 6.5 - Power circuit used to test the AC-DC converter as an off-grid VSI.

For this test, it is intended to supply the load *R* with a sinusoidal current. For that, a DC workbench power supply was used to simulate the regulation of the DC-link. The value of V_{DC} was set at 30 V.

As mentioned before, the switches on the same leg of the converter must be complementary so before the experiment was made it was important to validate if the correct PWM signal is being applied to the gates of the IGBTs. Because no semiconductor can switch instantly it is necessary to implement a dead time during which all IGBTs on the same leg are off. This prevents a situation in which one semiconductor turns on while the other is still not completely turned off. That would result in a short circuit across the leg of the converter which despite being brief could cause damage to the integrity of the converter itself. These dead times can be implemented by software or, like in this case, by the driver circuits of the IGBTs.

Figure 6.6 shows the gate signals applied to one leg of the converter. It can be seen that both PWM signals are complementary and that the dead time imposed by the driver circuit is 4 μs.

Development of Power Converters for Electric Vehicle Charging with Photovoltaics Interface
Júlio André Machado Fernandes - University of Minho

103
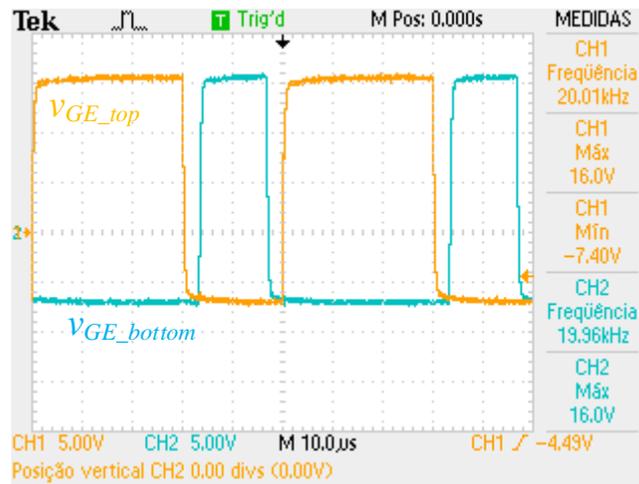
Figure 6.6 - PWM signals applied to the top IGBT (CH1: 5 V/div) and bottom IGBT (CH2: 5 V/div).

The experimental results obtained during this test are shown in Figure 6.7 and Figure 6.8, in which the measured waveforms for the load voltage (v_R) and current (i_L) can be seen. Firstly, in Figure 6.7, it is intended to supply the load with a sinusoidal current with a peak amplitude of 1 A. Lastly, in Figure 6.8, the reference was altered to a peak amplitude of 2 A.
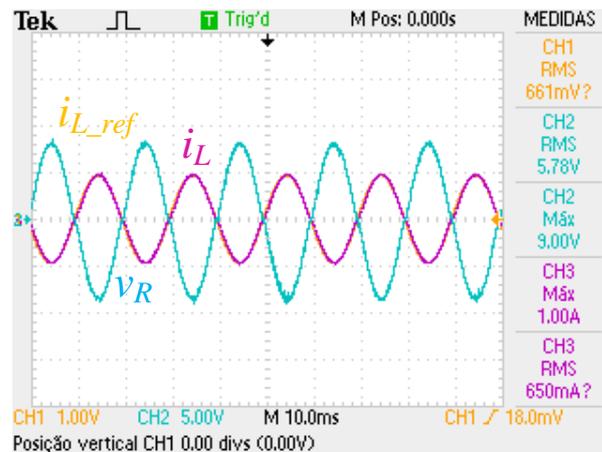
Figure 6.7 - Experimental results obtained when the AC-DC converter is operating as an off-grid VSI (1 peak): reference current (CH1: 1 A/div), synthesized current (CH3: 1 A/div) and load voltage (CH2: 5 V/div)
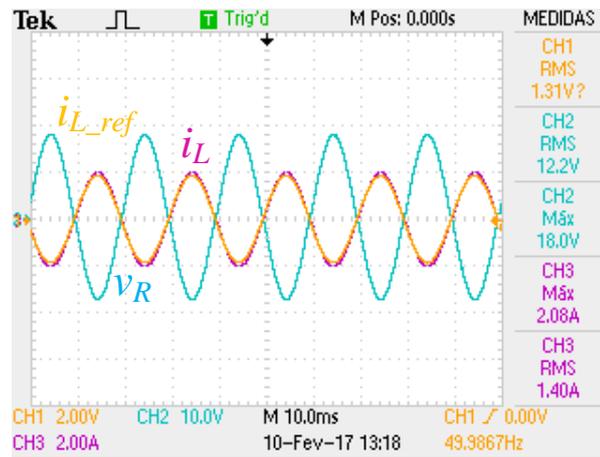
Figure 6.8 - Experimental results obtained when the AC-DC converter is operating as an off-grid VSI (2 peak): reference current (CH1: 2 A/div), synthesized current (CH3: 2 A/div) and load voltage (CH2: 10 V/div).

The results presented above show that, for both tests made, the controller is able to synthesize a sinusoidal current that is 180° out of phase with the load voltage and also with the desired amplitude.

In Figure 6.9 it is presented the power circuit utilized to test the functioning of the AC-DC converter as an active rectifier. The transformer is used to lower the voltage of the power grid form 230 V RMS to 30 V RMS. In this time, the load was connected to the DC-link and comprised of a rheostat.
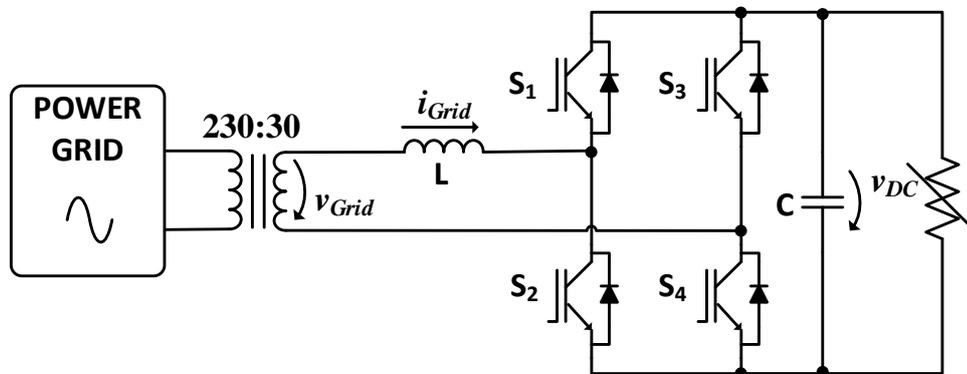
Figure 6.9 - Power circuit used to test the AC-DC converter in rectifier mode.

The main goal of this experimental test is to validate the correct regulation of the DC-link voltage. It is intended to maintain the DC-link at a constant 75 V and the current flowing through the input inductor should be sinusoidal and in-phase with the grid voltage. Figure 6.10 shows the waveforms obtained when the control system is turned off. This that means the converter is operating as an uncontrolled rectifier. In this case, the DC-link voltage will be roughly equal to the peak voltage of the power grid.

Development of Power Converters for Electric Vehicle Charging with Photovoltaics Interface
Júlio André Machado Fernandes - University of Minho

105
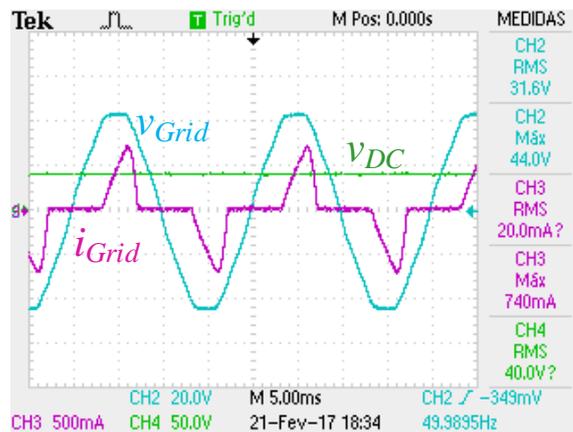
Figure 6.10 - Experimental results obtained when the AC-DC converter is operating as an uncontrolled rectifier: DC-link voltage (CH4: 50 V/div), grid current (CH3: 0.5 A/div) and grid voltage (CH2: 20/div).

When the controller is working, it can be seen that the current drawn from the grid is almost sinusoidal and in-phase with the voltage. The DC-link is also kept constant at 75 V. These results are illustrated in Figure 6.11.
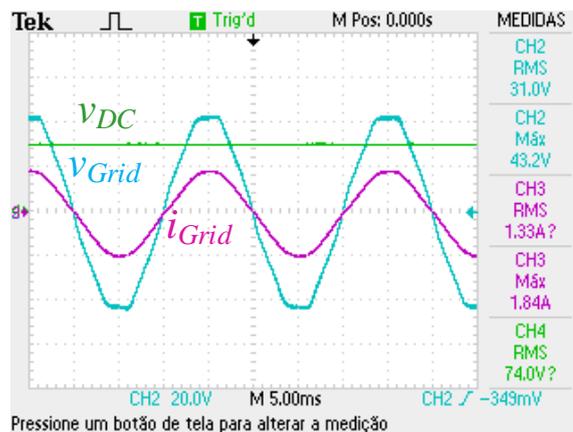
Figure 6.11 - Experimental results obtained when the AC-DC converter is operating as an active rectifier: DC-link voltage (CH4: 50 V/div), grid current (CH3: 2 A/div) and grid voltage (CH2: 20 V/div).

To further assess the behavior of the controller, the rheostat was varied to a lower level of resistance. The aim of this is to verify if, despite the changes in the current drawn from the grid, the controller can adapt and regulate the DC-link voltage. The results are presented in Figure 6.12 and it can be seen that the controller properly regulates the DC-link voltage despite the increase of the grid current.
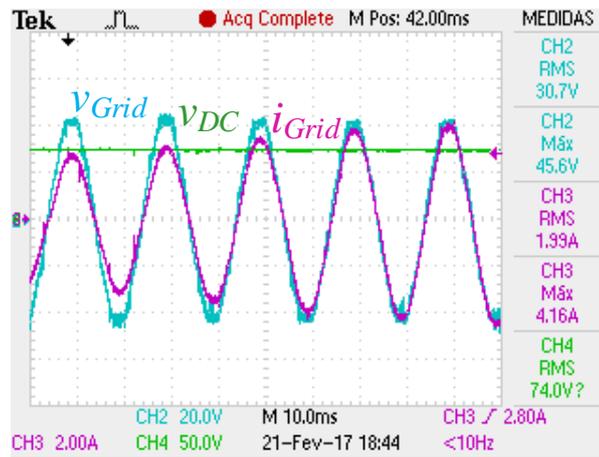
Figure 6.12 - Experimental results obtained when the AC-DC converter is operating as an active rectifier, with variation of the load: DC-link voltage (CH4: 50 V/div), grid current (CH3: 2 A/div) and grid voltage (CH2: 20 V/div).

Lastly, the final experiment made to validate the functioning of the AC-DC converter was to inject the energy from the DC-link into the power grid. For this, the circuit shown in Figure 6.13 was used.
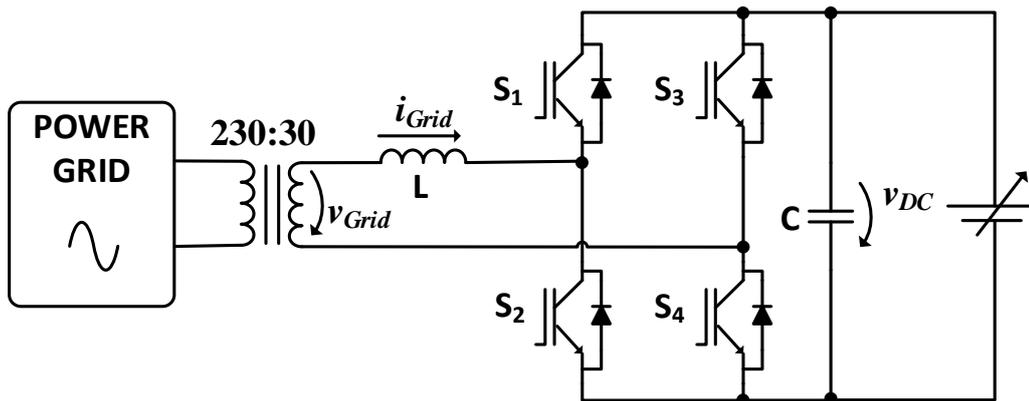
Figure 6.13 - Power circuit used to test the AC-DC converter as a grid connected VSI.

The DC workbench power supply was set at 75 V thus simulating the DC-link voltage regulation. The same conditions were used as in the test made to validate the off-grid operation. As such, it was intended to inject a sinusoidal current into the grid with an amplitude of, firstly, 1 A and, lastly, 2 A. Naturally, the grid current should be 180° out of phase with the voltage. The obtained results are presented in Figure 6.14 and Figure 6.15.

Development of Power Converters for Electric Vehicle Charging with Photovoltaics Interface
Júlio André Machado Fernandes - University of Minho

107
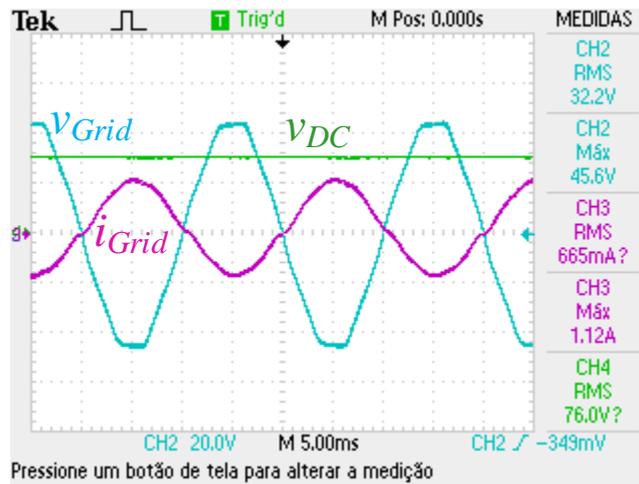
Figure 6.14 - Experimental results obtained when the AC-DC converter is operating as a grid connected VSI (1 A peak): DC-link voltage (CH4: 50 V/div), grid current (CH3: 1 A/div) and grid voltage (CH2: 20 V/div).
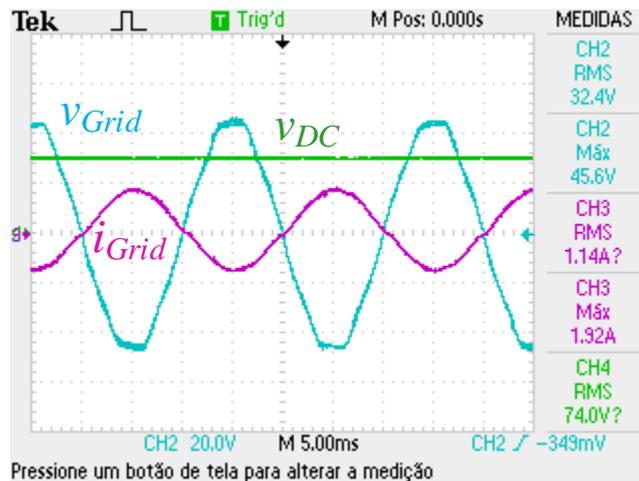

Figure 6.15 - Experimental results obtained when the AC-DC converter is operating as a grid connected VSI (2 A peak): DC-link voltage (CH4: 50 V/div), grid current (CH3: 2 A/div) and grid voltage (CH2:20 V/div).

It can be observed that the quality of the injected current increases with the amplitude. This was also noted in the simulations made earlier in the development of the converter.

6.4. Experimental Results of the MPPT Algorithm

Unfortunately there were no PV panels available at the lab. To get around this and to validate the Incremental Conductance MPPT that was implemented, a PV panel was simulated using a DC workbench power supply in series with a rheostat. The variations in the rheostat simulate the impact of changes in the temperature and irradiance in a real PV panel. The circuit used to validate the MPPT algorithm is presented in Figure 6.16.
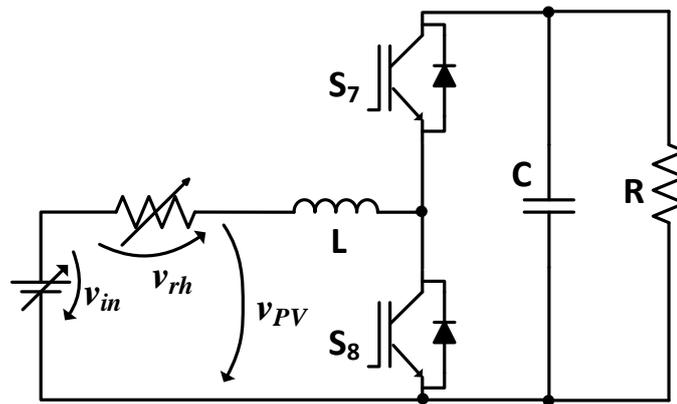
Figure 6.16 - Power circuit used to test the MPPT algorithm.

As seen above, the series connection of the DC supply and the rheostat simulate an actual PV panel. The values of L and C are, respectively, 3 mH and 5 mF. Considering an input voltage of 30 V (V_{in} = 30 V), the maximum power will be extracted when the voltage across the rheostat (v_{rh}) is equal to v_{PV}, that is, both voltages should be 15 V. One of the obtained results, for a value of rheostat resistance of 17.3 Ω, is shown in Figure 6.17. It can be seen that both voltages (v_{rh} and v_{PV}) converge to 15 V, as the controller finds the MPP.
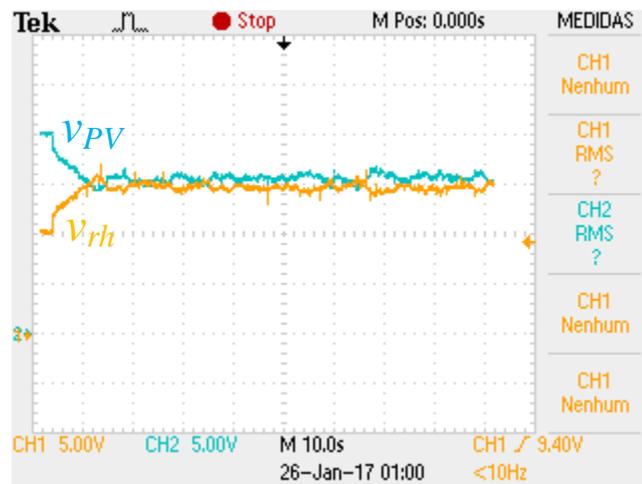
Figure 6.17 - Experimental results obtained for the Incremental Conductance MPPT algorithm: voltage across the rheostat (CH1: 5 V/div) and PV panel (CH2: 5 V/div).

Experimental results were also taken for different values of resistance. As such, Table 6.1 contains the obtained results in which the highest value of extracted power can be seen in relation to the maximum power available. Again, all tests were performed considering an input voltage of 30 V. By consulting the values below, it can be seen that the efficiency of the MPPT tends to be better for lower values of maximum power. Nonetheless, the obtained results show that, for the values of rheostat used, the efficiency of the MPPT is higher than 95%.

Development of Power Converters for Electric Vehicle Charging with Photovoltaics Interface
Júlio André Machado Fernandes - University of Minho

109

Table 6.1 - Experimental results of the MPPT algorithm.

R_{rh} [Ω]	V_{rh} [V]	V_{PV} [V]	I_{PV} [A]	P_{max} [W]	P_{PV} [W]	P_{max}%
5.4	13.1	16.9	2.4	41.6	40.56	97.5
10.7	14.1	15.9	1.31	21	20.8	99
17.3	14.6	15.4	0.84	13	12.93	99.5
24.1	15.1	14.9	0.63	9.34	9.33	99.8

6.5. Experimental Results of the Bidirectional DC-DC Converter

The next step was to validate the functioning of the bidirectional DC-DC converter, operating in both buck and boost modes. In the cases where it is desired to charge the batteries, an RC load was used in order to simulate a real battery, as it is shown in Figure 6.18. The load is comprised by the parallel association of a 47 mF capacitor with 3, series connected, 4 Ω resistors.

Figure 6.18 - RC load used to simulate the charging of the battery.

The circuit used to validate the buck mode of operation can be found in Figure 6.19. The values of *L*, *C1* and *C2* are 3 mH, 5 mF and 0.7 mF, respectively. Also, the DC workbench power supply that was connected to the DC-link was set to a voltage of 30 V.
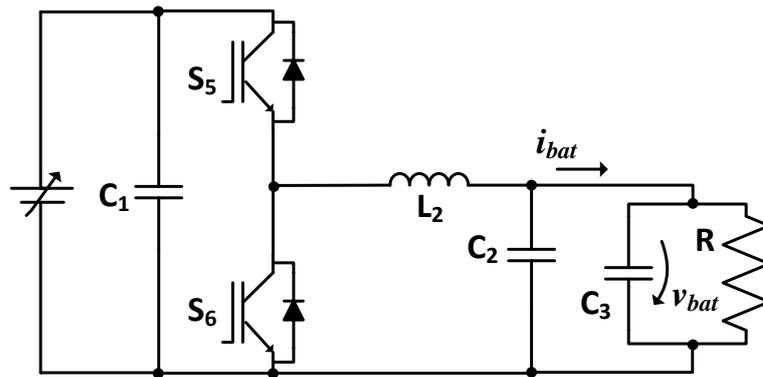
Figure 6.19 - Power circuit used to test the bidirectional DC-DC converter in buck mode.

The objective of this experimental test is to deliver to the load a constant current of 1 A and the obtained results are shown in Figure 6.20.
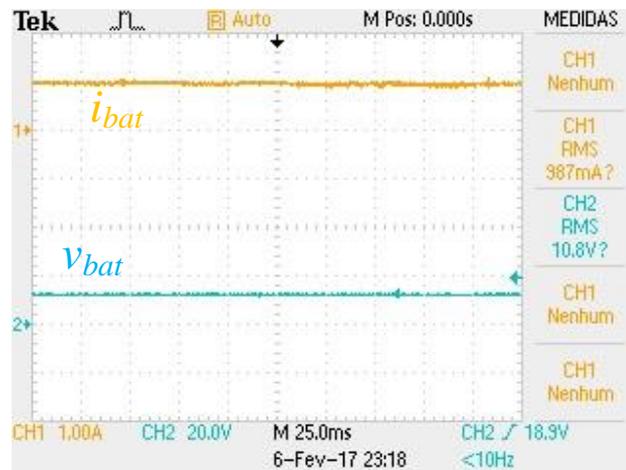
Figure 6.20 - Experimental results obtained during buck operation: battery current (CH1: 1 A/div) and voltage (CH2: 20 V/div).

It can be seen that a constant current of nearly 1 A is indeed being delivered to the load, which validates the implemented controller.

Finally, in order to validate the boost mode of operation, the circuit depicted in Figure 6.21 was utilized. For this test, the battery was simulated using a DC workbench power supply set to 12 V. The values of L, C_1 and C_2 remain unchanged from the previous circuit presented in Figure 6.19. The chosen value of R was 25 Ω.

Development of Power Converters for Electric Vehicle Charging with Photovoltaics Interface
Júlio André Machado Fernandes - University of Minho

111
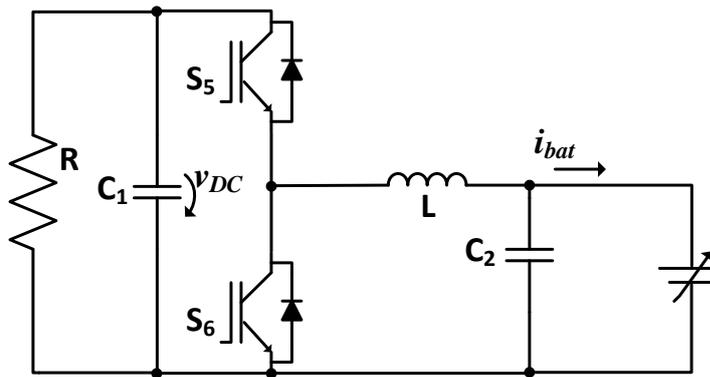
Figure 6.21 - Power circuit used to test the bidirectional DC-DC converter in boost mode.

It is intended, at this time, to deliver a constant current of 2 A to the load connected to the DC-link thus simulating the discharging of a battery. The obtained results are presented in Figure 6.22. The analysis of the results presented below allows concluding that the DC supply is delivering a constant current of 2 A to the load that is connected to the DC-link. This effectively simulates the expected behavior when discharging a battery, thus the controller was successfully tested and validated.
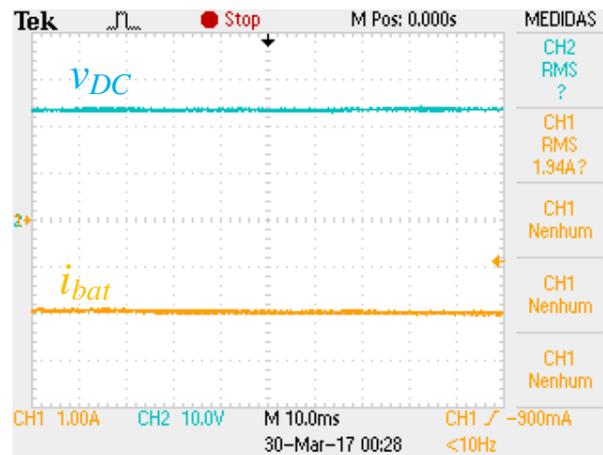
Figure 6.22 - Experimental results obtained during boost mode: battery current (CH1: 1 A/div) and DC-
-link voltage (CH2: 10 V/div).

6.6. Experimental Results of the Charging of the Batteries by the PV Panel

So far, each of the converters utilized for the integrated battery charger with interface for renewable energy sources were tested individually. Suffice it to say, given the results obtained, that the performance of each converter working independently was positive enough in order to validate its correct operation.

Naturally, for the whole system to operate, more than one converter will be working hence the reason why it is of the upmost importance to test and validate the

operation of multiple converters. As such, the first experimental test was performed in an effort to validate the charging of the batteries directly from a renewable energy source (i.e. PV panel). As it was stated in the initial chapter, the charging of the batteries directly from the PV panel is one of the key aspects of this dissertation, as it presents a change to conventional battery charging systems.

To assess this mode of operation, the following power circuit was used.
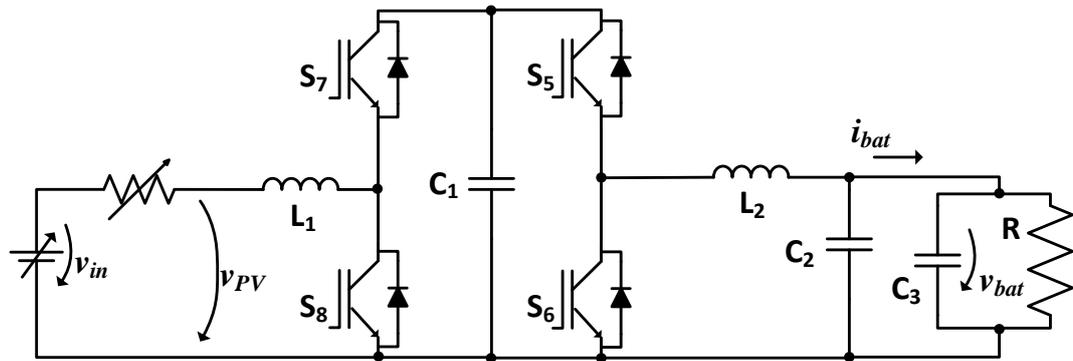
Figure 6.23 - Power circuit used to test the charging of the batteries by the renewable energy source.

Once again, the PV panel is simulated by a DC workbench power supply in series with a rheostat. Like in previous tests, the value of v_{in} is 30 V which means that the maximum power is extracted when v_{pv} = 15 V. The battery is again simulated by the RC load that was used in previous experiments. Nonetheless, the values of the other components remain unchanged from previous tests.

It should be noted that, in this case, where the AC-DC converter is not present to regulate the DC-link, it is not possible to extract the maximum power from the PV panel and charge the batteries with a specified current while maintaining the DC-link regulated. As such, some control strategies needed to be adapted considering these factors. If the battery pack has a voltage that is lower than the voltage across the terminals of the PV panel, the converter responsible for the MPPT must work as a buck converter. In this case, IGBTs *S6*, *S7* and *S8* will be permanently open. Therefore, the switching signal resulting from the MPPT algorithm is applied only to *S5*. On the other hand, if the battery voltage is higher than the PV panel voltage, the converter will operate in boost mode. In this case, *S6* and *S7* will be permanently open and *S5* permanently closed with the PWM signal being applied to *S8*. In both these cases, there is no control over the charging current of the batteries. Experimental tests were carried out for both these cases. For the first case described above, the experimental results that were obtained are shown in Figure 6.24. There it can be seen

Development of Power Converters for Electric Vehicle Charging with Photovoltaics Interface
Júlio André Machado Fernandes - University of Minho

113

the waveforms, in steady-state, of the voltage across the PV panel, the voltage across the battery and also the charging current of the battery.
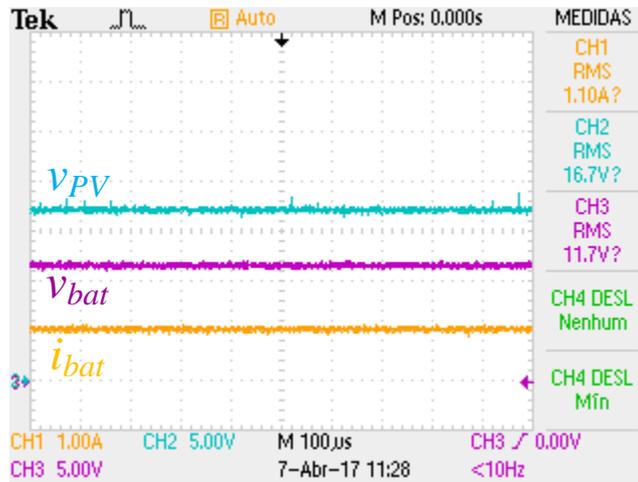
Figure 6.24 - Experimental results obtained during charging in buck mode: battery voltage (CH3: 5 V/div), battery current (CH1: 1 A/div) and PV panel voltage (CH2: 5 V/div).

It can be seen from the analysis of Figure 6.24 that the batteries are indeed being charged, being evident that v_{PV} is higher than v_{bat}. Furthermore, the value of the voltage across the PV panel is close to 15 V which allows concluding that nearly the maximum power is being extracted. It should be noted that there are deviations in the measurements obtained in the oscilloscope. Actually, the measured values by the ADC of v_{PV} were never higher than 16 V. These deviations are explained by the fact the sensors were modeled for higher values of voltage and current. Nevertheless, the obtained results are good enough to validate what was proposed.

On to the next step, Figure 6.25 shows the acquired waveforms when the converter is performing the charge of the batteries in boost mode.
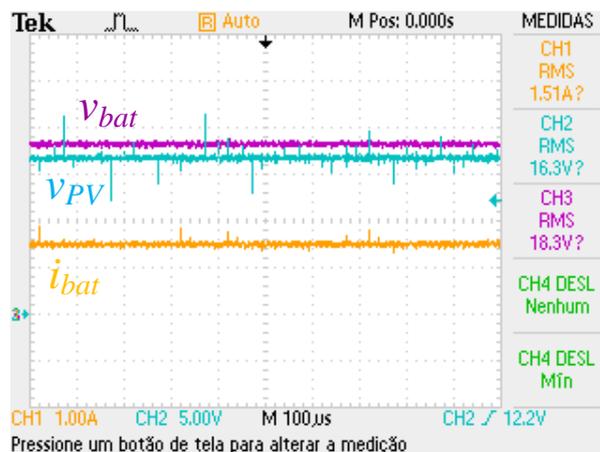
Figure 6.25 - Experimental results obtained during charging in boost mode: battery voltage (CH3: 5 V/div) and current (CH1: 1 A/div) and PV panel voltage (CH2: 5 V/div).

Once again the obtained results prove that the batteries are being charged with the energy provided by the renewable energy source. In addition, the converter is also operating near its MPP and it can be seen that the battery voltage is higher than the voltage across the PV panel.

6.7. Experimental Results of the G2V Mode

As it was previously mentioned, this mode is characterized by the charging of the EV's batteries being performed by the power grid. To test and validate this operation mode experimentally, the power circuit presented in Figure 6.26, was used.
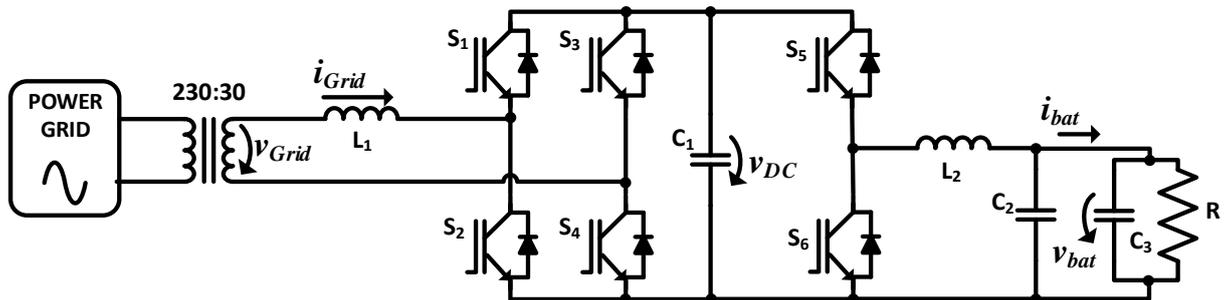
Figure 6.26 - Power circuit used to test the G2V mode.

For this operation mode to be successfully validated, it is intended to deliver to the battery a constant current, thus simulating the stage of constant current charging of a real battery. The battery will be charged by the power grid so it is desired that the grid current (i_{Grid}) be sinusoidal and in-phase with the grid voltage (v_{Grid}). The DC-link voltage (v_{DC}) should be kept at a higher voltage than the peak of v_{Grid}, the reference voltage being 75 V. Initially, the battery reference charging current was defined as 1 A. The obtained results are presented in Figure 6.27.
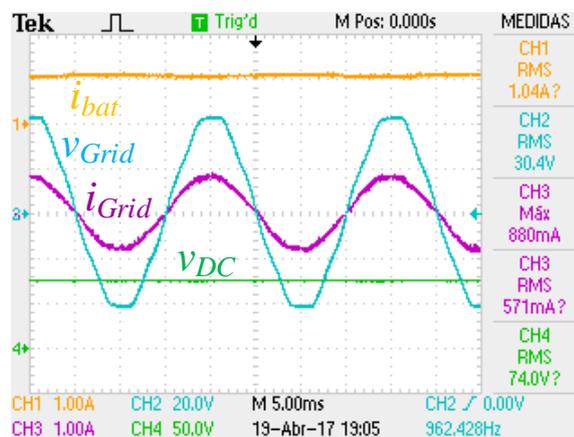
Figure 6.27 - Experimental results obtained during G2V mode with a reference charge current of 1 A: battery current (CH1: 1 A/div), grid voltage (CH2: 20 V/div), grid current (CH3: 1 A/div) and DC-link voltage (CH4: 50 V/div).

Development of Power Converters for Electric Vehicle Charging with Photovoltaics Interface
Júlio André Machado Fernandes - University of Minho

115

It is possible to conclude through the analysis of Figure 6.27 that the battery is being charged with a constant current that follows the 1 A reference imposed. A slight ripple is visible on i_{bat}, caused by the oscillation of the DC-link voltage. However, it can be seen that the ripple of i_{bat} does not exceed 0.2 A. On the grid side, it can be seen that the current (i_{Grid}), although not perfectly sinusoidal, is in phase with the voltage (v_{Grid}). The DC-link voltage is also kept regulated around the desired reference. The same experiment was made, this time with the reference charge current raised to 2 A. The obtained results are visible in Figure 6.28.
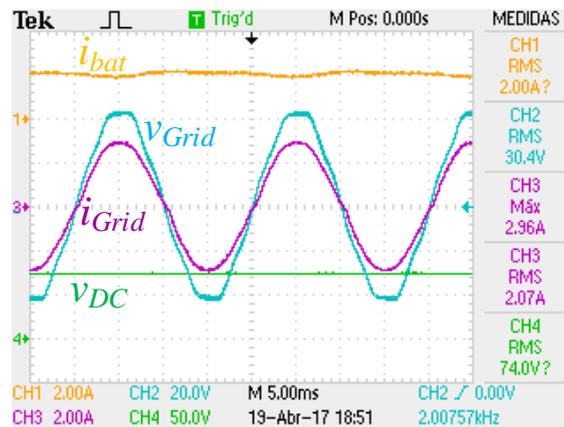
Figure 6.28 - Experimental results obtained during G2V mode with a reference charge current of 2 A: battery current (CH1: 2 A/div), grid voltage (CH2: 20 V/div), grid current (CH3: 2 A/div) and DC-link voltage (CH4: 50 V/div).

The obtained results for a charging current of 2 A are also positive, showing a visible improvement to the quality of the waveform of the grid current. This coincides with the previous experimental results obtained with the AC-DC in which it was verified that the overall quality of the synthesized wave by the controller is directly proportional to its amplitude.

Considering these results, and although there is still room for improvement, they are sufficient to experimentally validate the control strategies employed in this mode of operation.

6.8. Experimental Results of the V2G Mode

In this mode of operation, the batteries discharge their stored energy into the electrical power grid. As such, the power circuit used to test this mode is illustrated in Figure 6.29.
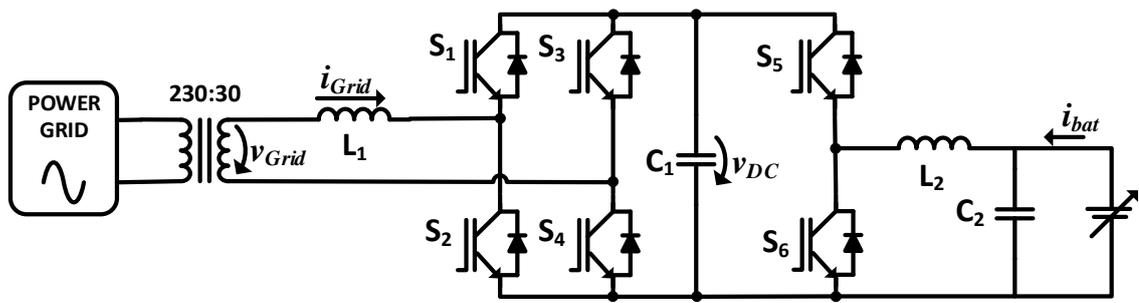
Figure 6.29 - Power circuit used to test the V2G mode.

Like in the previous experimental tests involving the operation of the bidirectional DC-DC converter in boost mode, that is, when it is intended to discharge the battery, a DC workbench power supply was used to simulate the battery. The value of the voltage provided by the supply was set to 30 V.

In the experimental tests that were made, the goal was to successfully discharge the battery with a constant power, which in this case corresponds to a constant current, while maintaining the DC-link voltage regulated to a reference value of 75 V. The grid current should be sinusoidal but in phase opposition with the voltage, as the energy will flow from the DC workbench power supply to the power grid. Initially, the reference discharge power was defined to 60 W, translating into a discharge current of 2 A. The experimental results that were obtained can be seen in Figure 6.30.
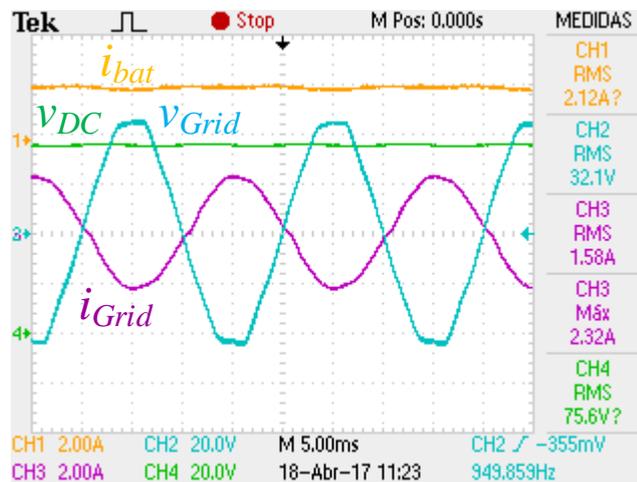

Figure 6.30 - Experimental results obtained during V2G mode with a reference discharge power of 60 W: battery current (CH1: 2 A/div), grid voltage (CH2: 20 V/div), grid current (CH3: 2 A/div) and DC-link voltage (CH4: 20 V/div).

The waveforms presented above indicate that energy is being successfully injected into the electrical power grid. The controller on the battery side is able to keep the discharging power practically constant, with the current possessing a low value of ripple. On the grid side, the results are encouraging. It can be seen that the grid current has a fairly acceptable waveform and that the regulation of the DC-link is achieved.

Development of Power Converters for Electric Vehicle Charging with Photovoltaics Interface
Júlio André Machado Fernandes - University of Minho

117

Finally, Figure 6.31 presents the obtained experimental results for a reference discharge power of 90 W. It can be seen that the discharge current is kept constant at 3 A and the quality of the injected current into the power grid visibly increases.
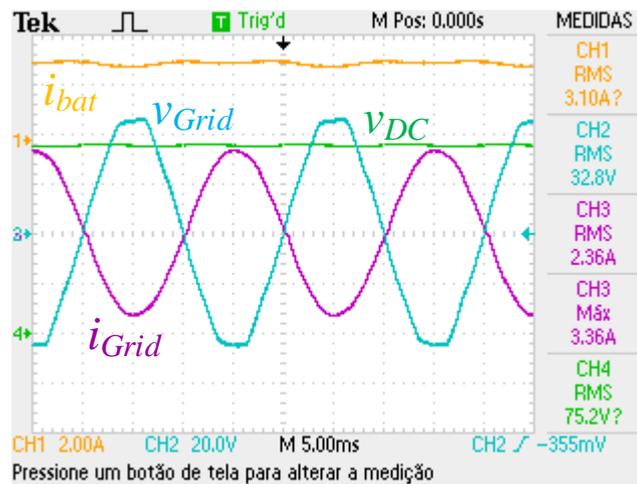

Figure 6.31 - Experimental results obtained during V2G mode with a reference discharge power of 90 W: battery current (CH1: 2 A/div), grid voltage (CH2: 20 V/div), grid current (CH3: 2 A/div) and DC-link voltage (CH4: 20 V/div).

The above presented results allow the experimental validation of the V2G operation mode.

6.9. Conclusions

The results obtained during the experimental stage of the development of this integrated power converter for EV battery charging with interface to renewable energy sources were presented and discussed in the present chapter. A key aspect to consider is that the values of the quantities used, either for voltage or current, are below the nominal values for which the converter was designed to operate. As such, when performing experiments in which the connection to the power grid is required, a transformer was used to provide isolation and also to lower the grid voltage from 230 V to 30 V.

The methodology in this chapter closely follows the approach that was taken during the simulations of the system. As such, each converter was firstly tested individually in order to simplify the process of adjusting and validating the control strategies proposed in Chapter 4.

Initially, the analysis of the grid synchronization algorithm (PLL) was carried out. The results that were obtained show that the implemented SOGI PLL is well capable of generating a phase locked sinusoidal reference from a distorted input signal, provided by the grid voltage. Moreover, when the controller is enabled, the synchronization with

the power grid is established in less than 2 cycles of the grid voltage, as evidenced in Figure 6.3, which for the application in question, is a very positive result.

After the confirmation that the PWM signals were being correctly applied to the IGBTs of the AC-DC converter, this converter was tested in different operation modes. Firstly, operating as a VSI and supplying a resistive load, it is concluded that both the converter and the control system operate as intended and in accordance with the results obtained in simulation. When the operation as a grid connected VSI was tested, it was demonstrated that the current control algorithm previously tested working together with the PLL allowed for a sinusoidal current with a close to unitary power. As for the inverse operation, as an active rectifier, it was verified that the control system forces the converter to draw a sinusoidal current from the power grid, in phase with the voltage. Also, the correct regulation of the DC-link voltage was achieved by connecting a resistive load to the DC-link thereby introducing losses to the system.

Next, the performance of the MPPT controller was evaluated. A PV panel was simulated using a DC workbench power supply connected in series with a rheostat, the purpose of which was to limit the amount of power the DC supply could deliver. The MPPT algorithm proved to be capable of producing fairly satisfactory results. Despite still being possible to improve the parameters of the MPPT, as a way of increasing its overall efficiency, it should be noted that, because of the low values of voltage and current used, the variations in the extracted power are more accentuated in percentage terms relative to the maximum power available.

As for the batteries, the experimental results obtained for the bidirectional DC-DC converter, both in buck and boost operation revealed that the controller was capable of keeping the battery current practically constant and in conformity with the stipulated reference.

With each converter's individual operation validated, the next step was to evaluate the performance of the system when two converters were required to function at the same time.

One of the major aspects of this dissertation that was successfully tested was the charging of the batteries directly from the renewable energy source. Because in the case in question the AC-DC converter was not working, the control over the charging current had to be sacrificed under penalty of the DC-link voltage rising to values that could potentially endanger the integrity of the system. As such, the batteries would be charged entirely with the energy provided by the PV, operating in its MPP. Two distinct cases were tested and both produced the expected results.

Development of Power Converters for Electric Vehicle Charging with Photovoltaics Interface
Júlio André Machado Fernandes - University of Minho

119

The obtained results for the AC-DC converter working simultaneously with the bidirectional DC-DC converter, in G2V mode, proved the system was able to perform the charge of the batteries from the power grid with a constant charging current. Again, the AC-DC converter was able to keep the DC-link voltage regulated around the reference while consuming a sinusoidal current, in phase with the grid voltage.

The same results were obtained for the V2G mode. In this case, the system was able to discharge the batteries with a constant power and inject the energy into the power grid.

Despite the obtained results and the control algorithms that were validated during this stage, the tests involving the three converters are yet to be made. As such, it would be interesting to evaluate the operation of the system during the G2V and V2G modes with the assist of the PV panel.

CHAPTER 7

Conclusions

7.1. Conclusions

It was presented in this Master's Dissertation the development of an integrated power converter for electric vehicle charging with optimized interface for renewable energy sources. This work is yet another contribution to the on-going global effort towards the reduction of pollution, focused primarily on Electric Mobility and also in the production of clean, renewable energy. As such, the developed solution offers the possibility of charging the batteries of an EV directly from the renewable source, reducing losses, and thus increasing the efficiency of the process. Furthermore, the possibility of bidirectional energy flow is also enabled which means that it is possible to both charge the batteries of the EV and deliver part of their stored energy back to the power grid, when the circumstances are propitious. In the growing context of the Smart Grids, in which the communication of the vehicles with the local utilities will happen in order to ensure that the batteries are charged when the electricity is cheapest and the impact of the charging systems on the grid is smallest, this work also aims to make its contribution.

Initially, in Chapter 1, a review of some statistical data, disclosed by their respective competent authorities, concerning the present day energy demands was presented. The fact is that, in 2016, the world is still heavily dependent on fossil fuels and that renewable energies are just a needle in a haystack when it comes to worldwide energy production. This exalts the importance of developing new solutions and technologies to turn the tide towards a cleaner planet Earth. Still in this chapter, a brief summary of the World's production of photovoltaic energy was made. The objectives drawn for year 2020 under the NREAP program, which establish the minimum installed capacity for photovoltaic energy production, were presented. Currently, Portugal is still far from reaching its designated installed capacity. Having to install roughly 60 MW a year in order to reach the goal set for 2020, it is of the upmost importance to internally develop solutions for solar photovoltaic energy production. Despite still not being able to compete with other renewable energy sources like the hydroelectric and wind, the production of photovoltaic energy is rapidly growing.

Development of Power Converters for Electric Vehicle Charging with Photovoltaics Interface
Júlio André Machado Fernandes - University of Minho

122

In Chapter 2, the major aspects regarding Electric Mobility were approached. A review was made of the more recent technologies employed in EVs, such as the different types of batteries that can be used and even the existing power electronics associated with EV battery charging systems. It was also shown how an EV would integrate a Smart Grid, with concepts such as V2G, G2V and V2H being explained. It is well known that, despite being arguably identical to an ICE vehicle with the same characteristics, the low autonomy of an EV is definitely its Achilles' heel. Nevertheless, major investigations and investments are currently under way with the goal of developing new technology capable of increasing the vehicle's autonomy. Also in this chapter, the composition of a PV panel and the processes that occur during the electricity production through solar radiation (i.e. photovoltaic effect) were briefly described. The effects that solar radiation and temperature have on, respectively, the current and voltage of a PV panel were also taken into account. Finally in this chapter, a review of MPPT algorithms employed in today PV systems was made. Several algorithms were studied, including those in which disconnection of the PV panel from the rest of the system is required (e.g. Open Voltage) and those in which it is not required (e.g. Perturb & Observe). At the end, the choice fell on the Incremental Conductance in which disconnection is not required and the oscillation around the MPP is theoretically lower than in the P&O algorithm.

The proposed system, in order to fully meet the specified requirements, would need to be comprised of a bidirectional AC-DC converter, a bidirectional DC-DC converter and a unidirectional DC-DC converter. As such, the next step on the development of this integrated converter was the study of existing solutions for the power converters aforementioned and it was presented in Chapter 3. This review of the state of the art of bidirectional AC-DC and DC-DC power converters resulted in the choice of the AC-DC Full-Bridge topology and the DC-DC buck-boost topology. While it is not the case here, it should be noted that, if the discrepancy between the voltage levels of the batteries and the DC-link is too high, the existence of galvanic isolation becomes crucial. The bipolar and unipolar SPWM modulation techniques, applicable to AC-DC converters, were then presented. Next, the variable frequency current control techniques, namely the hysteresis and the periodic sampling current control are presented. In terms of fixed frequency, the PI current control is also presented. It was concluded that the use of unipolar SPWM modulation, allied with the use of a fixed frequency current control technique, would produce the best results.

Development of Power Converters for Electric Vehicle Charging with Photovoltaics Interface
Júlio André Machado Fernandes - University of Minho

123

The computer simulations of the proposed integrated power converter are the main focus of Chapter 4. Regardless, before proceeding to the simulations, the modeling of the passive filters for each converter was made. The values of the inductors and capacitors were calculated aiming for admissible values of current and voltage ripples, resulting in a better quality of the synthesized waves. It should be noted that the calculated values correspond to the minimum values advised. The final choice to implement will always be influenced by the results of the simulation and also the standard values of the components. The simulations were made using the software PSIM. Each converter was simulated individually and then simultaneously. The results obtained prove that the designed system is viable and all of the proposed operation modes were validated. The simulated system successfully operated in V2G, G2V and in PV to Grid.

Chapter 5 focused on the implementation of the power converter. The choices for the control system and the power stage were individually presented and justified. The developed boards for the control system were introduced in full such as the command board and the signal conditioning board. The DSC in which the control algorithms were implemented was also presented along with its associated IDE.

Finally, the experimental results of the power converter are illustrated and discussed in Chapter 6. The obtained results met with the expected results, confirming the choices made during the developmental stages of this work. The charging/discharging of the batteries with a constant current was successfully performed. Moreover, the charging of the batteries directly from a DC workbench power supply, simulating a renewable energy source and operating in its MPP, was also verified. The obtained experimental results of the AC-DC converter show that the current in the power grid is sinusoidal and the power factor is close to unitary. Furthermore, the regulation of the DC-link is also achieved. However, there are still aspects to improve. The parameters of the MPPT algorithm can still be improved in order to minimize the oscillation around the MPP, ensuring a better efficiency. Also, the parameters of the PI controllers can also be modified in order to improve the obtained current and voltage waveforms. It is important to mention that the experimental tests were made for values lower than the nominal for which this converter was designed.

In terms of personal developments, this work allowed me to acquire knowledge that was not lectured during the degree, as it is expectable in an investigation project. Additionally, some not so fresh concepts were reacquired, especially in terms of microcontroller programming.

124

Development of Power Converters for Electric Vehicle Charging with Photovoltaics Interface
Júlio André Machado Fernandes - University of Minho

Unfortunately, I cannot hide the dissatisfaction for not being able to validate all the operation modes with the originally developed hardware, by the time the mobility period ended. However, given the amount of work of this project, the challenge that it was to develop it abroad and, more importantly, the significantly lesser time available for its completion, I would have to conclude that what was achieved has a positive balance in the end. Not to understate, of course, the importance of the results obtained at University of Minho which allowed me to perform the experimental tests on a more "controlled" environment, with enabled access to other components (i.e. DAC) which is a huge help in times of troubleshooting. Nonetheless, the achievements and failures throughout this project are part of a much vaster learning experience that has carried through and materialized to this Dissertation.

7.2. Proposals for Future Work

As mentioned above, this work can still be subject to improvements to its overall performance. Although the chosen topologies and control algorithms were experimentally validated, it is necessary to redo the tests, increasing the values at stake closer to their nominal values. It also would be interesting to carry out experimental tests with the goal of validating an entire battery charge cycle. Only then the constant voltage stage of charging would be verified.

Besides the aforementioned improvements to the MPPT algorithms, it would be important to perform again the tests to the unidirectional boost converter, only this time with a real PV panel instead of the DC workbench power supply in series with the rheostat. These tests could be made with different values of solar radiation and temperature as a way to determine the behavior of the MPPT in real conditions of operation.

Naturally, there are still modes of operation that were not validated in the hardware developed abroad that need to be verified. As such and although difficult, it would be important for this project as a whole to reacquire and redo the experimental tests to the original hardware. Also, as stated in the previous chapter, the performance of the system in V2G and G2V modes with the assist of the PV panel is yet to be assessed.

These are the major improvements to be made to this project. However, some other changes can be made to the benefit of the developed system such as:

- Create a user interface in which factors like the SoC of the batteries would be visible to the user. Also, the user would be given the chance to choose whether to charge or discharge the batteries, according to his needs;

- Utilize a bidirectional DC-DC converter that offers galvanic isolation therefore contributing to increase the safety of the system. An example of such converter is the Dual Active Bridge;

- Given that lead-acid batteries are only mainly used when converting ICE vehicles to EVs, the DC-DC converter's controller could be adapted to suit the charging/discharging needs of other types of batteries such as the lithium-ion, which are more frequently employed in EVs and PHEVs;

- The developed boards could be converted to PCBs, as it was originally planned, in order to reduce the size of the converter and improve the overall look of the converter;

- Finally, the converter could be adapted to a 3-phase system, allowing for faster charge times.

126

Development of Power Converters for Electric Vehicle Charging with Photovoltaics Interface
Júlio André Machado Fernandes - University of Minho

References

[1]   BP, "BP Statistical Review of World Energy 2016," June 2016. [Online].
       Available: https://www.bp.com/content/dam/bp/pdf/energy-economics/statistical-
       review-2016/bp-statistical-review-of-world-energy-2016-full-report.pdf. [Accessed
       22 3 2017].

[2]   PORDATA, "Consumo de energia primária: total e por tipo de fonte de energia -
       Portugal," 9 March 2017. [Online]. Available:
       http://www.pordata.pt/Portugal/Consumo+de+energia+prim%C3%A1ria+total+e+
       por+tipo+de+fonte+de+energia-1130. [Accessed 26 May 2017].

[3]   E. Proença, "A Energia Solar Fotovoltaica em Portugal," Msc
       Dissertation,Technical University of Lisbon, Lisbon, Portugal, 2007.

[4]   F. Naves, "Depois das barragens e das eólicas, chegou a vez da aposta no solar,"
       Diário de Notícias, 8 October 2016. [Online]. Available:
       http://www.dn.pt/sociedade/interior/depois-das-barragens-e-das-eolicas-chegou-a-
       vez-da-aposta-no-solar-5430494.html. [Accessed 25 March 2017].

[5]   Inês Almeida, "Avaliação e comparação do potencial solar e fotovoltaico em zonas
       urbanas," Msc. Dissertation, Universidade Nova de Lisboa, Lisbon, Portugal, 2013.

[6]   Green Rhino Energy, "Annual Solar Irradiance, Intermittency and Annual
       Variations," 2013. [Online]. Available:
       http://www.greenrhinoenergy.com/solar/radiation/empiricalevidence.php.
       [Accessed 25 March 2017].

[7]   M. Prado, "Produção de energia solar em Portugal acelerou em Agosto," Jornal de
       Negócios, 2 September 2014. [Online]. Available:
       http://www.jornaldenegocios.pt/empresas/energia/detalhe/producao_de_energia_so
       lar_em_portugal_acelerou_em_agosto. [Accessed 25 March 2017].

[8]   P. Pereira, "A Produção Fotovoltaica em Portugal - Análise da Legislação em
       Vigor e do Custo/benefício," Msc Dissertation, FEUP, Porto, Portugal, 2015.

[9]   Solar Power Europe, "Global Market Outlook for Solar Power 2015-2019," 2015.
       [Online]. Available: https://helapco.gr/pdf/Global_Market_Outlook_2015_-
       2019_lr_v23.pdf. [Accessed 25 March 2017].

[10] J. C. N. Freitas, "Projeto e Análise ao Funcionamento de Carros Elétricos," Msc.
       Dissertation, University of Minho, Guimarães, 2012.

[11] J. Martins and F. Brito, Carros Elétricos, Guimarães: Publindústria, 2011.

[12] J. Goldman, "Comparing Electric Vehicles: Hybrid vs. BEV vs. PHEV vs. FCEV,"
       Union of Concerned Scientists, 12 February 2014. [Online]. Available:
       http://blog.ucsusa.org/josh-goldman/comparing-electric-vehicles-hybrid-vs-bev-vs-
       phev-vs-fcev-411. [Accessed 26 May 2017].

[13] V. Monteiro, "Desenvolvimento de um Sistema Inteligente de Carregamento de Baterias," Msc. Dissertation, University of Minho, Guimarães, 2009.

[14] Texas Instruments, "Characteristics of Rechargeable Batteries," 2011. [Online]. Available: http://www.ti.com/lit/an/snva533/snva533.pdf. [Accessed 3 March 2017].

[15] Battery University, "How does the Lead Acid Battery Work?," 15 April 2016. [Online]. Available: http://batteryuniversity.com/learn/article/lead_based_batteries. [Accessed 22 March 2017].

[16] Northern Tool, "NPower Sealed Lead-Acid Battery — AGM-Type, 12V, 18 Amps," [Online]. Available: http://www.northerntool.com/shop/tools/product_200514451_200514451. [Accessed 3 May 2017].

[17] Ningbo Sealake Storage Battery Co.,Ltd, "NPower Sealed Lead-Acid Battery — AGM-Type, 12V, 18 A," Datasheet. [Online]. Available: http://www.northerntool.com/images/downloads/msds/829421.pdf. [Accessed 3 May 2017].

[18] Battery University, "BU-403: Charging Lead Acid," 4 March 2017. [Online]. Available: http://batteryuniversity.com/learn/article/charging_the_lead_acid_battery. [Accessed 3 May 2017].

[19] STA, "Manual das Baterias Recarregáveis, Pilhas e Carregadores," [Online]. Available: http://www.sta-eletronica.com.br/resources/downloads/manual.pdf. [Accessed 22 March 2017].

[20] Battery University, "BU-407: Charging Nickel-cadmium," 2 April 2016. [Online]. Available: http://batteryuniversity.com/learn/article/charging_nickel_based_batteries. [Accessed 3 May 2017].

[21] R. M. Dell and D. J. Rand, Understanding Batteries, Cambridge: The Royal Society of Chemistry, 2001.

[22] B. M. Sutin, "1976 Alfa Romeo EV Conversion," Skewray Research, 11 April 2013. [Online]. Available: http://www.skewray.com/articles/1976-alfa-romeo-spider-veloce-ev-conversion. [Accessed 3 March 2017].

[23] Battery University, "BU-304a: Safety Concerns with Li-ion," 21 September 2016. [Online]. Available: http://batteryuniversity.com/learn/article/safety_concerns_with_li_ion. [Accessed 3 May 2017].

[24] Battery University, "BU-204: How do Lithium Batteries Work?," 5 March 2016. [Online]. Available: http://batteryuniversity.com/learn/article/lithium_based_batteries. [Accessed 3 May

Development of Power Converters for Electric Vehicle Charging with Photovoltaics Interface
Júlio André Machado Fernandes - University of Minho

129

2017].

[25] H. Barbosa, "Sistema de Carregamento Externo de Baterias de Veículos Elétricos com Interface a Fonte de Energia Renovável," Msc. Dissertation, University of Minho, Guimarães, 2013.

[26] H. Boeriu, "BMW i3 range will be increased in 2016 with a new battery," 22 October 2015. [Online]. Available: http://www.bmwblog.com/2015/10/22/bmw-i3-range-will-be-increased-in-2016-with-a-new-battery/. [Accessed 3 March 2017].

[27] Battery University, "BU-409: Charging Lithium-ion," 21 February 2017. [Online]. Available: http://batteryuniversity.com/learn/article/charging_lithium_ion_batteries. [Accessed 3 May 2017].

[28] Green Car Reports, "The Ultimate Guide: Toyota Prius Battery Life, Cost, and Warranty.," 13 May 2011. [Online]. Available: http://www.greencarreports.com/news/1059907_the-ultimate-guide-toyota-prius-battery-life-cost-and-warranty. [Accessed 3 March 2017].

[29] Schneider Electric, "Connection Method for Charging Systems - a key element for Electric Vehicles.," 2010. [Online]. Available: http://www.schneider-electric.co.uk/documents/electrical-distribution/en/local/ev/Connection-method-for-charging-systems.pdf. [Accessed 22 March 2017].

[30] V. Monteiro, H. Gonçalves and J. L. Afonso, "Impact of Electric Vehicles on Power Quality in a Smart Grid Context," in *13th IEEE International Conference on Electrical Power Quality and Utilization (EPQU)*, Lisbon, 2011.

[31] V. Monteiro, H. Gonçalves, J. C. Ferreira and J. L. Afonso, "Batteries Charging Systems for Electric and Plug-In Hybrid Electric Vehicles," in *New Advances in Vehicular Technology and Automotive Engineering*, InTech, 2012.

[32] V. Monteiro, J. C. Ferreira, J. G. Pinto, B. Exposto, D. Pedrosa and J. L. Afonso, ""Comparison of Charging Systems for Electric Vehicles and Their Impact on Electrical Grid"," in *Annual Seminar on Automation, Industrial Electronics and Instrumentation 2012 - SAAEI'12*, Guimarães, Portugal, 2012, pp. 440-445.

[33] V. Monteiro, J. C. Ferreira, J. G. Pinto, D. Pedrosa and J. L. Afonso, ""iV2G Charging Platform"," in *13th International IEEE Conference on Intelligent Transportation Systems (ITSC)*, , pp 409-414, Madeira, Portugal, 2010.

[34] S. Shandilya, "Handbook of Research on Emerging Technologies for Electrical Power Planning, Analysis, and Optimization (Advances in Computer and Electrical Engineering)", 1st ed., IGI Global, 2016.

[35] C. Honsberg and S. Bowden, "Module Structure," PV Education, 2017. [Online]. Available: http://pveducation.org/pvcdrom/modules/modules-structure. [Accessed 25 March 2017].

130

Development of Power Converters for Electric Vehicle Charging with Photovoltaics Interface
Júlio André Machado Fernandes - University of Minho

[36] C. Honsberg and S. Bowden, "The Photovoltaic Effect," PV Education, 2017. [Online]. Available: http://pveducation.org/pvcdrom/the-photovoltaic-effect. [Accessed 25 March 2017].

[37] A. D. Dhass, P. Lakshmi and E. Natarajan, "Investigation of Performance Parameters of Different Photovoltaic Cell Materials using the Lambert-W Function," in *5th International Conference on Advances in Energy Research, ICAER 2015*, Mumbai, India, 15-17 December.

[38] A. D. Hansen, P. E. Sørensen, L. H. Hansen and H. W. Bindner, "Models for a Stand-alone PV System," Technical University of Denmark, Roskilde, 2001.

[39] Coastal Climate Control, "Estimating Daily Power Output from Solar Panels," 2017. [Online]. Available: https://www.coastalclimatecontrol.com/index.php/blog/130-estimating-daily-power-output-from-solar-panels.html. [Accessed 25 March 2017].

[40] Alternative Energy, "Common Types of Solar Cells," 2015. [Online]. Available: http://www.altenergy.org/renewables/solar/common-types-of-solar-cells.html. [Accessed 25 March 2017].

[41] R. F. Coelho and D. C. Martins, "An Optimized Maximum Power Point Tracking Method Based on PV Surface Temperature Measurement," in *Sustainable Energy - Recent Studies*, Dr. Alemayehu Gebremedhin (Ed.), InTech, DOI: 10.5772/51167, 2012.

[42] K. Kobayashi, H. Matsou and Y. Sekine, "An Excellent Operating Point Tracker of the Solar-Cell Power Supply System," *IEEE Transactions on Industrial Electronics,* Vols. 53, No 2, April 2006.

[43] A. Dolara, R. Faranda and S. Leva, "Energy Comparison of Seven MPPT Techniques for PV Systems," *J. Electromagnetic Analysis & Applications,* vol. 3, pp. 152-162, July 2009.

[44] S. Sengar, "Maximum Power Point Tracking Algorithms for Photovoltaic System: A Review," *International Review of Applied Engineering Research,* Vols. 4, No 2, pp. 147-154, 2014.

[45] D. S. Morales, "Maximum Power Point Tracking Algorithms for Photovoltaic Applications," Msc Dissertation, Aalto University, 2010.

[46] T.-C. Yu and Y.-C. Lin, "A Study on Maximum Power Point Tracking Algorithms for Photovoltaic Systems," Lunghwa University of Science and Technology, Taiwan, 2010.

[47] N. Moubayed, A. El-Ali and R. Outbib, "A Comparison of Two MPPT Techniques for PV System," Aix-Marseille University, Marseille, France, 2009.

[48] Fraunhofer Institute for Solar Energy Systems, "New world record for solar cell efficiency at 46% – French-German cooperation confirms competitive advantage of European photovoltaic industry," 1 Decemeber 2014. [Online]. Available:

Development of Power Converters for Electric Vehicle Charging with Photovoltaics Interface
Júlio André Machado Fernandes - University of Minho

131

https://www.ise.fraunhofer.de/en/press-media/press-releases/2014/new-world-record-for-solar-cell-efficiency-at-46-percent.html. [Accessed 26 March 2017].

[49] T. Sousa, "Filtro Ativo de Potência Paralelo Monofásico com Conversor CC-CC Bidirecional para Interface com Baterias," Msc. Dissertation, University of Minho, Guimarães, Portugal, 2016.

[50] H. R. Karshenas, H. Daneshpajooh, A. Safaee, P. Jain and A. Bakhshai, "Bidirectional DC - DC Converters for Energy Storage Systems," in *Energy Storage in the Emerging Era of Smart Grids*, InTech, 2011, pp. 162-178.

[51] D. C. Erb, O. C. Onar and A. Khaligh, ""Bi-Directional Charging Topologies for Plug-in Hybrid Electric Vehicles"," Illinois Institute of Technology, 2010.

[52] C. Kamalakannan, L. P. Suresh, S. S. Dash and B. K. Panigrahi, "Power Electronics and Renewable Energy Systems," in *Lecture Notes in Electrical Engineering*, Springer, New Delhi, 2014.

[53] T. Polsevi and R. Muthu, "Comparison of Cascaded H-Bridge, Neutral Point Clamped and Flying Capacitor Multilevel Inverters using Multicarrier PWM," 2011.

[54] A. K. Sharma, A. K. Sharma and N. Vijay, "Unipolar and Bipolar SPWM Voltage Modulation Type inverter for Improved Switching Frequencies," in *International Journal of Engineering Sciences & Research Technology*, 2014.

[55] R. Almeida, "Desenvolvimento de um Filtro Ativo Paralelo Monofásico Compacto e Didático Utilizando MOSFETs," Msc Dissertation, University of Minho, Portugal, 2013.

[56] L. A. Serpa, "Current Control Strategies for Multilevel Grid Connected Inverters," Swiss Federal Institute of Technology, Zurich, 2007.

[57] M. P. Kazmierkowski and L. Malesani, "Current Control Techniques for Three-Phase Voltage-Source PWM Converters: A Survey," in *IEEE Transactions on Industrial Electronics*, 2013.

[58] K. Sundararajan, A. Nachiappan and G. Veerapathiran, "Comparison of Current Controllers for a Five-level Cascaded H-Bridge Multilevel Inverter," in *International Journal Of Computational Engineering Research*, 2012.

[59] A. Araújo, J. G. Pinto, B. Exposto, C. Couto and J. L. Afonso, "Implementation and Comparison of Different Switching Techniques for Shunt Active Power Filters," in *IECON – 40th Annual Conference of the IEEE*, Dallas, TX, USA, 2014.

[60] A. I. Maswood and E. Al-Ammar, "Analysis of a PWM Voltage Source Inverter with PI Controller under Non-ideal conditions," in *Conference Proceedings IPEC*, Singapore, 2010.

[61] R. Macedo, "Desenvolvimento de um Inversor Multinível Monofásico para Aplicações de Qualidade de Energia Elétrica," Msc. Dissertation, University of

132

Development of Power Converters for Electric Vehicle Charging with Photovoltaics Interface
Júlio André Machado Fernandes - University of Minho

Minho, Guimarães, Portugal, 2015.

[62] A. Abouloifa, F. Giri, I. Lachkar, M. Haloua, J. Rodellar and F. Ikhouane, "Concurrent and Simple Controller for AC/DC Power Converters - Theoretical Design and Experimental Evaluation," in *2007 IEEE International Symposium on Industrial Electronics*, 4-7 June 2007.

[63] G. Benysek and M. Pasko, Power Theories for Improved Power Quality, Springer-Verlag London, 2012.

[64] J. G. Pinto, V. Monteiro, H. Gonçalves and J. L. Afonso, "Onboard Reconfigurable Battery Charger for Electric Vehicles With Traction-to-Auxiliary Mode," *IEEE Transactions on Vehicular Technology,* vol. 63, pp. 1104-1116, March 2014.

[65] L. P. Mandal and R. W. Cox, "A transient-based approach to estimation of the electrical parameters of a lead-acid battery model," in *Energy Conversion Congress and Exposition (ECCE)*, 12-16 September 2010.

[66] A. Nikolian, J. d. Hoog, K. Fleurbay, J.-M. Timmermans, O. Noshin, P. V. d. Bossche and J. V. Mierlo, "Classification of Electric modelling and Characterization methods of Lithium-ion Batteries for Vehicle Applications," in *European Electric Vehicle Congress*, Brussels, Belgium, 3-5 Dec 2014.

[67] M. Green, "Design Calculations for Buck-Boost Converters," Texas Instruments Application Report nº SLVA535A, 2012.

[68] S. Danielak, J. Haverstock, D. Krebs and D. Spaulding, "Bidirectional DC-DC Converter Drive System for Electric Vehicle," Purdue University Fort Wayne, Indiana, USA, 2014.

[69] Kyocera, "High Efficiency Multicrystal Photovoltaic Module," KD215GX-LPU Datasheet, 2008.

[70] B. Hauke, "Basic Calculation of a Boost Converter's Power Stage," Texas Instruments Application Report nº SLVA372C, 2009.

[71] K. Możdżyński, K. Rafał and M. Bobrowska-Rafal, "Application of the second order generalized integrator in digital control systems," *Archives of Electrical Engineering,* vol. 63, pp. 423-437, 2014.

[72] LEM, "Voltage Transducer LV 25-P," Datasheet, 2014. [Online]. Available: http://www.lem.com/docs/products/lv_25-p.pdf. [Accessed 16 October 2016].

[73] LEM, "Current Transducer LA 55-P," Datasheet, 2014. [Online]. Available: http://www.lem.com/docs/products/la_55-p_e.pdf. [Accessed 16 October 2016].

[74] Texas Instruments, "TL43xx Precision Programmable Reference," Datasheet, 2015. [Online]. Available: http://www.ti.com/litv/pdf/slvs543o. [Accessed 27 October 2016].

Development of Power Converters for Electric Vehicle Charging with Photovoltaics Interface
Júlio André Machado Fernandes - University of Minho

133

[75] Texas Instruments, "TL07xx Low-Noise JFET-Input Operational Amplifiers," Datasheet, 2015. [Online]. Available: http://www.ti.com/lit/ds/symlink/tl072.pdf. [Accessed 28 October 2016].

[76] Texas Instruments, "TMS320F2833x, TMS320F2823x Digital Signal Controllers (DSCs)," Datasheet, 2016. [Online]. Available: http://www.ti.com/lit/ds/symlink/tms320f28335.pdf. [Accessed 27 October 2016].

[77] Texas Instruments, "SNx4LV06A Hex Inverter Buffers/Drivers With Open-Drain Outputs," Datasheet, 2016. [Online]. Available: http://www.ti.com/lit/ds/symlink/sn74lv06a.pdf. [Accessed 27 October 2016].

[78] NXP, "74HC540, 74HCT540 Octal buffer/line driver, 3-state, inverting," Datasheet, 2016. [Online]. Available: http://www.nxp.com/documents/data_sheet/74HC_HCT540.pdf. [Accessed 27 October 2016].

[79] MeanWell, "60W Triple Output Switching Power Supply," Datasheet, 2005. [Online]. Available: http://pdf1.alldatasheet.com/datasheet-pdf/view/259473/MEANWELL/T-60C.html. [Accessed 27 October 2016].

[80] PowerSyS, "P3G 1000W Instruction Manual," PowerSyS, Poland, 2008.

[81] Semikron, "IGBT Peak Voltage Measurement and Snubber Capacitor Specification," Application Note AN-7006, 2008. [Online]. Available: https://www.semikron.com/dl/service-support/downloads/download/semikron-application-note-igbt-peak-voltage-measurement-and-snubber-capacitor-specification-en-2008-03-17-rev-00. [Accessed 27 March 2017].

[82] CDE Cornell Dubilier, "Designing RC Snubber Networks," 2013. [Online]. Available: http://www.cde.com/resources/catalogs/igbtAPPguide.pdf. [Accessed 27 March 2017].

[83] NXP, "Designing RC snubbers," 2012. [Online]. Available: http://www.nxp.com/documents/application_note/AN11160.pdf. [Accessed 27 March 2017].

[84] University of California, "Inductor Construction," [Online]. Available: http://www.ece.ucsb.edu/~long/ece145b/Lab2_218b/INDUCTOR_w02.pdf. [Accessed 24 April 2017].

[85] MW Power, "MW 40-12," Datasheet, 2008.

[86] EU, "EU Energy Markets in 2014," 13 October 2014. [Online]. Available: http://ec.europa.eu/energy/sites/ener/files/documents/2014_energy_market_en_0.pdf. [Accessed 22 March 2017].

[87] J. Balsa, "Avaliação do Impacto da Introdução de Veículos Elétricos na Procura de Combustíveis em Portugal," Msc. Dissertation, University of Coimbra, Coimbra, 2013.

134

Development of Power Converters for Electric Vehicle Charging with Photovoltaics Interface
Júlio André Machado Fernandes - University of Minho

[88] P. Mao, M. Zhang, S. Cui, W. Zhang and B.-H. Kwon, "A Review of Current Control Strategy for Single-Phase Grid-Connected Converters," *Indonesian Journal of Electrical Engineering and Computer Science,* vol. 12, p. 563, 2014.

Appendix
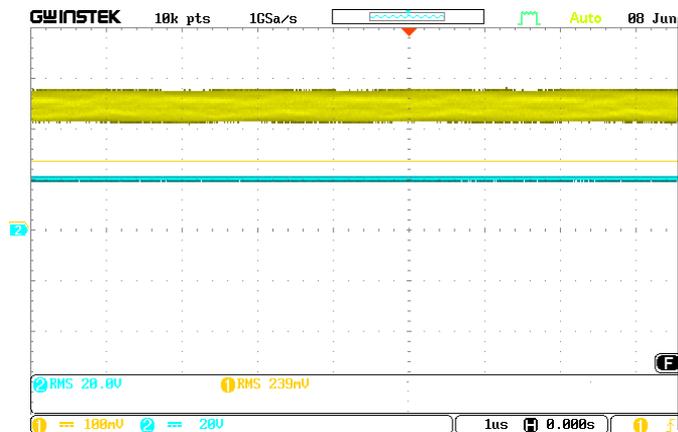
Appendix i - Voltage sensor board test results for a 20 V input signal: output signal (CH1: 100 mV/div) and input signal (CH2: 20 V/div).
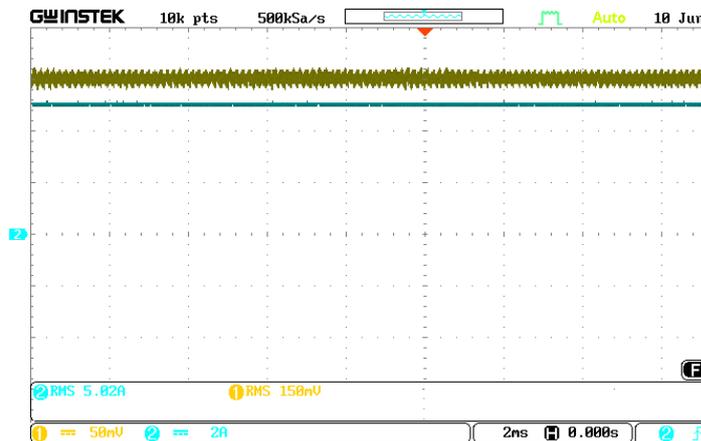

Appendix ii - Current sensor board test results for a 5 A current in the primary: output signal (CH1: 50 mV/div) and input signal (CH2: 2 A/div).
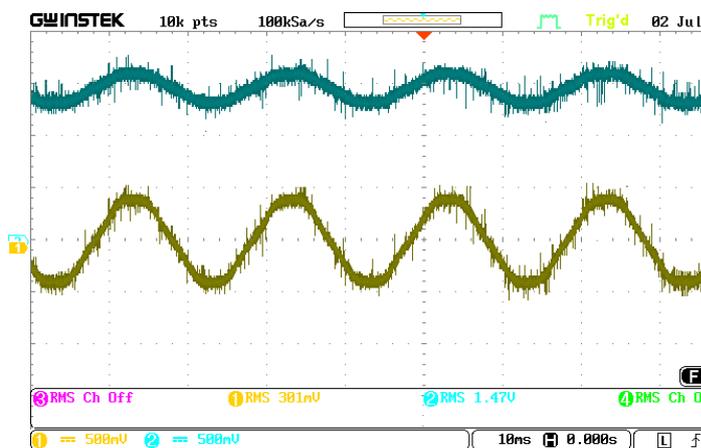

Appendix iii - Signal conditioning board test results for the voltage sensor: input signal (CH1: 500 mV/div) and output signal (CH2: 500 mV/div).

Development of Power Converters for Electric Vehicle Charging with Photovoltaics Interface
Júlio André Machado Fernandes - University of Minho
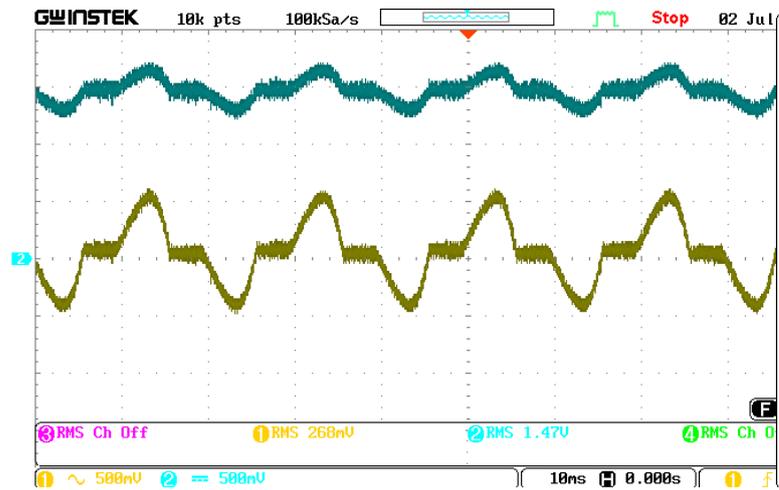
Appendix iv - Signal conditioning board test results for the current sensor: input signal
(CH1: 500 mV/div) and output signal (CH2: 500 mV/div).
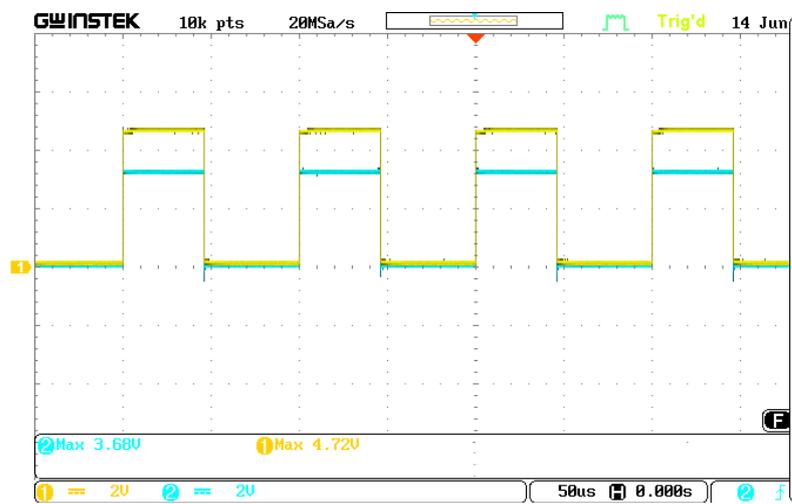
Appendix v - Command board test results: PWM signal from the DSC (CH2: 2 V/div) and output signal
of the command board (CH1: 2 V/div).
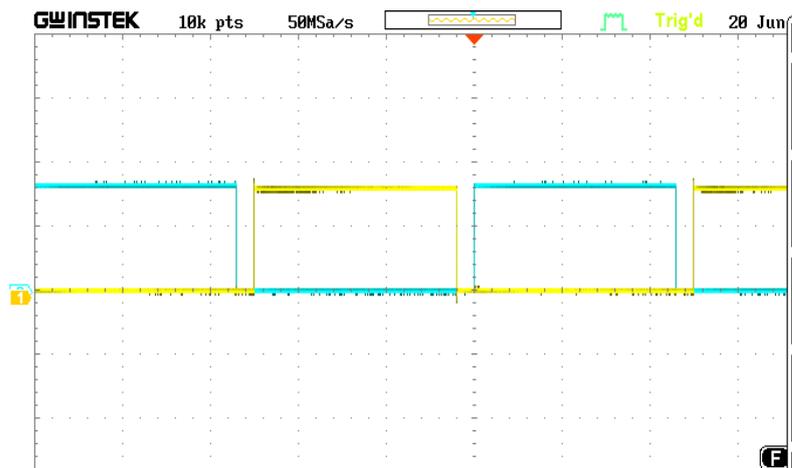
Appendix vi - PWM signals from the DSC applied to one leg of the AC-DC converter (CH1: 2 V/div and
CH2: 2 V/div).
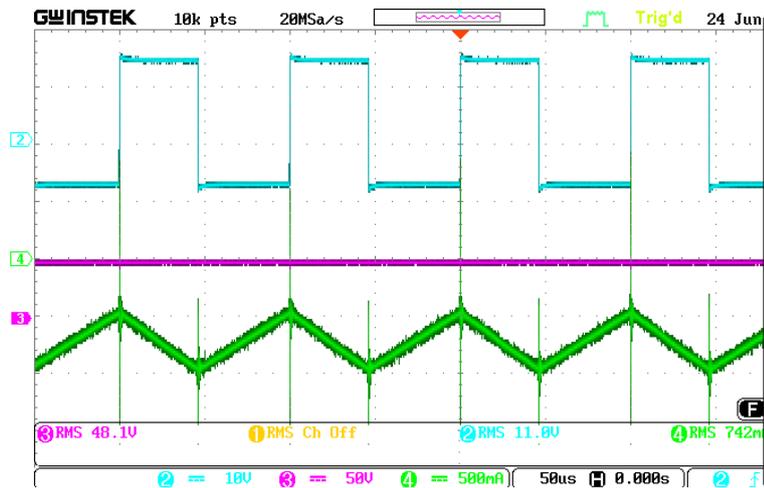
Appendix vii - Experimental results obtained in of the open-loop test to discharge the battery pack: PWM signal coming from the driver circuit (CH2: 10 V/div), DC-link voltage (CH3: 50 V/div) and battery current (CH4: 500 mA/div).
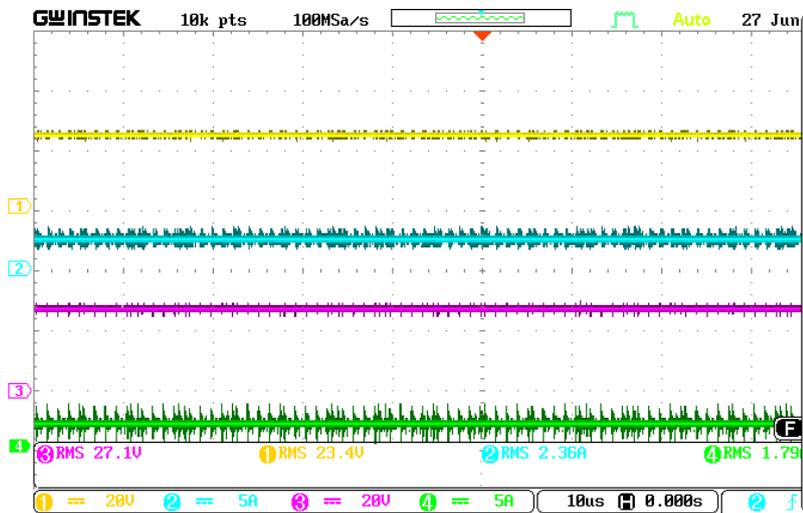

Appendix viii - Experimental results obtained during charge of the batteries by a DC source simulating a PV panel: DC lab source voltage (CH3: 20 V/div) and current (CH2: 5 A/div); Battery voltage (CH1: 20 V/div) and current (CH4: 5 A/div).
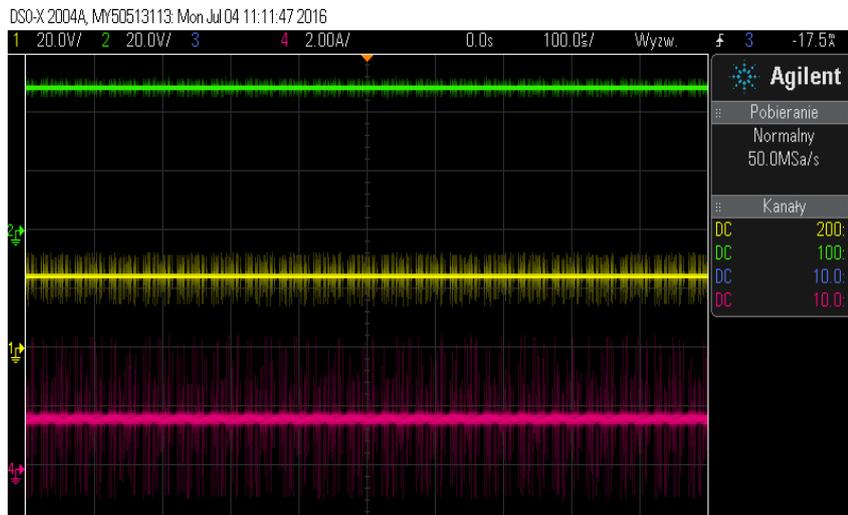
Appendix ix - Experimental results obtained for the bidirectional DC-DC converter, during constant current charge: DC-link voltage (CH2: 20 V/div), battery voltage (CH1: 20 V/div) and battery current (CH4: 2 A/div),.
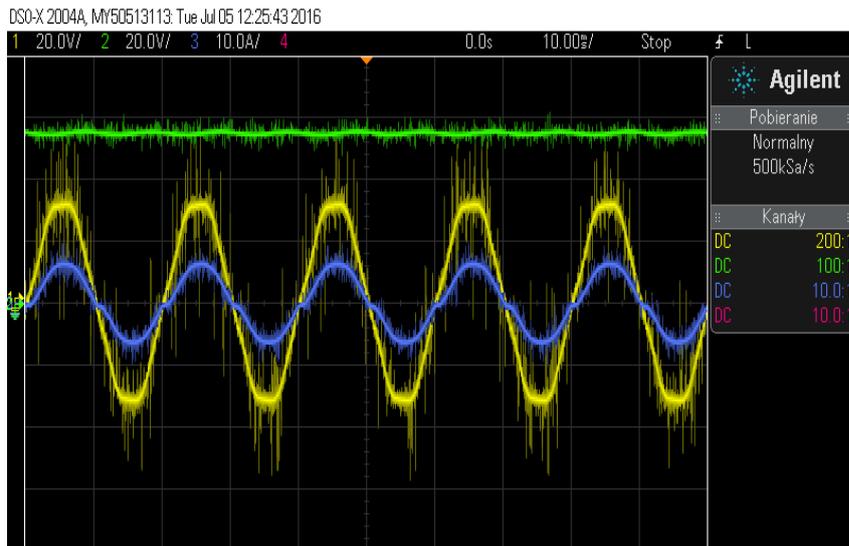
Appendix x - Experimental results obtained during DC-link voltage regulation test to 55 V: Grid voltage (CH1: 20 V/div), grid current (CH3: 5 A/div) and DC-link voltage (CH2: 20 V/div).
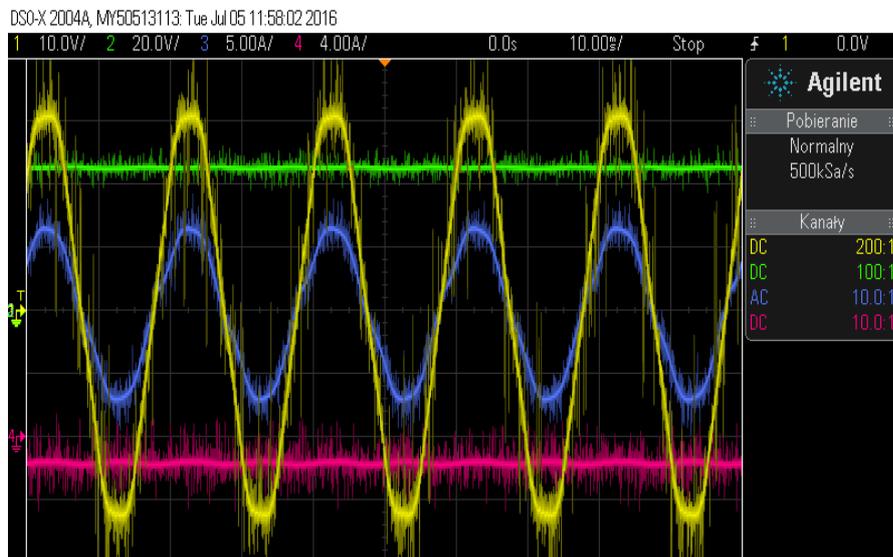
Appendix xi - Experimental results of G2V operation with a reference charge current of 2 A: Grid voltage (CH1: 10 V/div), grid current (CH3: 5 A/div), DC-link voltage (CH2: 20 V/div) and battery current (CH4: 4 A/div).

Development of Power Converters for Electric Vehicle Charging with Photovoltaics Interface
Júlio André Machado Fernandes - University of Minho

139